PB98-148976

FINAL REPORT

FHWA-WY-98/01F

State of Wyoming
Department of Transportation

U.S. Department of Transportation
Federal Highway Administration

DETERMINING BRIDGE RESPONSES TO OVERWEIGHT LOADS

Submitter:

Bridge Diagnostics, Inc.
5398 Manhattan Circle #100
Boulder, CO 80303-4239
(303) 494-3230

March, 1998

DISCLAIMER

The contents of this report reflect the views of the author(s) who are responsible for the facts and accuracy of the data presented herein. The contents do not necessarily reflect the official views or policies of the Wyoming Department of Transportation or the Federal Highway Administration. This report does not constitute a standard, specification, or regulation.

The United States Government and the State of Wyoming do not endorse products or manufacturers. Trade or manufacturers' names appear in this report only because they are considered essential to the objectives of the document.

Technical Report Documentation Page

Report No.	Government Accession No.	Recipients Catalog No.
FHWA-WY-98/01F		

Title and Subtitle	Report Date
DETERMINING BRIDGE RESPONSES TO OVERWEIGHT LOADS	MARCH 1998
	Performing Organization Code

Author(s)	Performing Organization Report No.
Jeffrey L. Schulz, Brett C. Commander, George G. Goble	

Performing Organization Name and Address	Work Unit No.
Bridge Diagnostics, Inc. 5398 Manhattan Circle #100 Boulder, CO 80303-4239	RS08(197) Job No. R1H6
	Contact or Grant No. 49565

Sponsoring Agency Name and Address	Type of Report and Period Covered
Wyoming Department of Transportation P.O. Box 1708 Cheyenne, WY 82003-1708 Programming - Research Unit (307) 777-4182	Final
	Sponsoring Agency Code

Supplementary Notes

WYDOT Technical Contact: Jerry L. Ellerman, Bridge Operations Engineer

Abstract

The Wyoming Department of Transportation (WYDOT) Office of Overweight Loads issues overload permits to motor carriers based on the results of conventional structural analysis of bridges along the anticipated permit route.

This study was initiated to determine if current analytical methods accurately represent the actual live-load response of common bridge types, or if the results are over- or under-conservative in predicting maximum stresses. Field test procedures consisted of performing diagnostic load tests on each structure type as it was subjected to both a standard vehicle load and then an overload/permit vehicle. Finite element models (FEM) were developed and an analysis performed with the same loads as those applied in the field. Comparisons between the measured strains and the analytical strains were made, and each model systematically modified until comparisons were in good agreement.

The three bridge types used in the study are:

- Reinforced Concrete (R/C) Slab Bridge
- R/C T-Beam Bridge
- Slab/Steel Girder Bridge

Results:

The results demonstrated that the concrete slab bridge rated significantly higher than conventional analysis dictated. The actual load capacity of the steel bridge was also greater than conventional analysis predicted. While the capacity of the concrete t-beam was not as high as anticipated, in no instance were the actual capacities determined to be lower than conventional analysis indicated.

Key Words	Distribution Statement
WYOMING, R/C SLAB BRIDGE, R/C T-BEAM BRIDGE, SLAB/STEEL GIRDER BRIDGE, FEM, STRAIN COMPARISON, STATIC, DYNAMIC, BEAM, STRAIN MAGNITUDE, OVERWEIGHT LOADS	Unlimited

Security Classif. (of this report)	Security Classif. (of this page)	No. of Pages	Price
Unclassified	Unclassified	103	

Form DOT F 1700.7 (8-72) Reproduction of form and completed page is authorized.

SI* (Modern Metric) Conversion Factors

Approximate Conversions from SI Units

Symbol	When You Know	Multiply By	To Find	Symbol
Length				
mm	millimeters	0.039	inches	in
m	meters	3.28	feet	ft
m	meters	1.09	yards	yd
km	kilometers	0.621	miles	mi
Area				
mm^2	square millimeters	0.0016	square inches	in^2
m^2	square meters	10.764	square feet	ft^2
m^2	square meters	1.195	square yards	yd^2
ha	hectares	2.47	acres	ac
km^2	square kilometers	0.386	square miles	mi^2
Volume				
ml	milliliters	0.034	fluid ounces	fl oz
l	liters	0.264	gallons	gal
m^3	cubic meters	35.71	cubic feet	ft^3
m^3	cubic meters	1.307	cubic yards	yd^3
Mass				
g	grams	0.035	ounces	oz
kg	kilograms	2.202	pounds	lb
Mg	megagrams	1.103	short tons (2000 lbs)	T
Temperature (exact)				
°C	Centigrade temperature	1.8 C + 32	Fahrenheit temperature	°F
Illumination				
lx	lux	0.0929	foot-candles	fc
cd/m^2	$candela/m^2$	0.2919	foot-Lamberts	fl
Force and Pressure or Stress				
N	newtons	0.225	poundforce	lbf
kPa	kilopascals	0.145	pound-force per square inch	psi

Approximate Conversions to SI Units

Symbol	When You Know	Multiply By	To Find	Symbol
Length				
in	inches	25.4	millimeters	mm
ft	feet	0.305	meters	m
yd	yards	0.914	meters	m
mi	miles	1.61	kilometers	km
Area				
in^2	square inches	645.2	square millimeters	mm^2
ft^2	square feet	0.093	square meters	m^2
yd^2	square yards	0.836	square meters	m^2
ac	acres	0.405	hectares	ha
mi^2	square miles	2.59	square kilometers	km^2
Volume				
fl oz	fluid ounces	29.57	milliliters	ml
gal	gallons	3.785	liters	l
ft^3	cubic feet	0.028	cubic meters	m^3
yd^3	cubic yards	0.765	cubic meters	m^3
Mass				
oz	ounces	28.35	grams	g
lb	pounds	0.454	kilograms	kg
T	short tons (2000 lbs)	0.907	megagrams	Mg
Temperature (exact)				
°F	Fahrenheit temperature	5(F-32)/9 or (F-32)/1.8	Celsius temperature	°C
Illumination				
fc	foot-candles	10.76	lux	lx
fl	foot-Lamberts	3.426	$candela/m^2$	cd/m^2
Force and Pressure or Stress				
lbf	pound-force	4.45	newtons	N
psi	pound-force per square inch	6.89	kilopascals	kPa

PREFACE

Purpose

The purpose of the proposed project is to measure the stresses actually induced in the load carrying members of the selected bridge structures and compare these stresses with those calculated by conventional structural analysis. This research should provide WYDOT with a better understanding of the accuracy of our structural analysis methodology as it applies to various structure types and indicate bridges for which conventional analysis may be overly conservative.

Anticipated Benefits

The proposal is anticipated to provide a better understanding of the actual criticality of various structure types when subjected to the effects of heavy loading. This information will be valuable in addressing requests for routing of overweight loads on the State highway system. The findings of this study will determine if procedures followed in the past for allowing or denying the movement of heavy loads within the State are justified and should continue to be adhered to, or if changes in this procedure should result. This may ultimately accelerate the process of analyzing the effects of overweight loads on Wyoming's bridges, resulting in a cost savings to both the State and the trucking industry

Description of the Project

Three structures were selected for instrumentation and analysis by the Bridge Program. These bridges consisted of a three span continuous concrete slab bridge, a three span continuous cast-in-place concrete tee beam bridge, and a three span continuous composite welded plate steel girder bridge. These structure types are representative of large groups of bridges existing within the State.

The structures noted above were instrumented by the consultant at different times. The typical procedure involved several steps. The Office of Overweight Loads would advise the Bridge Program of the proposed movement of an overweight permit vehicle and the anticipated route to be traveled. The Bridge Program would select a bridge on that route based on the desired structure type and accessibility. The consultant would arrive at the bridge the day before movement of the load, and place the strain transducers. Control loads consisting of fully loaded WYDOT dump trucks would be weighed and run across the structure along prescribed paths. Several passes of this vehicle were made at crawl speed and at high speed. The high speed passes helped determine the effects of impact on the structure. The overload vehicle then crossed the structure and strain measurements were recorded.

The strain measurements taken from the several passes of the control vehicle were used to develop an accurate model utilizing a rational analysis. A finite element model (FEM) was defined and the field testing data reproduced in this model. Elements representing the curbs, and load transfer characteristics of the deck were included in the model. Based on measured bending

responses, realistic constraints were established at support locations, i.e. abutments and bents. Parameters including stiffness of the curbs, actual concrete modulus, effective deck stiffness, and moment resistance at the supports were assumed for initial analysis and later modified as required to produce realistic results based on comparison of the measured and computed behavior.

Live loads, simulating the control vehicle are input into the model at several locations and strains calculated. These strains were compared to the field measured data. Stiffness parameters are then modified to result in a Best-Fit correlation between measured and computed strains.

Live loads, simulating the permit vehicle, are then input into the calibrated model. The calculated stresses are compared to the stresses derived from the measured strains to verify the accuracy of the calibrated model.

Comparison of BDI & WYDOT Load Rating Results

Concrete Slab

	BDI		WYDOT	
Vehicle	Inventory	Operating	Inventory	Operating
HS20	1.25	2.11	0.77	1.29
Type 3	1.55	2.58	1.03	1.72
Type 3S2	1.51	2.51	1.03	1.72
Type 3-3	1.81	3.03	1.16	1.94
Permit Vehicle	2.37	3.96	0.58	0.97

Note: Some of the WYDOT ratings were governed by positive moment, other by negative moment. BDI ratings were governed by negative moment with the exception of the permit vehicle which was controlled by shear.

Concrete Tee Beam

	BDI		WYDOT	
Vehicle	Inventory	Operating	Inventory	Operating
HS20	0.98	1.64	0.92	1.54
Type 3	1.27	2.11	1.27	2.12
Type 3S2	1.17	1.95	0.99	1.65
Type 3-3	1.15	1.92	1.06	1.77
Permit Vehicle #1	0.74	1.23	0.63	1.06
Permit Vehicle #2	1.21	2.02	1.04	1.74

Note: The ratings for HS20 and Type 3S2 were governed by shear in the WYDOT calculations. the ratings for all other trucks were governed by negative moment at the first pier in the WYDOT calculations. All of the BDI ratings were governed by negative moment at the first pier.

Steel Girder

	BDI		WYDOT	
Vehicle	Inventory	Operating	Inventory	Operating
HS20	1.63	2.72	1.01	1.69
Type 3	2.24	3.74	1.38	2.30
Type 3S2	1.85	3.10	1.27	2.12
Type 3-3	1.77	2.95	1.31	2.18
Permit Vehicle #1	1.41	2.35	0.89	1.57

Note: Both the BDI and WYDOT ratings for HS20 and Type 3S2 were governed by positive moment in the center span. Ratings for the other three trucks governed by negative moment at the first pier.

Realized Benefits

For the most part, the results of this study were as anticipated. It was presumed before the study that the concrete slab bridge would rate significantly higher than conventional analysis would dictate. Likewise, it was assumed that the actual load capacity of the steel bridge would be greater than conventional analysis shows.

Conversely, the resulting capacity of the concrete Tee beam was not as high as anticipated. These results surprised the Consultant as much as us. The consultant demonstrated that the girders and deck were not as stiff as anticipated. The consultant has concluded that this must be due to cracking, voids, or poor concrete in the deck. However, the cause has not been determined with certainty.

Even though the ratings for the concrete Tee beam were lower than anticipated, in no instance, for any of the bridges, were the actual capacities determined to be lower than conventional analysis indicates. Based on the results of this study, our present procedure for authorizing the movements of overweight loads would seem to be sound. Typically, we do not allow any significant overstress of our bridges, as determined by conventional analysis, with the exception of concrete slab structures which are sometimes allowed to see loading exceeding the calculated maximums. Even in these instances, the overstress is and should be controlled. Although a specific factor has not been identified with any certainty for the less than anticipated capacity of the concrete Tee beam, it serves as an example of how deterioration might affect the capacity of a structure. The study shows us that even though our calculations are probably conservative in the majority of cases, authorizing the movements of overloads which exceed the calculated capacity of a structure must be controlled with care.

Jerry Ellerman, P.E.
WYDOT Bridge Engineer

Table of Contents

List of Figures

List of Tables

INTRODUCTION

Every month, several overload permits are issued to motor carriers by the Wyoming Department of Transportation (WYDOT) Office of Overweight Loads. In each case, the bridges along the anticipated permit route must be evaluated for their ability to handle these very heavy live loads. Traditional evaluation methods often indicate that a particular structure may be loaded up to or above its operating limit if the overload is allowed to pass. This means that an alternate route must be selected, often causing a significant cost increase to the carrier. This decision is based on an analysis that may be quite conservative and significantly over-predicting the live-load effects. Or, conversely, the conventional analysis may be under-predicting maximum stresses, meaning that overload permits might be issued that allow excessive loading to occur.

Therefore, a study was initiated by WYDOT to determine if their current analytical methods accurately represent the actual live-load response of common bridge types. The basis for the comparison was developed by collecting field data on three bridges subjected to overloads. The field test procedures consisted of performing diagnostic load tests on each structure as it was subjected to both a standard vehicle load and then an overload/permit vehicle. Finite element models of the structures were then developed, and an analysis performed with the same loads as those applied in the field. Comparisons between the measured strains and the analytical strains were made, and each model systematically modified until these comparisons were in good agreement. Finally, load ratings were performed for the required Wyoming rating vehicles and for the respective overload permit vehicles.

By comparing the results of these "calibrated" models to the results from their standard analysis methods, WYDOT can evaluate whether their techniques for evaluating overloads are over- or under-conservative. This report outlines the field testing, analysis and load rating procedures used for each bridge, and provides the results in a tabular form that should allow a relatively easy comparison to be made by WYDOT.

TESTING AND ANALYSIS METHODOLOGY

Three bridges on I-25 were selected by WYDOT as representatives of particular "families" such as steel or reinforced concrete. Another consideration in the bridge selection process was the ease of access to the superstructures. Since WYDOT and the testing crew would usually have only a day's notice (and sometimes shorter) as to when a permit load was coming, easy accessibility by the testing crew was necessary in order to minimize instrumentation time. Also, to reduce traffic control requirements below the structures, only bridges that crossed over lightly-traveled roads were selected for testing.

The first bridge to be tested was a reinforced concrete (R/C) slab bridge located near Glendo. WYDOT has a significant number of these continuous slab bridges on their interstate routes, and this bridge was a typical three-span structure. The second bridge was an R/C T-beam bridge located near Wheatland. Again, WYDOT owns a large number of these types of

structures. The third bridge was a steel girder/concrete slab bridge with a slight skew located near Douglas. In each case, instrumentation was installed and a set of tests was first completed on each structure with a standard tandem-axle dump truck vehicle supplied by WYDOT. The testing crew then waited until the permit load arrived and collected data as it crossed at crawls speed as well. In each case, the required boom trucks and/or ladders, traffic control, and test vehicles were all supplied by WYDOT.

The goal was to use the data from the dump truck tests to "calibrate" the analytical models, and then verify their accuracy by comparing the predicted strains to measured strains from the permit vehicles.

RESULTS

Since the detailed results from each test are provided in appendices A through C, only the overall results are discussed here. In each case, the final models predicted the effects of the permit loads quite well, and therefore could be considered much more accurate than an model developed without load test data. In general, the improved accuracy can be attributed to the more realistic load distribution characteristics of the "calibrated" models. AASHTO's guideline for evaluating existing structures was used for load rating all three bridges. While the calibrated models represented the live-load effects quite accurately, the member capacities were calculated by following the current AASHTO design specifications. Although the dynamic effects from high-speed truck passes were measured, the AASHTO impact factors were applied in all of the rating procedures. The following is a brief outline of the results obtained from each bridge:

R/C SLAB BRIDGE:

- The effective stiffnesses of the slabs and curbs were approximately 30 percent stiffer than initially assumed with the gross concrete cross-sections. It was likely that Young's modulus of the concrete was greater than that assumed and/or the overlay contributed to the slab stiffness.
- Rotational restraints of the piers provided nearly fixed-end conditions for the slabs and curbs. The piers also had significant rotational restraint.
- The effective stiffness of the end span was approximately 10 percent greater than the interior span.
- The measured dynamic or impact effect obtained during the high-speed truck crossing appeared to be negative, meaning that the dynamic strain magnitudes were typically less than the static responses.
- Strain comparisons from the permit load had the same degree of accuracy as the test vehicle used to calibrate the model, verifying a linear-elastic response of this structure, even under a heavy load.
- The permit load rating factors were less critical for the superstructure than the factors for the standard Wyoming rating vehicles.
- The critical component for all the ratings was the moment capacity of the curbs at the face of the transverse floor beams.

R/C T-BEAM BRIDGE:

- The exterior beams were approximately 28 percent stiffer than the interior beams, due primarily to the increased flange thickness provided by the curbs.
- The abutments provided approximately 50 percent of completely fixed-end conditions for the beams.
- The measured dynamic or impact effects obtained during the high-speed truck crossings were in the range of 0 to 40 percent. Average values obtained from the most heavily-loaded beams were approximately 25 percent, indicating that the AASHTO impact factor of 30 percent is reasonable.
- With the exception of the exterior beams, the resulting stiffness parameters were reduced significantly from the original values based on the gross member cross-sections, indicating that the actual concrete modulus may be lower than expected.
- Measurements taken from the center beam near the pier indicated unusual behavior, indicating that special attention should be paid at this location during future visual inspections.
- Strain comparisons from the permit load had the same degree of accuracy as the test vehicle used to calibrate the model, verifying linear elastic behavior under heavy load.
- This structure was significantly more flexible than the majority of R/C bridges previously evaluated with this technique. The fact that the resulting beam stiffnesses were less than those obtained with gross concrete sections suggests that the crack density in the concrete has become significant.
- The unusual measurements obtained from the center beam near the pier were an indication that some type of deterioration has occurred or that some defect was present in the vicinity.
- There were considerable differences between the critical rating values obtained by the ASD and LFD rating methods.

SLAB/STEEL GIRDER BRIDGE:

- The exterior beams had approximately the same stiffness as the interior beams.
- Fully-composite behavior was observed in the positive moment region of span 2, and the resulting beam stiffness was 22 percent greater than the initial stiffness calculated for a composite section.
- Beam sections designed as non-composite were observed to behave partially-composite due to friction between the top flange of the steel I-beam and the concrete deck.
- There was minimal rotational restraint provided by the rockers at the supports.
- The measured impact effects obtained during the high-speed truck crossings were in the range of 0 to 22 percent
- Strain comparisons from the permit load produced approximately the same degree of accuracy as did the test vehicle used to calibrate the model. This indicated that the majority of measured responses (with the exception of the top flange measurements in the non-composite regions) were linear with respect to load magnitude and that the model's accuracy was not dependent on the applied load.
- The sections of the superstructure that were designed as non-composite were observed to behave partially-composite due to friction between the top flange and the deck. The degree of

unintended composite action varied with load position and indicated that the responses in these areas were somewhat nonlinear.
- The rating factors indicated that this structure had a relatively high load capacity.

Appendix D contains a detailed outline of the field testing procedures, and the techniques used to correlate the models with the field data are described in detail in appendix E. Also, the methods used to develop the load rating factors are discussed in appendix F.

CONCLUSIONS

The procedures used for testing and validating each of the analytical models produced reasonable, if not excellent, results for this type of study. In addition to using these models as a basis for comparison with their standard analysis techniques, WYDOT can use them to develop load ratings on these structures for future overloads.

APPENDIX A – R/C SLAB BRIDGE

DESCRIPTION OF STRUCTURE

Table 1 Structure description – R/C slab bridge.

Structure Identification	Project I-25-2(7)102
Location	Wyoming, Southbound I-25 milepoint 98.51
Structure Type	R/C slab, 3-span continuous
Span Length(s)	20ft-25ft-20ft (6.1m-7.6m-6.1m)
Roadway/Structure Widths	38ft/41ft (12m/12.5m)
Slab Depth(s)	10in (254mm) at midspans, 12-1/2in (318mm) @ piers, haunch begins @ 4ft 6in (1.4m) from edge of floor beam.
Abutments	R/C abutment on top of cast-in-place piles, connected to slab by dowels and shear key.
Piers	(8) 12.75in (324mm) ∅ steel pipe piles filled with concrete. Spaced @ 5ft-4in (1.6m) o.c. 24in x 24in (0.6m x 0.6m) R/C transverse floor beam.
Comments	Structure appears to be in good condition. No indication of distress, minimal observed cracks on bottom surface of bridge. Some longitudinal cracks between curb and slab. Inspection personnel indicated that these bridges often have exceptionally rough decks.

INSTRUMENTATION AND TESTING PROCEDURES

The superstructure of the bridge was instrumented with 32 re-usable strain transducers as shown in Figure 1. Since the bridge was symmetric about two axes and there was no apparent structural damage, the majority of instrumentation was confined to one quarter of the bridge. All of the transducers were attached to the slab and the curbs. Transducers were placed at five locations across the midspan cross-section on span 2 and were oriented both longitudinally and transversely. Various positive and negative moment regions were instrumented as follows: midspan of spans 1 and 2, near the north abutment of span 1, both sides of the of the north pier, and the quarter span of span 2. The overall goal of the instrumentation was to establish the transverse and longitudinal stiffness characteristics of the structure and to evaluate the contribution of the various components such as the slab, curb, abutment and piers.

Transducers were mounted in pairs on the curbs so that flexural curvature and the neutral axis location could be computed from the strains. All of the slab gages were attached to the bottom surface of the slab and an assumed neutral axis location was used to compute curvature. Gage lengths of the strain transducers were extended from the standard 3in (76mm) to 12in (305mm) and 18in (458mm) in order to reduce the effects of tension cracks associated with

reinforced concrete. The purpose of the extensions was to obtain average surface strains that were consistent with a homogenous material.

A loaded three-axle tandem dump truck was provided by WYDOT for the purpose of controlled loading. The truck's gross wheel weights and axle configurations are shown in Figure 2. Three transverse truck paths (south curb, middle, and north curb) were defined so that the lateral load transfer characteristics could be established. The load tests were performed by driving the truck across the bridge at crawl speed along the prescribed paths. Data was recorded continuously during each pass and the truck position was monitored remotely. Truck crossings from each path were performed twice to ensure reproducibility. A total of six slow speed truck crossings were performed along with two high-speed passes along paths 2 and 3. The entire process including instrumentation and load testing with the WYDOT vehicle took approximately four hours.

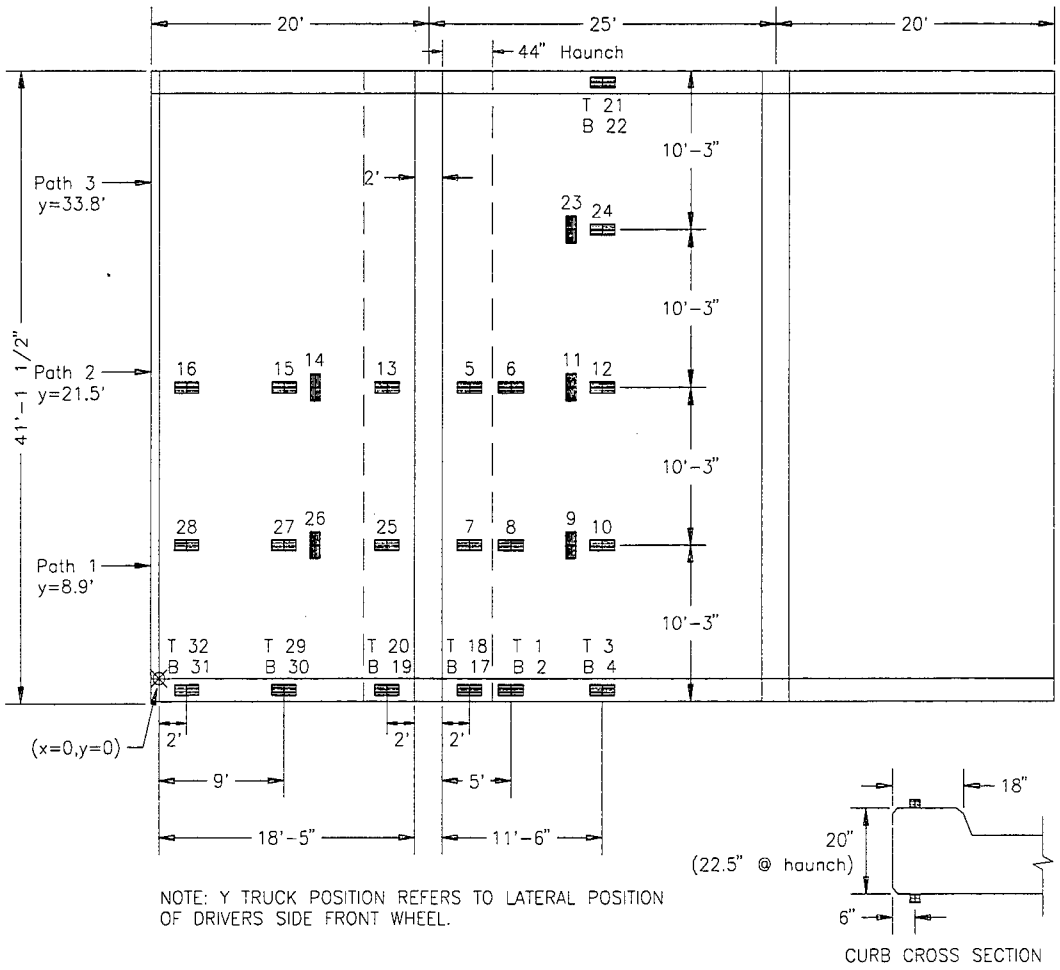

Figure 1 Instrumentation plan – R/C slab bridge.

Following the standard load testing procedures, strains were measured during a single crossing of a 252,000lb (1,121kN) permit load vehicle. Axle spacing and load magnitudes are shown in Figure 3. As with the dump truck, the longitudinal position was monitored as the

permit load followed a pre-defined path at crawl speed. The path for the overload was defined as the passenger side front wheel following the right lane. Note that this lateral position was not the same as those defined for the WYDOT dump truck crossings. As will be seen, data from this test was used to verify the ability of the calibrated analysis model to predict load responses due to an extremely large load.

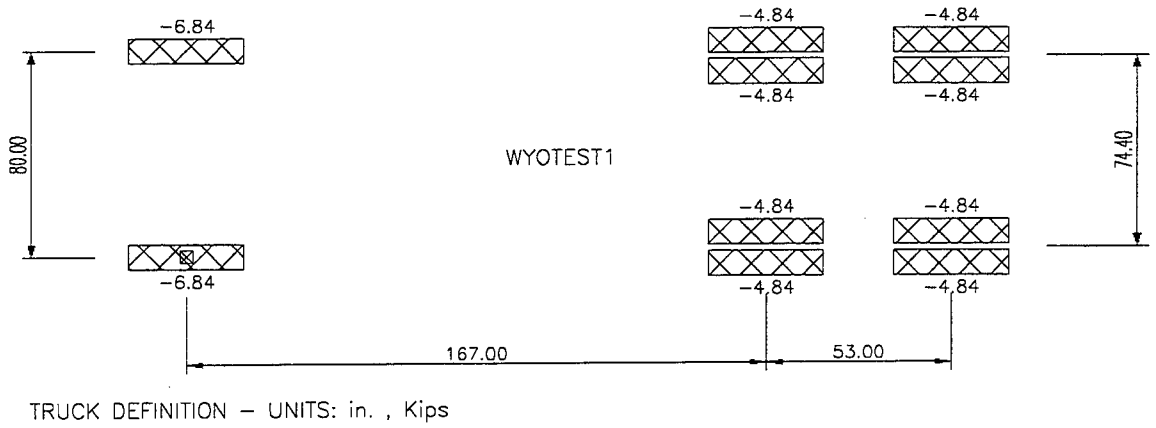

Figure 2 Initial test truck – R/C slab bridge.

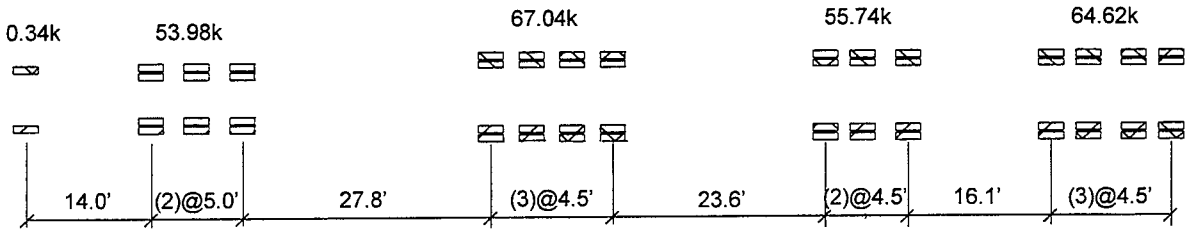

Figure 3 Overload permit vehicle – R/C slab bridge.

PRELIMINARY INVESTIGATION OF TEST RESULTS

A visual examination of the field data was fist performed to assess its quality and to make a qualitative assessment of the bridge's live-load response. It was determined that the structural responses were linear and elastic since there were no discontinuities and all of the strains returned to zero after each truck crossing. This was true for all of the dump truck crossings as well as the permit load crossing. Reproducibility of the data was verified by comparing strain histories from duplicate truck crossings. In every case, the correlation was excellent as shown in Figure 4.

Another observation made directly from the measurements was that rotational restraint at the abutments was inducing negative moment in the slab and curb near the abutment while the first span was loaded. Based on this observation, the rotational stiffness of the abutment had to be included in the model calibration procedure because it has a significant effect on the other measured strains.

The measured strains were considered normal for the span length and truck weight. The largest measured strain magnitude was 78 in^{-6}/in which corresponds to approximately 0.28 ksi (1.93MPa) in concrete (assuming E=3,600 ksi (24,840 MPa)) or 2.26 ksi (15.6 MPa) in steel. It is important to note that the measured strains are averaged over a 12in (305mm) or 18in (458mm) gage length. Because of the presence of cracks, these strains are **not** to be confused with **maximum** steel stress. Table 2 contains the maximum measured strains at various locations on the structure for each truck path and for the permit load. Unfortunately, a direct comparison could be made for the dump truck and permit load responses because the same truck paths were not followed. However, comparison of the maximum positive and negative measured strains indicated that the permit load generated stresses of approximately eight percent higher in positive moment and 30 percent higher in negative moment compared to the dump truck crossings.

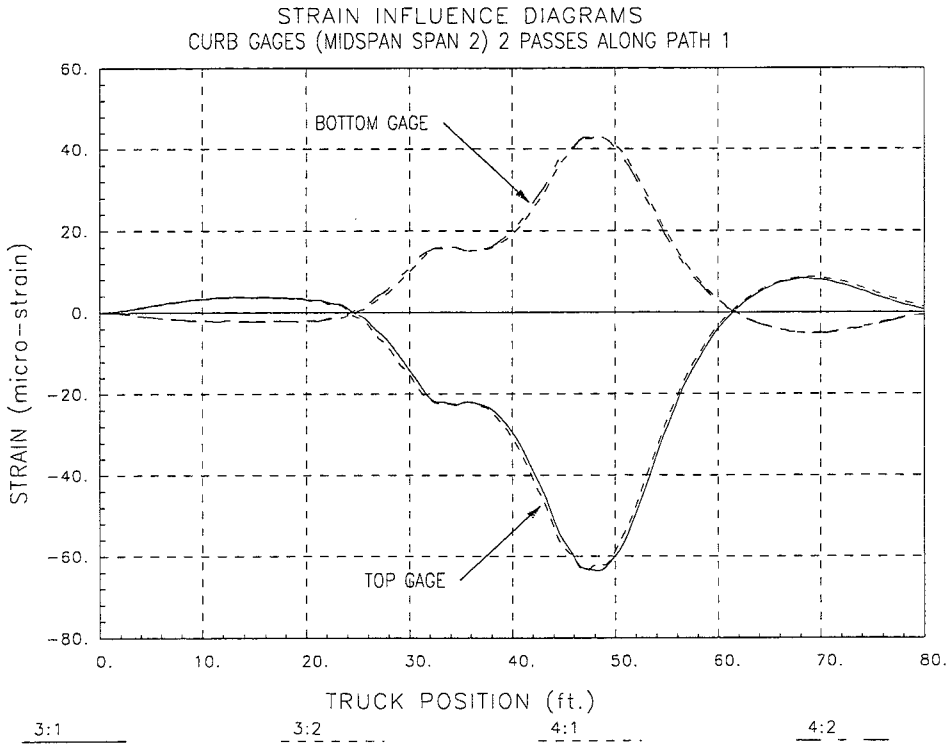

Figure 4 Reproducibility of test results – R/C slab bridge.

Table 2 Maximum measured strain magnitudes – R/C slab bridge.

Gage ID	Location	3 Axle Path 1	3 axle Path 2	3 Axle Path 3	Permit load Path 2
4	Midspan (2) West Curb	43	8	1	27
10	Midspan (2) West Slab	78	33	5	84
12	Midspan (2) Middle Slab	16	73	23	66
24	Midspan (2) East Slab	4	23	56	19
22	Midspan (2) East Curb	+0	5	32	4
17	West Curb near pier	-16	-2	-0	-10
7	West Slab near pier	-19	-10	-1	-35
5	Middle Slab near pier	-4	-27	-5	-33

Strains were also recorded from high-speed crossings of the dump truck along paths 2 and 3 in an effort to quantify any impact or dynamic effects on the structure. As shown in Figure 5, it is apparent that the high speed passes produced lower magnitude strains then the quasi-static passes. This was typical of all the strain histories from both high speed passes. The decrease in strain magnitudes was caused mainly by the short span lengths and the truck speed. Based on this, it was apparent that the AASHTO impact factor of 30 percent is conservative for the superstructure. However, the same could not be assumed for the supporting piers and substructure. Since the impact effect is dependent on many variables including vehicle speed, vehicle suspension, and road surface condition, the AASHTO impact factor was still used for the subsequent rating calculations.

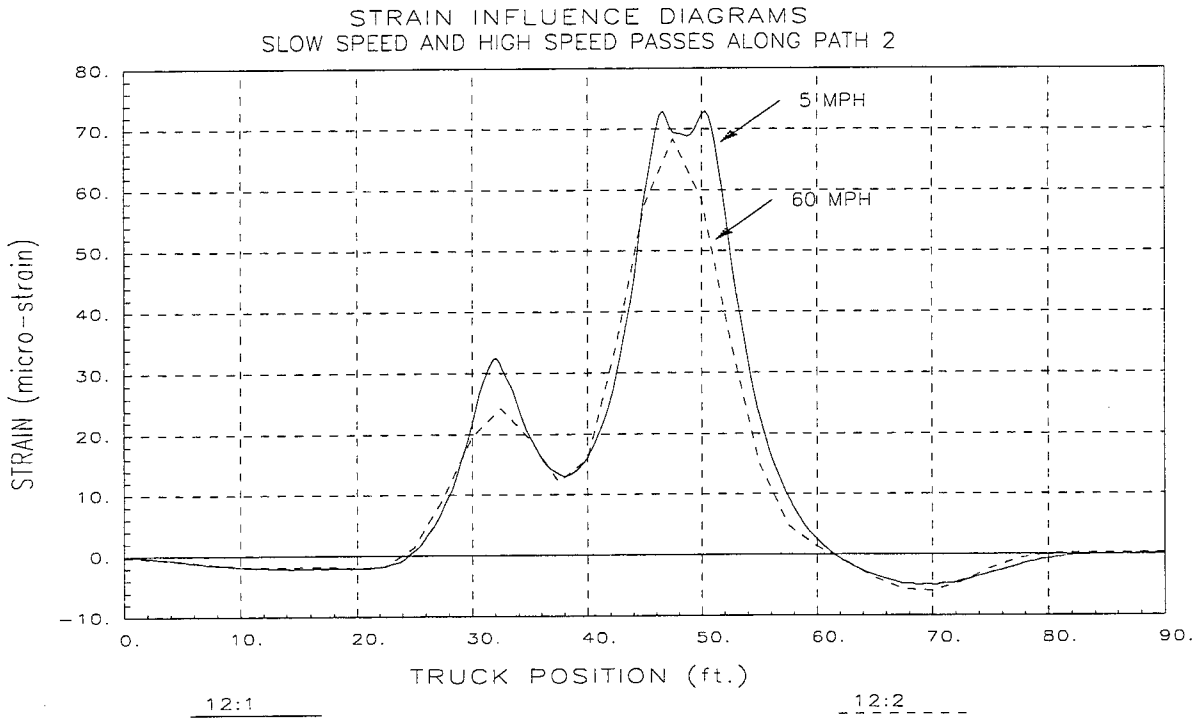

Figure 5 Static vs. dynamic strains – R/C slab bridge.

It should be noted that all of the above information was extracted directly from the field data only. The following section illustrates how the field data was used to generate and "calibrate" an analytical model of the structure.

MODELING, ANALYSIS, AND DATA CORRELATION

A simple grid finite element model (FEM) of the structure was defined and the entire field testing operation was essentially reproduced in the modeling and analysis procedures. Two-dimensional frame elements were used to represent the curbs and quadrilateral plate elements simulated the load transfer characteristics of the deck. Nodal points were defined longitudinally at the abutment and pier centerlines, edge of the transverse floor beam, and at 1/12-span locations. Transverse node placement was based on the overall width (W) of the slab and at W/18 locations to maintain a desirable aspect ratio of the plate elements. Based on the observed bending responses, elastic and rotational spring elements were placed at the abutment nodes and at all pier locations. To facilitate comparison of the computed and measured responses, strain gage locations were defined on the curbs and slab corresponding to the same locations defined in the field.

The entire model, including geometry, boundary conditions, member cross-sections, and gage locations, was generated graphically. A computer-generated display of the model is shown in Figure 6. Even though the geometry of the structure was well defined, there were various structural parameters that were not well known. These parameters included the effective stiffness (EI) of the curbs because of the presence of cracks, actual concrete modulus (E_c), the effective stiffness of the deck (Et^3), and the moment resistance of the support conditions (K_r). For the initial model, concrete properties were based on 3.0 ksi (20.7 MPa)concrete and the beam cross-sectional properties were based on the gross concrete sections. Initially, the effects of cracks, reinforcement steel, and overlay were ignored and the initial stiffness constants of the support springs were assumed to be zero. These properties were later modified based on the comparison of the computed and measured response behavior.

Loading of the model was accomplished by defining a two-dimensional model of the test vehicle (group of point loads) and then placing the truck model at discrete positions along the same paths used during the field test. During the comparison process, eleven longitudinal truck positions were defined for each test path. Therefore, during each analysis run, strains were computed at 32 gage locations for 33 different load conditions. The accuracy of the analysis was then determined by comparing the 1056 (32x33) computed strain values with their corresponding measured strains.

Initial comparisons between the computed and measured strains indicated that significant differences existed between the model and the actual structure. In general, the magnitudes of the computed strains were excessive by a range of 20 to 30 percent at the midspan locations. Relatively good agreement was observed at gage locations near the pier while the abutment gages had a negative correlation (opposite sign). Since simple supports were used in the initial model, the computed moments near the abutments were in the positive direction (tension on bottom surface). But as previously mentioned in the discussion of preliminary observations, negative moments were

measured near the abutment. It was also apparent that the lateral distribution was in error by observing the relative errors at the midspan gages for the various truck passes.

To improve the initial model's accuracy, the above-mentioned stiffness terms were modified through a parameter identification process until a best-fit correlation between the measured and computed strain was obtained. Reasonable upper and lower limits were defined for each parameter and the parameters were evaluated within those constraints. For instance, the upper- and lower-bound moment-of-inertia values for the curb members were defined through the gross and the elastic cracked sections, respectively. The effective slab thickness was given a range of plus and minus 50 percent to account for the stiffening effect of the reinforcement, the presence of cracks, and any error in the estimated concrete modulus. Lower and upper bounds for the abutment and pier spring stiffnesses were defined by the ratio of EI/KL, where E, I and L refer to the curb or slab properties and span lengths, and K is the rotational spring stiffness in terms of moment-per-unit measure of rotation. Reasonable ranges for this ratio are between 0.1 and 4.0, which correspond to nearly fixed and nearly simple supports. Common end restraints for typical beam supports have a stiffness ratio (EI/KL) of around 1.0.

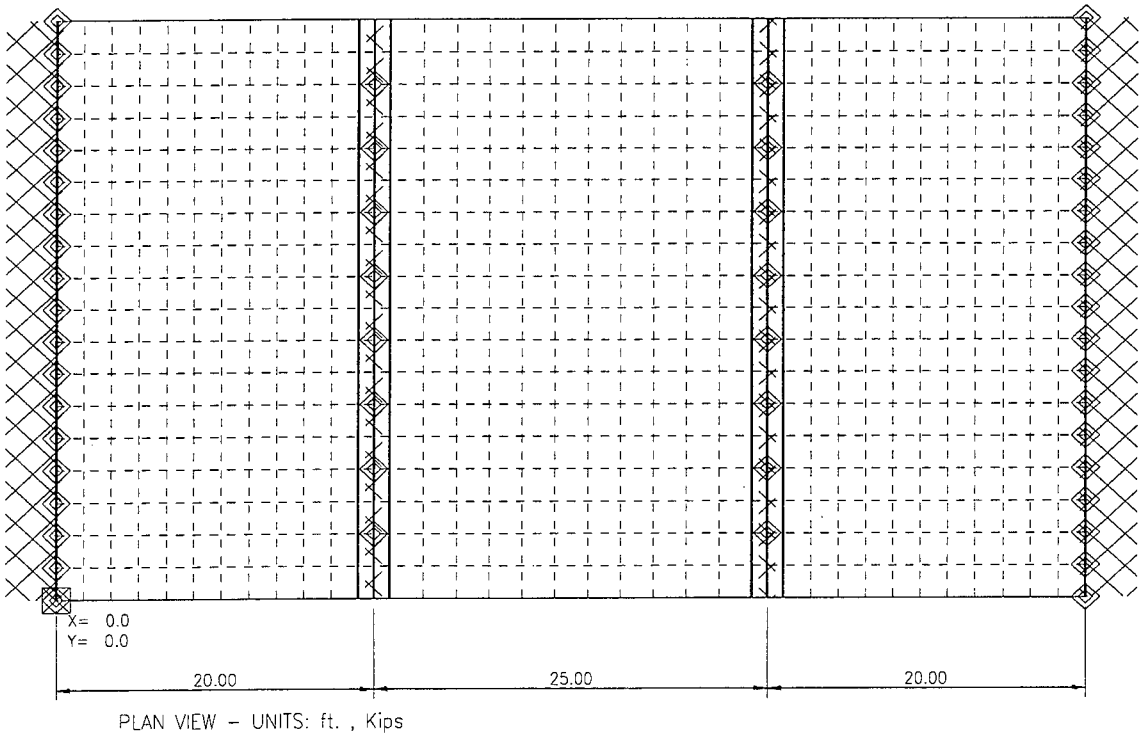

Figure 6 Computer model of R/C slab bridge.

For the first set of iterations, it was assumed that the relatively rigid abutment support stiffnesses might different for the slab and the curb because of the curb support detail and the wingwall. Therefore, separate spring parameters where defined for these locations. Initially, it was

assumed that the slab properties were the same for the end and interior spans. Also, the haunched areas were simulated by proportionally graduating the thickness of the plates near the piers. After several iterations, it was apparent that the end spans were stiffer than the interior span and that the haunched slab stiffnesses were not directly related to the slab thickness. For instance, the thickest portion of the tapered slab nearest the pier was slightly less stiff than the thinner sections. Intuitively, this result seemed unlikely. However, this is possible because the thicker portion of the slab experiences higher moments and stresses and could therefore have a slightly higher concentration of flexural cracks, resulting in a reduction in stiffness. After allowing the different slab sections to be calibrated independently, the parameter identification process was repeated. At the end of this cycle, an excellent correlation was obtained, Table 3 contains the initial and final values for each of the variable properties. To illustrate how the parameter modification improved the accuracy of the model, the initial and final error values are shown in Table 4.

Table 3 Initial and final parameter values.

Member Property	Units	Initial Value	Identified Value
Curb – I	in^4 (cm^4)	16,420 (683,400)	20,500, 853,210
Curb @ haunch – I	in^4 (cm^4)	19,620 (816,580)	34,000 (1,415,080)
Slab Span 1 –t	in (mm)	10.0 (254)	12.8 (325)
Slab Span 2- t	in (mm)	10.0 (254)	10.1 (257)
Slab @ haunch A – t	in (mm)	10.625 (270)	11.3 (287)
Slab @ haunch B- t	in (mm)	11.875 (302)	10.2 (259)
Abutment Restraint – Kr	k-in/radian (N-m/radian)	0.0 (0.0)	95% = $1.15x10^6$ ($1.30x10^8$)
Abutment Curb Restraint - Kr	k-in/radian (N-m/radian)	0.0 (0.0)	70% = $2.00x10^6$ ($2.26x10^8$)
Pier Rotational Restraint - Kr	k-in/radian (N-m/radian)	0.0 (0.0)	20% = $2.88 x10^5$ ($3.25 x 10^8$)

Following the parameter identification procedure, a 2-D model of the permit load was generated and applied to the calibrated model. The purpose of this exercise was to verify that the model could reasonably predict the responses from a much heavier load with a completely different geometry. The analysis was run for the single pass of the permit load with the truck positions incremented at 3-ft (0.92-m) intervals. A total of 36 truck positions were defined and strains were computed at each gage location. As shown in Table 5, the same level of accuracy was obtained from the permit load crossing as for the dump truck which was used to calibrate the model. The absolute and scale error values were larger, but this was expected since there was a much larger volume of strain due to a much longer load cycle. Measured and computed strain comparisons are provided for both load vehicles in Figure 7 through Figure 16.

Table 4 Accuracy of initial and refined models – R/C slab bridge.

Error Value	Initial Model	Refined Model
Absolute Error	3624	1465
Percent Error	28.7	6.9
Scale Error	6.3	2.6
Correlation Coefficient	.89	.96

Table 5 Model accuracy with permit load – R/C slab bridge.

Error Value	Calibrated Model
Absolute Error	2504
Percent Error	7.1
Scale Error	6.5
Correlation Coefficient	.96

At this point, the model has been "calibrated" to the field measurements and it has been verified that the model will provide the same degree of accuracy regardless of the load configuration. Since the load responses of the model are very similar to those of the actual structure, it can be assumed that the stiffness and load transfer characteristics are correct.

DISCUSSION OF RESULTS

The accuracy obtained by this evaluation process was typical of continuous R/C bridge structures. Most of the strain comparisons were within the tolerance obtainable by the load test. The primary observations made from the load test data evaluation and during the parameter identification process are as follows:

- The effective stiffnesses of the slabs and curb were approximately 30 percent stiffer than initially assumed based on the gross concrete cross-sections. There are three possible situations that may be contributing to the higher-than-expected stiffness. First, the density of flexural cracks in the concrete was not high enough to have a significant impact on the overall stiffness. Secondly, since the resulting stiffness values were greater than what could be obtained by the gross cross-section, it is likely that the modulus of the concrete was greater than the initially-assumed value of 3,100 ksi (21,390 kPa) (corresponding to F_y = 3.0 ksi (20.7 kPa)). This result implies that the concrete was of relatively high strength, and a Young's modulus value of 3,600 ksi (24,840 kPa) (corresponding to F_y = 4.0 ksi (27.6 kPa)) could be conservatively used for rating purposes. An alternative explanation of the observed results is that the overlay applied to the slab contributed to the slab stiffness.

- Rotational restraints of the piers and abutment had a significant effect on the structural response. The abutments provided nearly fixed-ended conditions for the slab and curb. The piers also had significant rotational restraint which had the effect of reducing midspan moments but slightly increasing the maximum negative moments at the piers.
- The effective stiffness of the end span was approximately 10 percent greater than the interior span. An explanation for this result is that the end spans have experienced lower stress levels than the interior span because the end spans are only 20 percent shorter and the apparent end restraint induced by the abutments greatly reduces the midspan stresses of the end spans. The lower stresses may have resulted in a lower density of cracking in tension zones and therefore, a stiffer response behavior.
- The measured dynamic or impact effect obtained during the high-speed truck crossings appeared to be negative, meaning that the dynamic strain magnitudes were typically less than the static responses. This observation was based on the slab and curb responses and does not likely apply to the supporting structure. Because there are many variables associated with dynamic and impact responses, the AASHTO impact factor of 30 percent is still recommended for general rating calculations.
- Strain comparisons from the permit load had the same degree of accuracy as the test vehicle used to calibrate the model. This verified that all measured responses were linear with respect to load magnitude and that the model's accuracy was not dependent on the applied load.

LOAD RATING PROCEDURES AND RESULTS

The main reason for producing a field calibrated model was to have the ability to compute realistic load ratings. Given a realistic model, analyses and load ratings can be performed for any load configuration. In this section, a discussion of the load rating procedures is given and load limits are provided for standard Wyoming load configurations and for the permit load vehicle used in the field test.

Inventory and operating rating factors were computed using the Load Factor Design (LFD) method with the ultimate moment capacities of the slab and curb as the limiting criteria. Ratings based on ultimate shear capacities were also checked for the overload vehicle. It is important to note that there is inherent conservatism in this approach, because the analysis is based on a linear stress-strain relationship up to initial failure. In reality, the structure would undergo non-linear behavior and load redistribution would occur prior to initial failure of any component. Therefore, it is likely that a higher load would be resisted by the actual structure than what is predicted by the analysis.

The rating equation specified by the AASHTO *Manual for Condition Evaluation of Bridges* discussed in appendix F was used to generate inventory and operating load limits. The flexural capacities of the members were based on standard nominal strength calculations for the curb and one ft wide strips of the slab. Yield stresses and concrete strength values were not provided in the plans, therefore, F_y of 40 ksi (276 MPa) was assumed for the reinforcement steel based on the age of the structure and F'_c of 4.0 ksi (27.6 MPa) was assumed for the concrete due to the observed stiffness. Moment and shear capacities used to compute ratings for the slab and curb are listed in Table 6. The shear capacities were computed according to AASHTO specifications as the sum of

the steel and concrete shear capacities ($V_n = V_s + V_c$) since there was little significant cracking. The appropriate load factors were applied to the dead and live-load effects based on the level of rating (A_1=1.3, A_2=2.17 for inventory and A_1=1.3, A_2=1.3 for operating). An impact factor of 30.0 percent specified by AASHTO was used even though the dynamic strains were less than the static strains.

It is important to note that the primary benefit of this approach is that the load effects are more realistically determined. With the exception of estimating a conservative concrete strength, the approach has little impact on component capacity calculations. In the rating equation, dead- and live-load effects were computed from the calibrated model. The dead-load was computed from the structure's self-weight plus an extra 45 lbf/ft^2 (2,156 N/m^2) on the deck to account for the railings and overlay. Critical live-load effects were determined by computing shear and moment envelopes for several different truck paths. Multiple lane load situations (two and three lanes) were obtained by superimposing envelopes for truck paths separated by 12 ft (3.66m) or more. Effects of three-lane loading were reduced by 10 percent as specified by AASHTO 3.12.1. Rating values for various components are listed in Table 7 for the HS-20 design vehicle.

Table 6 Component capacities – R/C slab bridge.

Member	Moment (Mn = AsFy(d-a/2)	Shear (Vn = (V_s+V_c))
Slab @ Midspan	437 k-in/ft (161,909 N-m/m)	11.0 k/ft (160.6 kN/m)
Slab @ Pier	592 k-in/ft (219,336 N-m/m)	14.2 k/ft (207.3 kN/m)
Curb @ Midspan (w/6t slab)	5,754 k-in (650,202 N-m)	53.2 kips (53.2 kN)
Curb @ Pier (w/6t of slab)	1,806 k-in (204,080 N-m)	62.4 kips (277.7 kN)

Table 7 HS-20 load rating factors – R/C slab bridge.

Member	Inventory Rating Factor A_1=1.3, A_2=2.17	Operating Rating Factor A_1=1.3, A_2=1.3
Curb @ Pier	0.97 (moment)	1.62 (moment)
Slab Midspan	1.67 (moment)	2.79 (moment)
Slab @ pier	1.25 (moment)	2.11 (moment)

Vehicle load limits are controlled by the lowest member rating factor resulting from the specific load configuration. The maximum vehicle load is then computed by multiplying the gross vehicle weight by the rating factor. This rating process was performed for four standard Wyoming truck configurations including the HS-20 and also for the permit vehicle used during the test, with the results being shown in Table 8. In all cases, the critical rating factor was controlled by moment capacity of the curb near the pier and, except for the permit vehicle, the three-lane loading configuration controlled. It should be noted that some of the rating factors induced by the permit load vehicle were controlled by shear.

Table 8 Vehicle rating factors and weight limits (tons) – R/C slab bridge.

Load Type tons (kN)	Inventory	Operating
HS-20: 36 (320.4)	0.97: 35 (311.5)	1.62: 58 (516.2)
Type 3*: 22 (196.0)	1.32: 29 (258.1)	2.21: 49 (436.1)
Type 3S2*: 40 (356.0)	1.16: 46 (409.4)	1.93: 77 (685.3)
Type 3-3*: 40.5 (360.5)	1.47: 60 (534.0)	2.46: 100 (890.0)
Permit 126**: (1121.4)	1.64: 207 (1842.3)	2.73: 344 (3061.6)

* Modified to Wyoming load configurations.

** Single lane loading (permit truck only).

To facilitate a conventional beam load rating, wheel distribution factors where computed from the calibrated model. The distribution factors were computed for the slab by dividing the maximum computed slab moment due to multiple HS-20 loads by the moment generated by an HS-20 wheel line on a continuous beam. Table 9 contains the wheel distribution factors for the slab at the piers and at midspan along with their corresponding AASHTO factors. It should be noted that these distribution factors are expressed in terms of percent of wheel line load carried by a unit width of slab. It is apparent that the computed distribution factors are relatively close in value to the AASHTO factors, particularly at midspan of the center span. It is important to note, however, that the appropriate support conditions must also be applied for in order for conventional beam analyses to be representative of the actual structure. The conventional and conservative approach is to assume simple supports.

Table 9 Wheel load distribution factors per unit width of slab.

Location	Computed Distribution Factor ft (m)	AASHTO* Multiple lane load wheel distribution factor
Slab @ Pier	0.23 (0.75)	0.18 (0.59)
Slab @ Midspan	0.18 (0.59)	0.18 (0.59)

*AASHTO 3.24.3.2

CONCLUSIONS

Because of the short span lengths and the distribution of the load provided by the large number of axles, the permit load was less critical to the super-structure than the standard rating vehicles. It is important to note that single-lane loading was assumed for the permit vehicle, where the critical loading conditions for the rating vehicles occurred with three lane loading. It was also apparent that shear capacity of the slab is likely to be critical with the heavier permit loads.

The critical component for all the ratings was the moment capacity of the curbs at the face of the transverse floor beam. It is possible that the curb was not intended to be a structural member so that limiting the load based on the curb's capacity may be overly conservative. However, future inspections should focus on the condition of the curbs as they currently affect the bridge's response behavior and they would likely experience the first effects due to overloading.

MEASURED AND COMPUTED STRAIN COMPARISONS

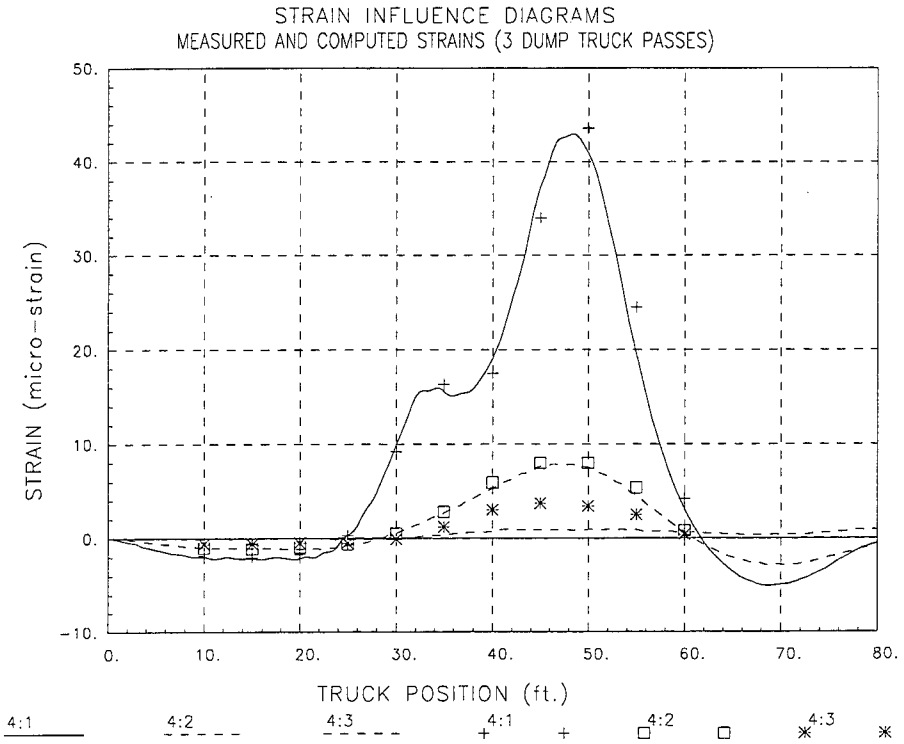

Figure 7 Strain comparison at midspan, span 2, west curb (3-axle truck).

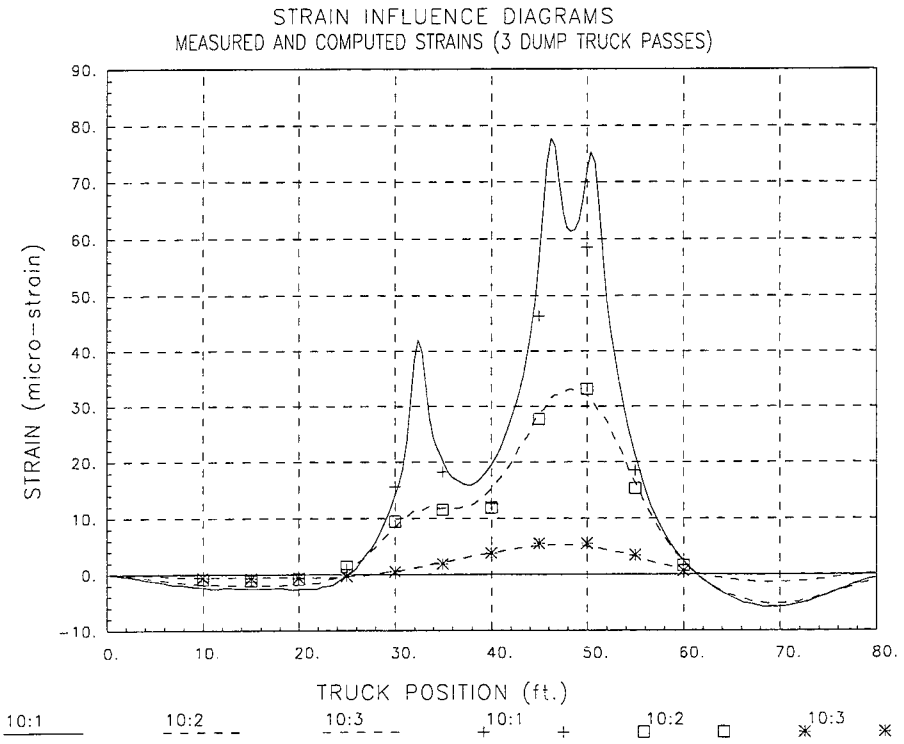

Figure 8 Strain comparison at midspan, span 2, west slab (3-axle truck).

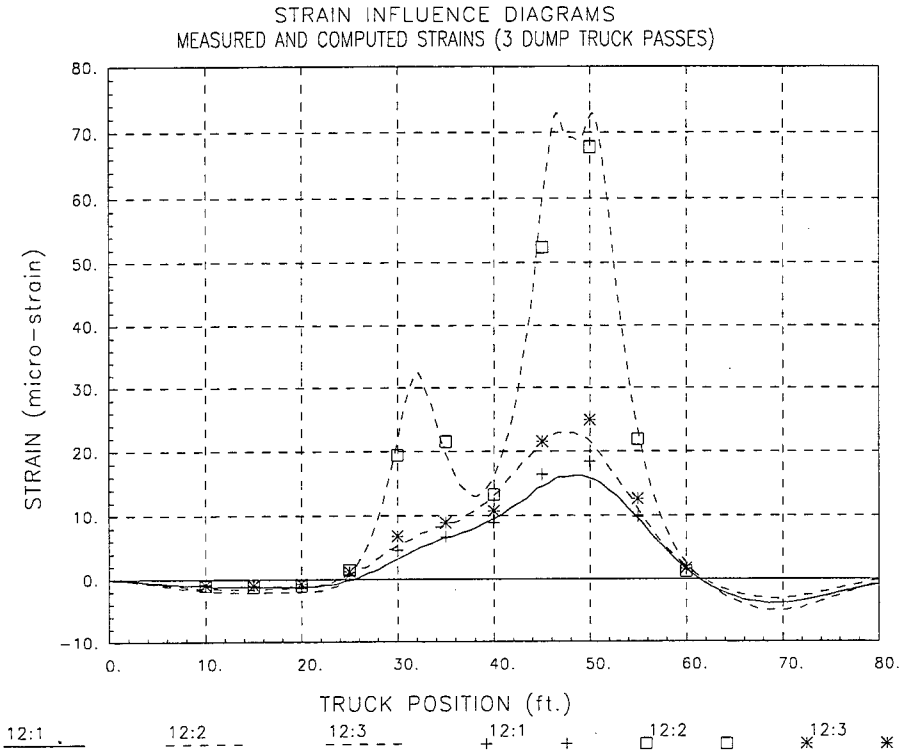

Figure 9 Strain comparison at midspan, span 2, centerline slab (3-axle truck).

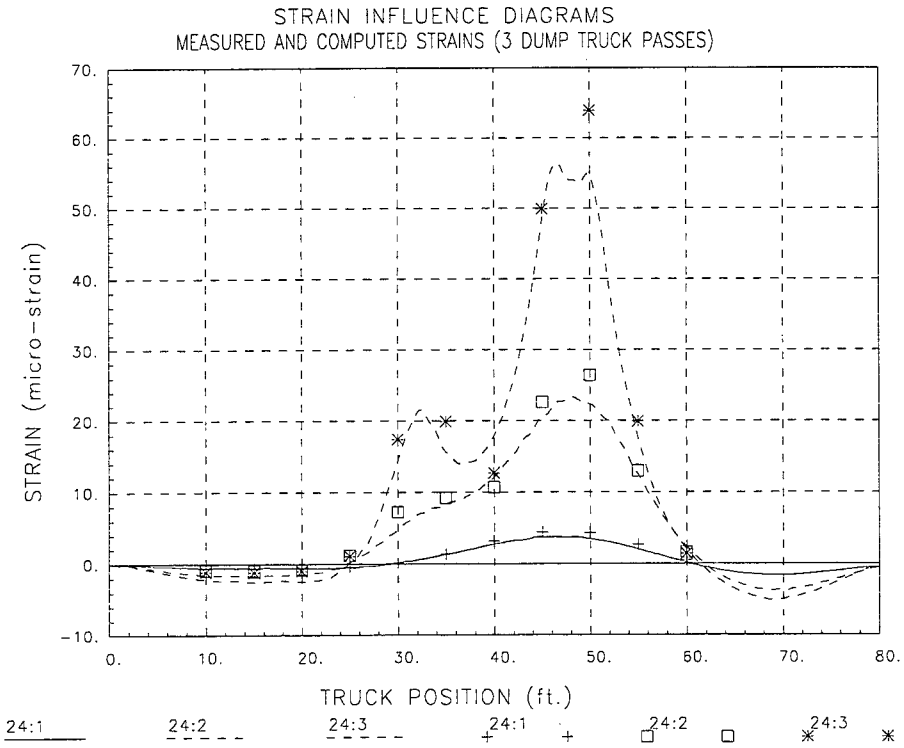

Figure 10 Strain comparison at midspan span 2, east slab (3 axle truck)

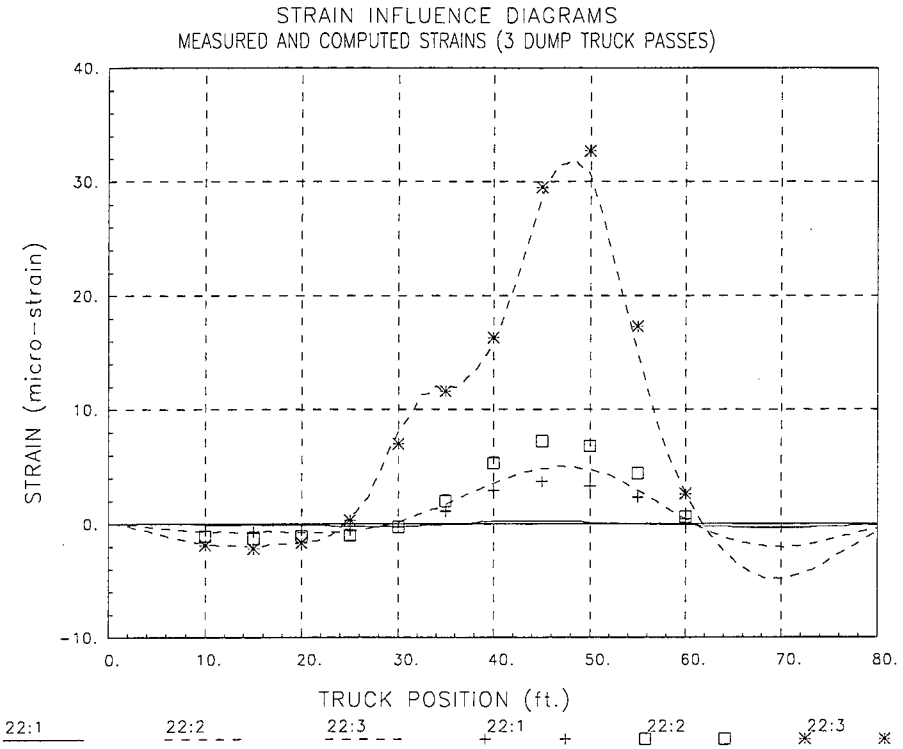

Figure 11 Strain comparison at midspan, span 2, east curb (3 axle truck).

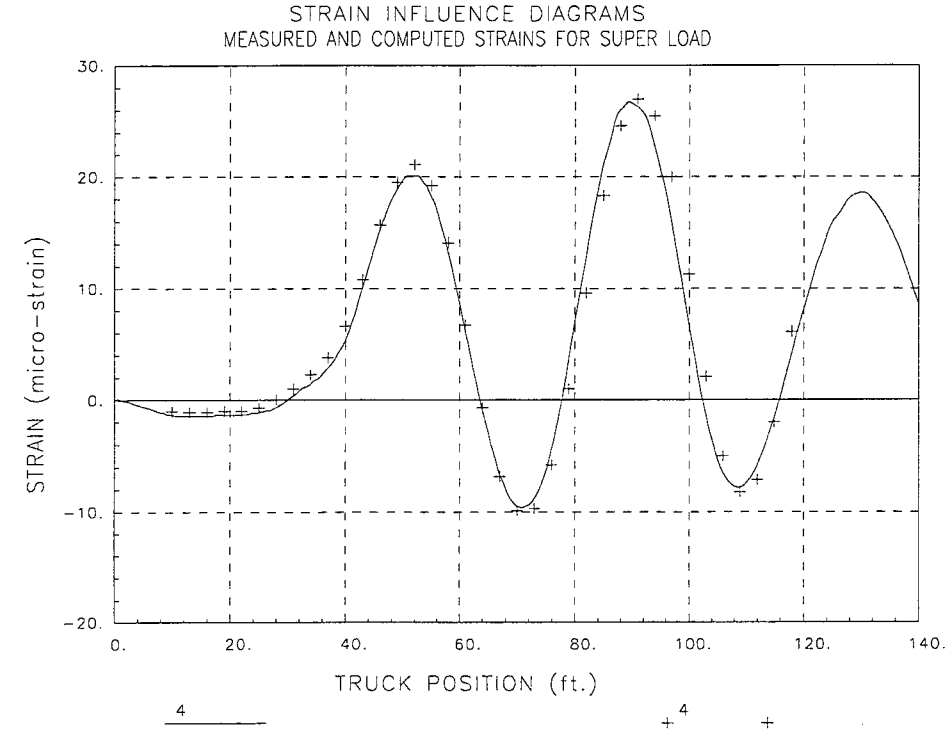

Figure 12 Strain comparison at midspan, span 2, west curb (permit truck)

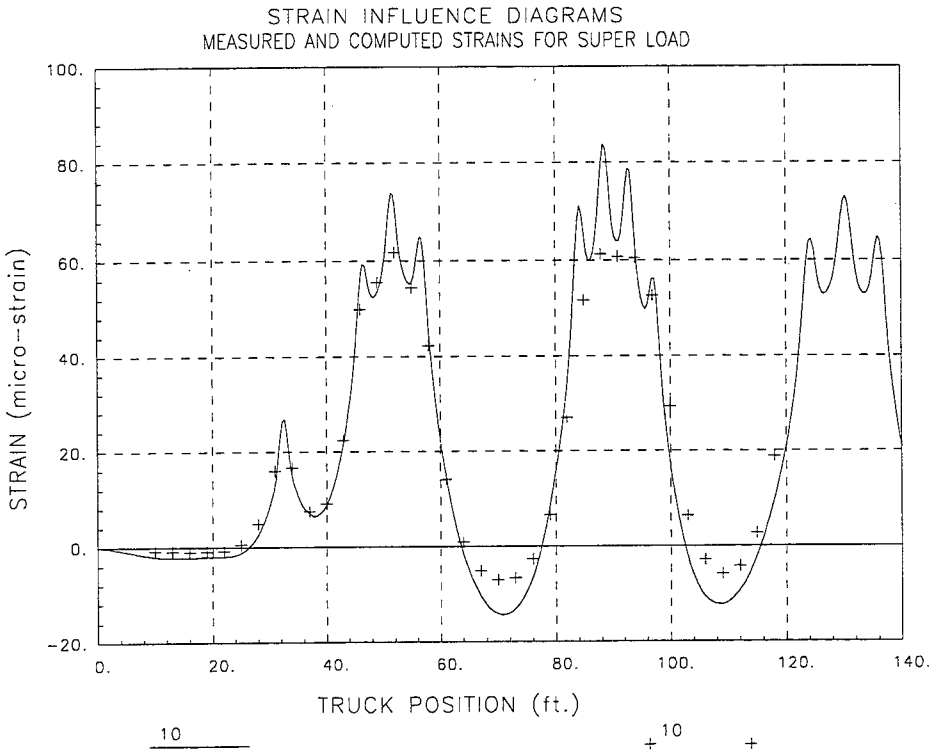

Figure 13 Strain comparison at midspan, span 2, west slab (permit truck).

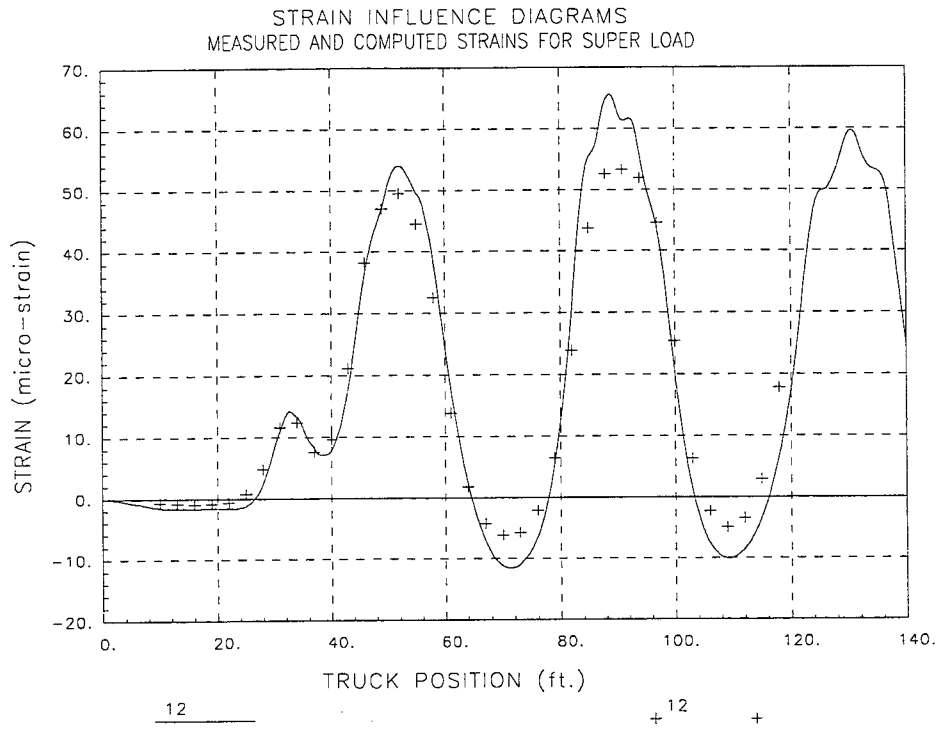

Figure 14 Strain comparison at midspan, span 2, centerline slab (permit truck).

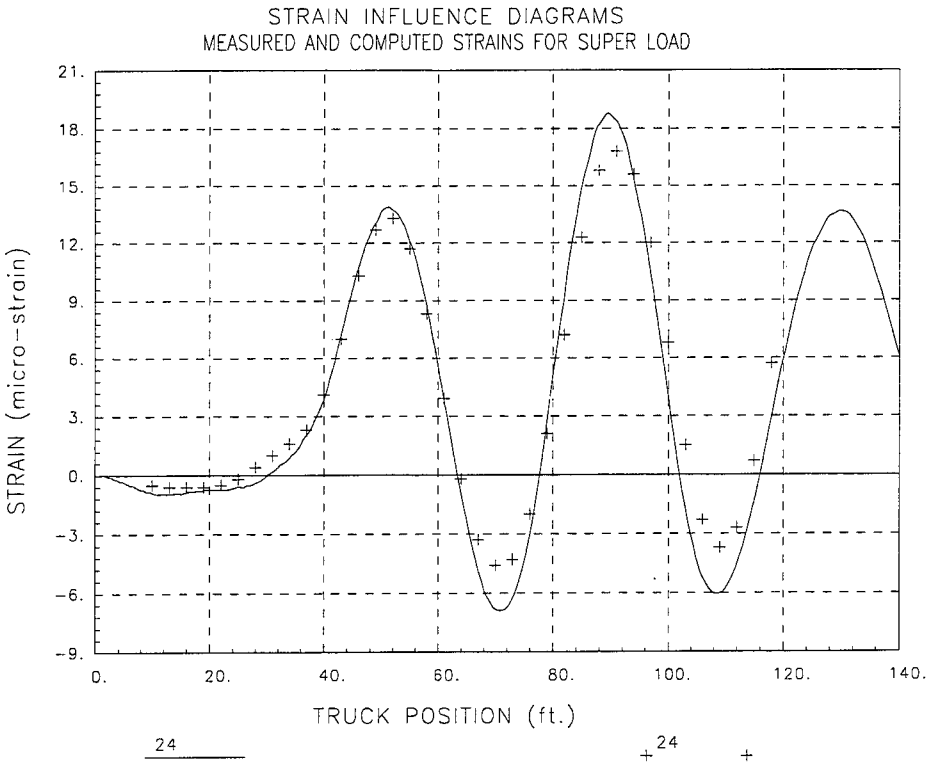

Figure 15 Strain comparison at midspan, span 2, east slab (permit truck).

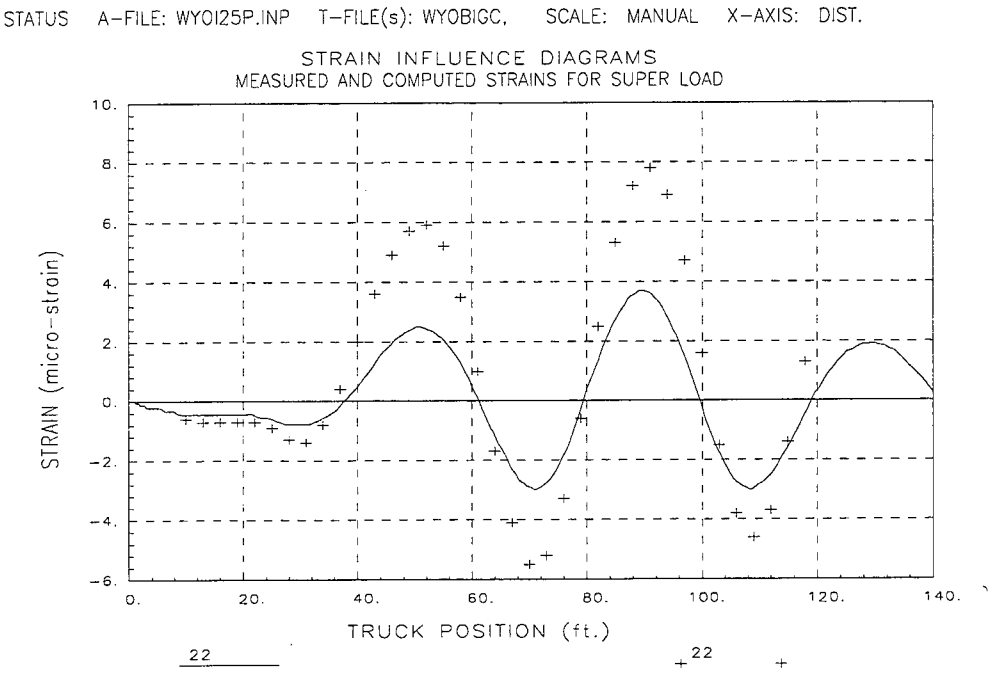

Figure 16 Strain comparison at midspan, span 2, east curb (permit truck).

APPENDIX B – R/C T-BEAM BRIDGE

DESCRIPTION OF STRUCTURE

Table 10 Structure description – R/C T-beam bridge.

Structure Identification	Project I-25-3(23)144
Location	Wyoming, Southbound I-25, milepoint 144
Structure Type	R/C T-Beam, 3-span continuous
Span Length(s)	26ft-3in-37ft-0in-26ft-3in (8.0m-11.3m-8.0m)
Roadway/Structure Widths	38ft-0in / 40ft-8in (12.0m/12.4m)
Beam Spacing	(5) T-beams @ 8ft-6in (2.6m)
Slab Depth(s)	7in (178mm)
Beams dimensions	Total depth including slab 27in (686mm) Web width 16in (406mm) Effective flange width varies
Exterior Beams	3ft-4in (1.0m) deck overhang from beam centerline with a 14inw x 6in (356mm x 153mm) concrete curb.
Abutments	R/C abutment on top of cast-in-place piles. Construction joint between superstructure and abutment
Bents	(3) 24in (610mm)Ø R/C Columns @ 11ft-0in (280mm) o.c. with 30in x 30in (762mm x 762mm) R/C floor beam.
Design Concrete Strength f'c	3,000 lbf/in^2 (20,700 kPa)
Comments	Structure appears to be in good condition. No indication of distress, minimal cracks on deck and beams. Some apparent patch work on underside of deck.

INSTRUMENTATION PROCEDURES

The superstructure of the bridge was instrumented with 32 re-usable strain transducers as shown in Figure 17. Since the bridge was symmetric about two axes and there was no apparent structural damage, the majority of instrumentation was confined to one quarter of the bridge. Transducers were located in pairs at 16 different beam cross-sections; one centered along the bottom of the web and the other on the side of the web 3in (76mm) from the bottom of the deck. All of the transducers were oriented longitudinally to measure axial strain responses. Beam flexural responses and neutral axis locations could then be measured directly since strains were obtained at two depths on each cross-section.

Instrumented beam cross-sections included midspans of all beams at the north-end and interior spans, and negative moment regions near the north abutment and north pier for beams 1, 2, & 3. The primary goal of this plan was to capture the longitudinal flexural behavior of the continuous beams and the transverse load distribution characteristics of the deck. Based on the construction details of the superstructure and experience with similar structures, it was desired to obtain the following stiffness parameters:

- Effective stiffness of the interior beams in positive and negative moment regions, including the effective flange width and thickness, effect of cracks in tension zones, and concrete stiffness.
- Effective stiffness of the exterior beams in positive and negative moment regions, including the effects of the attached curb, cracks in tension zones, and concrete stiffness.
- Effective rotational end restraints of the beams provided by the abutments.
- Rotational resistance provided by the piers.
- Effective transverse stiffness of the R/C deck, including the effective thickness with overlay, presence of cracks, and concrete stiffness.

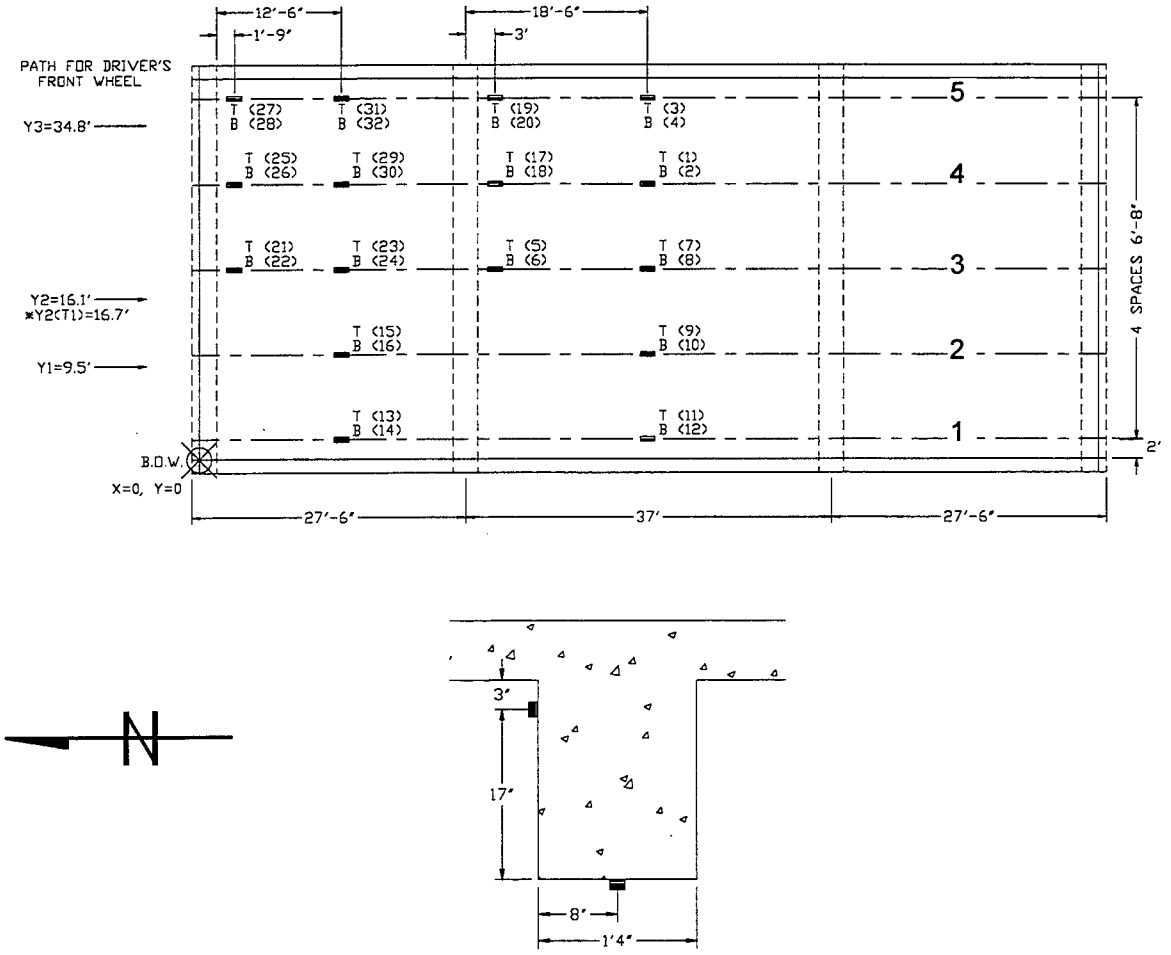

Figure 17 Instrumentation plan for R/C T-beam bridge.

All of these parameters significantly affect the structure's load distribution characteristics, therefore, evaluation of these parameters was necessary to accurately assess the effect on each component due to an applied load condition.

Gage lengths of the strain transducers were extended from the standard 3in (76mm) to 15in (381mm) and 21in (533mm) in order to reduce the effects of tension cracks associated with

reinforced concrete. The purpose of the extensions was to obtain average surface strains consistent with a homogenous material. The selection of gage length was based primarily on span lengths. It was desired to use the longest gage length possible without inducing significant error due to moment/strain gradients along the lengths of the beams. As a general rule, a maximum gage length of $1/20^{th}$ of the span length was followed.

All of the instrumentation procedures were accomplished during the afternoon of June 2^{nd}, 1997. Access to the underside of the structure was obtained by ladders and a lift truck provided by the Wyoming DOT (WYDOT).

LOAD TEST PROCEDURES

A loaded three-axle tandem dump truck was provided by WYDOT for the purpose of controlled loading. The test truck had a gross weight of 48.6 kips (216.3 kN) with wheel weights and axle configurations as shown in Figure 18. Three transverse truck paths (west shoulder, west lane, and east lane) were defined so that the bridge's lateral load transfer characteristics could be established. The load tests were performed by driving the truck across the bridge at crawl speed along the prescribed paths. Data was recorded continuously at 32 Hz during each pass and the truck position was monitored in order to record strain as a function of vehicle position. Truck crossings from each path were performed twice to ensure data reproducibility. A total of six slow-speed truck crossings were performed along with two high-speed passes along paths 2 and 3. Traffic control was provided by WYDOT which consisted of a single lane closure and approximately one-minute road blocks as the test truck crossed the bridge. The entire testing process with the dump truck was completed in approximately one hour.

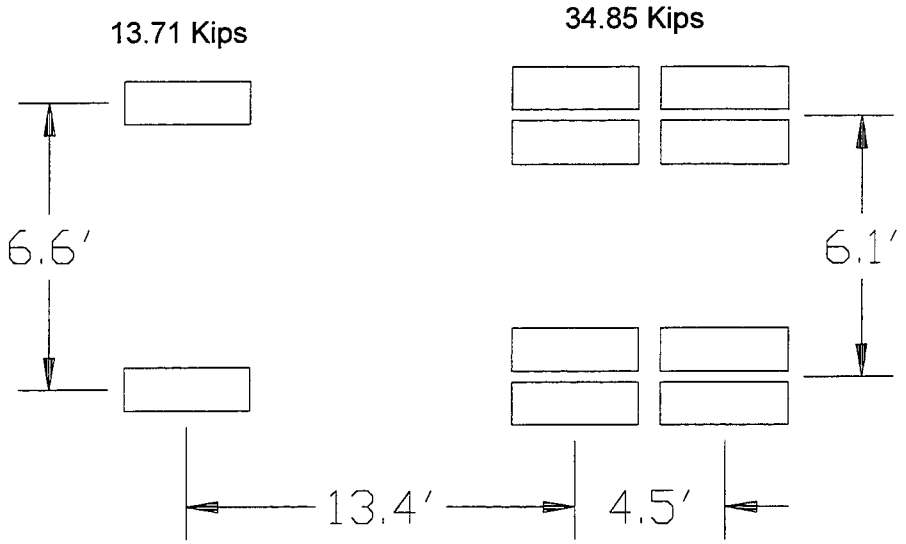

Figure 18 Initial test truck for R/C slab bridge.

After the load testing procedures with the 3-axle test truck were completed, strains were measured during single crossings of two overload permit vehicles. The first vehicle had a gross weight of 252.4 kips (1,123.2 kN) carried by nine axles as shown in Figure 19. The gross weight

of the second vehicle was 158.2 kips (704 kN) carried by ten axles, whose axle spacing and load magnitudes are shown in Figure 20. As with the initial test, the longitudinal position of the truck was monitored as the permit load followed a pre-defined path at crawl speed. The path for both overload vehicles was the same as path 2 of the test truck (passenger side steering wheel over the right lane line). Data from these crossings were used to observe the response behavior induced by the extremely large loads. It was also used to verify the ability of the calibrated analysis model to predict load responses due to loads significantly different in both magnitude and configuration than the original test truck.

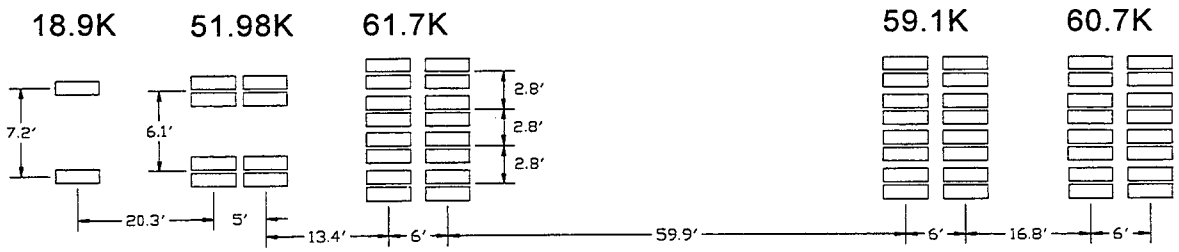

Figure 19 Load definition of permit vehicle 1 – R/C T-beam bridge.

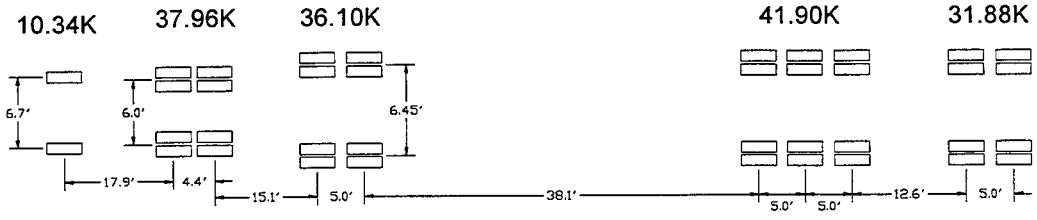

Figure 20 Load definition of permit vehicle 2 – R/C T-beam bridge.

PRELIMINARY INVESTIGATION OF TEST RESULTS

A visual examination of the field data was fist performed to assess the quality of the data and to make a qualitative assessment of the bridge's live-load response. It was determined that the structural responses were linear and elastic since there were no discontinuities in the strain histories and all of the strains returned to zero after each truck crossing. This was true for all of the dump truck crossings as well as the permit load crossings. Reproducibility of the data was verified by comparing strain histories from duplicate truck crossings. In every case, the correlation was excellent as shown in Figure 4. This is an additional indication of a linear stress/strain relationship throughout the load cycle and a quality check for the entire testing process.

Another observation made directly from the measurements was that the rotational restraints at the abutments were inducing negative moment in the beams while the first span was loaded. Based on this observation, the rotational stiffness of the abutment would need to be

included in the model calibration procedure since it had a significant effect on the other measured strains.

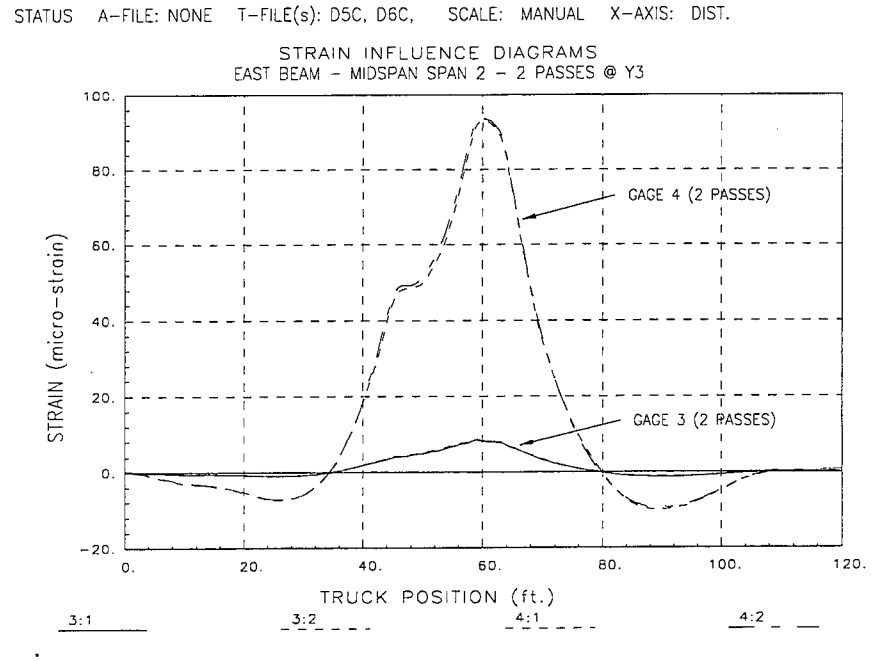

Figure 21 Reproducibility of test results – R/C T-beam bridge.

It was also observed that two gages (2 & 16) produced unreasonably low strain values. This conclusion was based on comparisons with similar gage locations under similar loading (symmetry). It was assumed that these gages were not attached properly, or broke loose during the night between the instrumentation and the load test procedures. Results from these gages were then assumed to be invalid and eliminated from further data evaluations.

A very unusual response was observed from beam 3 near the pier (Gage 5). There was no indication that the gage malfunctioned or that it was attached poorly because the strains magnitudes were relatively high and returned to zero after the load cycle. Calculation of the neutral axis location obtained from gages 5 and 6 showed large variations with each truck pass. Causes for this response could not be identified, however, it appeared to be a localized effect likely due to a crack or void in the deck. Investigation of photographs taken at the time of the test indicated that patch work had been done to the underside of the deck directly above the gage location. Because the observed behavior was very localized and too complex to be represented by the analysis, responses from gage 5 were not used in the subsequent model calibration process.

Overall, the measured strains were considered normal to high for the span length and truck weight. The largest measured strain magnitude was +122 in^{-6}/in which corresponds to approximately 0.4 ksi (2.76 MPa) in concrete (assuming E=3,200 ksi (22,080 MPa)) or 3.5 ksi

(24.2 MPa) in steel. It is important to note that the measured strains were averaged over a 15in (381mm) or 21in (533mm) gage length. Because of the presence of cracks, these strains are **not** to be confused with **maximum** steel stress. Table 11 contains the maximum measured strains at various locations on the structure for each truck path and for the permit loads. A reasonably direct comparison could be made for the test truck (path 2) and permit load responses because the truck paths were very similar. Some difference in lateral load distribution was expected due to the relative differences in axle widths. Comparison of the maximum measured strains between the test truck path 2 and the permit truck 1 indicated that the permit load generated responses approximately 47 percent higher in positive moment and 180 percent higher in negative. Also, the second permit truck generated approximately the same positive moment strains and higher negative moment strains by about 73 percent compared to those produced by the initial test truck.

Table 11 Maximum strain magnitudes (in^{-6}/in) – R/C T-beam bridge.

Gage ID	Location	3 Axle Path 1	3 axle Path 2	3 Axle Path 3	Permit 1 Path 2	Permit 2 Path 2
14	Bm 1 midspan 1	85	22	1	39	28
24	Bm 3 midspan 1	7	41	8	67	43
30	Bm 4 midspan 1	4	10	111	15	7
32	Bm 5 midspan 1	1	3	74	6	3
12	Bm 1 midspan 2	122	40	1	68	50
10	Bm 2 midspan 2	114	117	31	173	116
8	Bm 3 midspan 2	24	94	28	147	96
4	Bm 5 midspan 2	1	2	93	6	4
6	Bm 3 pier 1	-6	-40	-16	-111	-69
18	Bm 4 pier 1	-2	-5	-82	-14	-6
20	Bm 5 pier 1	-1	-2	-53	-3	-1

As a means of determining relative stiffnesses of the interior and exterior beams, neutral axis measurements were determined from the strain histories. This was done by using strain measurements at the different depths of the beam cross-sections and assuming linear strain distributions throughout the beam depth. Table 12 contains the measured neutral axis values for the various beam cross-sections and provides averaged values for the interior and exterior beams in the positive moment regions. From these results it is apparent that the curbs significantly influence the effective cross-section properties of the exterior beams. On average, the exterior beam neutral axis values were 1.0 in (25.4mm) higher than those calculated for the interior beams. Since the web dimensions and steel ratios were typical for all of the beams, this was a direct indication that the exterior beams had a thicker effective flange and were therefore stiffer than the interior beams.

Strains were recorded from high-speed crossings of the test truck along paths 2 and 3 to assess any impact or dynamic effects on the structure. Figure 5 contains strain histories from an end span gage and an interior span gage for both the slow speed and high speed crossings along path 2 (right lane). These strain histories show that there was only a minimal dynamic component (vibration) from this high-speed crossing. Although the end-span responses were

nearly identical, the-interior span responses were amplified by as much as 15 percent. Static and dynamic responses obtained from path 3 (left lane) generated a much different picture as shown in Figure 23. Both the end-span and interior-span beams experienced significantly higher strain amplifications during this high-speed truck pass. The maximum dynamic amplification appeared to be approximately 40 percent, which was obtained from gage 30. This result is an overestimate because it was apparent that the actual truck paths varied slightly causing beam 4 to receive a higher percentage of load during the 60 mi/h pass. An average of the dynamic amplification factors from the most heavily loaded beams was approximately 25 percent. Based on these calculations, the AASHTO impact factor of 30 percent appeared to be reasonable and was used in the subsequent rating calculations.

Table 12 Measured neutral axis locations – R/C T-beam bridge.

Cross-section location	Gage #s	Neutral axis location from bottom of beam – in. (mm)
Beam 1 span 1	13, 14	20.7 (525.8)
Beam 3 span 1	23, 24	19.2 (487.7)
Beam 4 span 1	29, 30	19.0 (482.6)
Beam 5 span 1	31, 32	20.2 (513.1)
Beam 1 span 2	11, 12	21.4 (543.6)
Beam 2 span 2	9, 10	19.9 (505.5)
Beam 3 span 2	7, 8	19.0 (482.6)
Beam 5 span 2	3, 4	19.0 (482.6)
Beam 4 @ pier	17, 18	19.2 (487.7)
Beam 5 @ pier	19, 20	24.4 (619.8)
Average Interior Beam (+Moment)		20.3 (515.6)
Average Exterior Beam (+Moment)		19.3 (490.2)

It should be noted that all of the above information was extracted directly from the field data only. The following section illustrates how the field data was used to generate and "calibrate" an analytical model of the structure.

Modeling, Analysis, and Data Correlation

A simple, grid-type finite element model (FEM) of the structure was defined and the entire field testing operation was reproduced in the modeling and analysis procedures. Two-dimensional frame elements were used to represent the beams, and quadrilateral plate elements simulated the load transfer characteristics of the deck. Nodal points were defined longitudinally at the abutment and pier centerlines, edge of the transverse floor beams, and at the 1/12 span locations. Transverse node placement was based on the overall width of the bridge and at the beam centerline locations. To maintain a desirable aspect ratio of the plate elements, intermediate node lines were located half way between the beam lines. Based on the observed bending responses, rotational spring elements were placed at the abutment nodes and at all pier locations. To facilitate comparison of the

computed and measured responses, gage locations were defined on the beams corresponding to the same locations defined in the field.

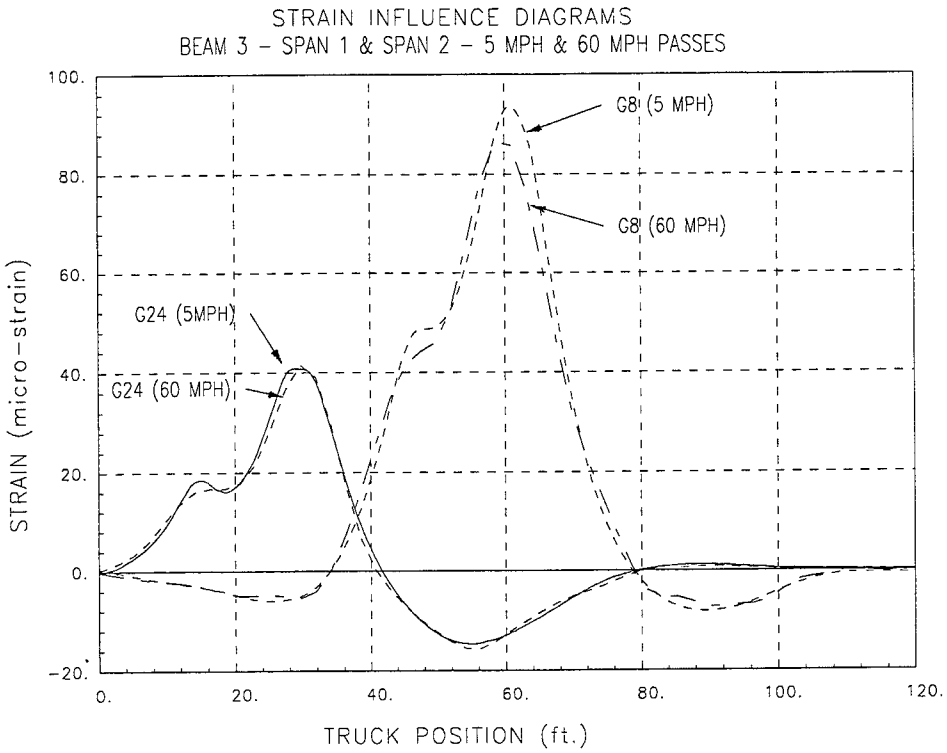

Figure 22 Static and dynamic strains - truck path 2 (right lane) – R/C T-beam.

The entire model, including geometry, boundary conditions, member cross-sections, and gage locations, was generated graphically. A computer-generated display of the model is shown in Figure 24. Even though the geometry of the structure was well defined, there were various structural parameters that were not well known. These parameters included the effective stiffness (EI) of the interior and exterior beams in both the positive and negative moment regions, the effective stiffness of the deck (Et^3), and the moment resistance of the support conditions at the abutments (K_a) and at the piers (K_p). For the initial model, concrete properties were based on 3.0 ksi (20.7MPa) concrete and the beam cross-sectional properties were based on the gross concrete sections. Also, the effects of cracks, reinforcement steel, and overlay were ignored and the initial stiffness constants of the support springs were assumed to be zero. These properties were later modified based on the comparison of the computed and measured response behavior.

Loading of the model was accomplished by defining a two-dimensional model (foot print) of the test vehicle consisting of a group of point loads and then placing the truck model on the structure model. Truck crossings were simulated by moving the truck model at discrete positions along the same paths used during the field test. During the comparison process, 14 longitudinal truck positions were defined for each test path. Therefore, strains were computed during each analysis run at 29 gage locations for 14 truck positions moving along three truck paths. The

accuracy of the analysis was then determined by comparing the 1218 (29x14x3) computed strain values with their corresponding measured strains.

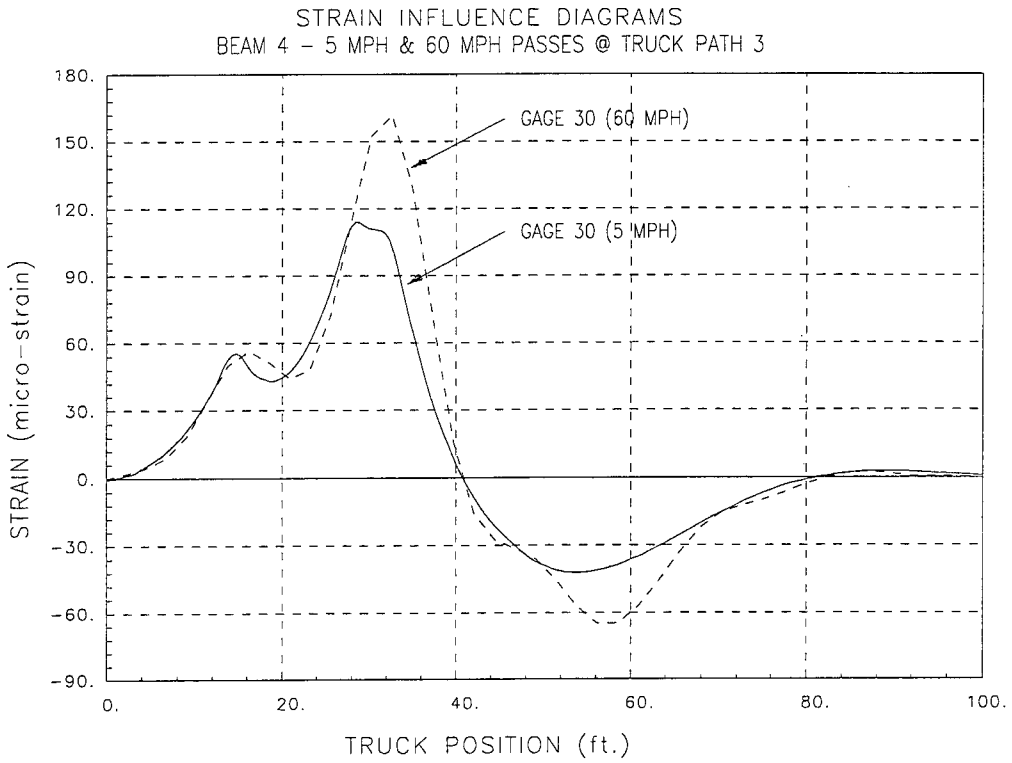

Figure 23 Static and dynamic strains - truck path 3 (left lane) – R/C T-beam.

Initial comparisons between the computed and measured strains indicated that the model was reasonably accurate, but that significant differences existed between the model and the actual structure. In general, the magnitudes of the computed strains were within 20 percent of the measured strains. Relatively good agreement was observed at gage locations near the pier while the abutment gages had a negative correlation, meaning the flexure near the supports was in the opposite direction. Since simple supports were used in the initial model, the computed moments near the abutments were very small in magnitude and had a positive value (tension on bottom surface). But as previously mentioned in the discussion of preliminary observations, negative moments were measured near the abutment. It was also apparent that the lateral distribution was in error by observing the relative errors at the midspan gages for the various truck passes.

To improve the model's accuracy, the above-mentioned stiffness terms were modified through a parameter identification process until a best-fit correlation between the measured and computed strain was obtained. Reasonable upper and lower limits were defined for each parameter and the parameters were evaluated within those constraints. For instance, the upper- and lower-bound moment-of-inertia values for the beam members were defined by the gross and the elastic cracked sections, respectively. An additional allowance of 30 percent on upper and lower limits was provided to account for likely differences between the assumed and actual concrete modulus (Ec).

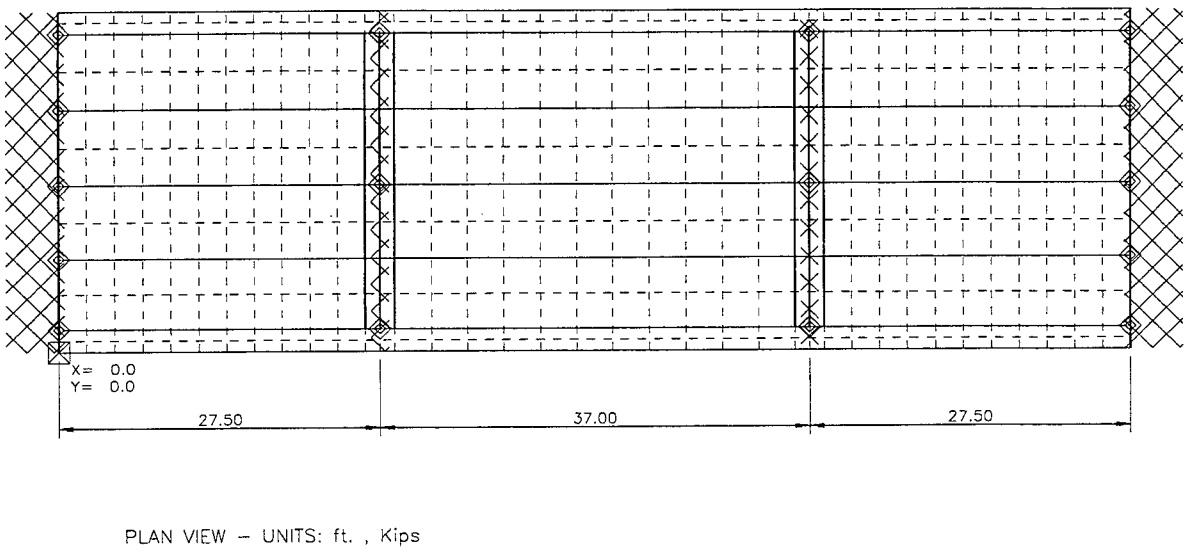

Figure 24 Computer model of R/C T-beam bridge.

The effective slab thickness was given a range of plus and minus 50 percent to account for the stiffening effect of the reinforcement, the presence of cracks, and any error in the estimated concrete modulus. Lower and upper bounds for the abutment spring stiffnesses were defined by the ratio of EI/KL, where E, I and L refer to the beam properties and span lengths, and K is the rotational spring stiffness in terms of moment-per-unit measure of rotation. Reasonable ranges for this ratio are between 0.1 and 4.0, which correspond to nearly fixed and nearly simple supports. Common end restraints for typical beam supports have a stiffness ratio (EI/KL) of around 1.0.

Even though the structural plans indicated that a hinged construction joint was furnished between the bent and the superstructure, it was assumed that the piers might provide some rotational restraint. While this occurrence typically has minimal effect on the superstructure's load rating, it can significantly affect the measured responses and therefore had to be evaluated in order to accurately assess the other stiffness parameters. An upper limit of 4EI/L was assigned to the pier springs, where E, I, and L refer to the properties and length of the pier. It was assumed that the stiffnesses of the interior and exterior beams were different due the different measured neutral axis values. It was also assumed that the positive moment regions might have different stiffness than the negative moment regions. Therefore, beam stiffness parameters were calibrated at four different regions.

A total of seven different stiffness parameters were calibrated through an iterative process of analysis, data comparison, and structural identification. At the end of this cycle, an excellent correlation was obtained. Table 13 contains the initial and final values for each of the variable properties. To illustrate how the parameter modification improved the accuracy of the model, the initial and final error values are shown in Table 14.

Table 13 Initial and final modeling parameter values – R/C T-beam bridge.

Member Property	Units	Initial Value	Identified Value
Int. Beams Pos. Moment - I	in^4 (cm^4)	60,071 (2,500,155)	41,570 (1,730,143)
Int. Beams Neg. Moment - I	in^4 (cm^4)	40,428 (1,682,613)	37,700 (1,569,074)
Ext. Beams Pos. Moment - I	in^4 (cm^4)	43,733 (1,820,168)	48,420 (2,015,240)
Ext. Beams Neg. Moment - I	in^4 (cm^4)	40,428 (1,682,613)	53,100 (2,210,022)
Abutment Restraint - Ka	k-in/rad (N-m/rad)	0 (0)	$2.19x10^6$ (2.44×10^8)
Pier Rotational Restraint - Kp	k-in/rad (N-m/rad)	0 (0)	$9.53X10^5$ (1.08×10^8)
Deck Thickness	In (mm)	8.0 (203)	6.1 (155)

Table 14 Accuracy of initial and refined models – R/C T-beam bridge.

Error Value	Initial Model	Refined Model
Absolute Error	3634.5	2359.3
Percent Error	13.2	4.3
Scale Error	4.4	3.1
Correlation Coefficient	0.94	0.98

Following the parameter identification procedure, 2-D models of the permit loads were generated and applied to the calibrated model. The purpose of this exercise was to verify that the model could reasonably predict the responses from the much heavier loads with completely different geometries. The analysis was run for the single pass of each permit load with the truck positions incremented at 3.0ft (0.92m) intervals. A total of 46 truck positions were defined and strains were computed at each gage location. As shown in Table 15, the same level of accuracy was obtained from the permit load crossings as for the dump truck that was used to calibrate the model. The absolute and scale error values are larger, but this was expected since there was a much larger volume of strain due to a much longer load cycle. Measured and computed strain comparisons are provided for the test truck and the two permit vehicles in Figure 7 through Figure 39.

Table 15 Accuracies for overload prediction – R/C T-beam bridge.

Error Value	Permit Truck 1	Permit Truck 2
Absolute Error	3380.7	1990.0
Percent Error	4.8	4.0
Scale Error	14.5	14.1
Correlation Coefficient	0.98	0.98

At this point, the model has been "calibrated" to the field measurements and it has been verified that the model will provide the same degree of accuracy regardless of the load configuration. Since the load responses of the model are very similar to those of the actual structure, it can be assumed that the stiffness and load transfer characteristics are correct.

DISCUSSION OF RESULTS

The accuracy obtained by this evaluation process was typical of continuous R/C bridge structures. Most of the strain comparisons were within the tolerance obtainable by the load test. The main observations made from the load test data evaluation and during the parameter identification process are as follows:

- The exterior beams were approximately 28 percent stiffer than the interior beams. This was primarily due to the increased flange thickness provided by the curbs. An additional factor may have been that the exterior beams had a lower density of tension cracks because they typically experienced less loading than the interior beams.
- Rotational restraints of the piers and abutment had a significant effect on the structural response. The abutments provided approximately 50 percent of completely fixed-end conditions for the beams. The piers also had noticeable rotational restraints which had the effect of reducing midspan moments but slightly increasing the maximum negative moments at the piers.
- The measured dynamic or impact effects obtained during the high-speed truck crossings were in the range of 0 to 40 percent. Average values obtained from the most heavily-loaded beams were approximately 25 percent, indicating that the AASHTO impact factor of 30 percent is reasonable. Based on test results from numerous bridges with similar span lengths, measured impact factors of more than 15 percent are relatively unusual.
- With the exception of the exterior beams, the resulting stiffness parameters were reduced significantly from the original values based on the gross member cross-section. This result is an indication that the actual concrete modulus may be lower than expected (3,200 ksi (22,080 MPa)) or that the density of flexural cracks in the concrete is high enough to affect the member stiffness.
- Measurements taken from the center beam near the pier indicated unusual behavior (Gages 5 & 6). Strain magnitudes from the upper gage and fluctuating neutral axis location were evidence that the primary response was not pure flexure, but appeared to be localized as it did not appear to affect load transfer elsewhere in the structure. The most likely cause for this response was a void or large crack in the deck near the instrumented cross-section. Visible patch work indicated that the deck had been previously repaired at that location. While the observed

behavior did not alter the subsequent rating values, special attention should be placed at this location during future visual inspections (formation of potholes, cracks in web or deck).

- Strain comparisons from the permit load had the same degree of accuracy as the test vehicle used to calibrate the model. This verified that all measured responses were linear with respect to load magnitude and that the model's accuracy was not dependent on the applied load.

LOAD RATING PROCEDURES AND RESULTS

Inventory and operating rating factors were computed using Allowable Stress Design (ASD) and Load Factor Design (LFD) methods. Member capacities were computed for the interior and exterior beams based on positive moment, negative moment, and shear. All capacities were computed using AASHTO design specifications for reinforced concrete. Allowable stress flexural capacities of the beams were based on steel stresses of 24 ksi (165.6 MPa) for inventory ratings and 36 ksi (248.4 MPa) for operating limits. Load factor capacities were based on standard nominal strength calculations using an F_y of 60 ksi (414 MPa)for the main reinforcement, 40 ksi (276 MPa) for the shear stirrups, and a concrete strength of 3.0 ksi ((20.7 MPa). The shear capacities were computed according to AASHTO specifications as the sum of the steel and concrete shear capacities ($V_n = V_s + V_c$) since there was not any significant cracking. The moment and shear capacities that were used to compute ratings for the slab and curb are listed in Table 16.

The effective flange widths of the T-beams in positive moment were computed according to AASHTO 8.10.1. While computing the negative moment capacity of the T-beams over the piers, the longitudinal steel in the deck was included in the area of steel (A_s). The amount of deck steel contributing to the beam's capacity was limited by the maximum steel ratio of 0.75 $_{bal.}$

The rating equation specified by the AASHTO *Manual for Condition Evaluation of Bridges* as given in appendix f was used to generate inventory and operating load limits. The appropriate load factors were applied to the dead- and live-load effects based on the level of rating ($A_1 = A_2 =$ 1.0 for ASD ratings, A_1=1.3, A_2=2.17 for LFD Inventory ratings, and A_1=1.3, A_2=1.3 for LFD Operating ratings). An impact factor of 30.0 percent, specified by AASHTO, was applied to the live load effects.

It is important to note that the primary benefit of the integrated approach is that the load effects are more realistically determined. With the exception of estimating a conservative concrete strength, the approach has little impact on component capacity calculations. In the rating equation, dead- and live-load effects were computed from the calibrated model. The dead-load was computed from the structure's self weight plus an extra 30 lb/ft^2 (1,437 N/m^2) on the deck to account for the railings and roadway wearing surface. Critical live-load effects were determined by computing shear and moment envelopes for several different truck paths. Multiple lane load situations (two and three lanes) were obtained by superimposing envelopes for truck paths separated by 12ft (3.7m) or more. Effects of three-lane loading were reduced by 10 percent as specified by AASHTO 3.12.1. Rating values for various components are listed in Table 17 for the HS-20 loading.

Table 16 Component capacities – R/C T-beam bridge.

Member	Moment Capacity k-in (kN-m)			Shear Capacity k (kN)		
	Inv.	Oper.	L. F.	Inv.	Oper.	L. F.
Int. Beams Spans 1&3	4,511.6 (509.8)	6,767.5 (764.7)	10,443.9 (1,180.2)	50.4 (224)	99.3 (441.9)	87.5 (389.4)
Ext. Beams Spans 1&3	4,343.4 (490.8)	6,515.2 (736.2)	9,581.3 (1,082.7)	50.4 (224.3)	99.3 (441.9)	87.5 (389.4)
Int. Beams @ Pier	2,675.3 (302.3)	-4,013.0 (453.5)	-5,426.4 (613.2)	68.8 (306.2)	126.3 (562.0)	118.8 (528.7)
Ext. Beams @ Pier	-2,675.3 (302.3)	-4,013.0 (453.5)	-5,426.4 (613.2)	68.8 (306.2)	126.3 (562.0)	118.8 (528.7)
Int. Beams Span 2	4,819.2 (544.6)	7,228.7 (816.8)	11,151.4 (1,260.1)	---	---	---
Ext. Beams Span 2	4,589.7 (518.6)	6,884.5 (777.9)	10,151.3 (1,147.1)	---	---	---

Table 17 HS-20 rating factors – R/C T-beam bridge.

Member	Allowable Stress R.F.		Load Factor R.F.	
	Inventory	Operating	Inventory	Operating
Int. beam spans 1&3	3.12	4.83	3.47	5.79
Ext. beam spans 1&3	3.52	5.45	3.72	6.20
Int. beam @ Pier	0.79	1.55	0.98	1.64
Ext. beam @ Pier	0.88	1.69	1.07	1.79
Int. beam span 2	2.15	3.45	2.51	4.18
Ext. beam span 2	2.21	3.58	2.47	4.13

Vehicle load limits are controlled by the lowest member rating factor resulting from the specific load configuration. The maximum vehicle load for a particular rating method was then computed by multiplying the gross vehicle weight by the rating factor. This rating process was performed for five standard Wyoming truck configurations including the HS-20 and H-20 and also for the two permit vehicles used during the test. The critical rating factors are shown in Table 18. In all cases, the lowest rating factors were obtained from the interior beams at the face of the bents (negative moment). The next most critical location was the negative moment regions of the exterior beams.

To facilitate a conventional beam load rating, wheel line distribution factors where computed from the calibrated model. The distribution factors were computed for each beam by dividing the maximum computed beam moment by the sum of the entire bridge cross-section moment. This was done for several single-lane loading scenarios and the worst case two- and three-lane loading conditions. Table 19 contains the experimentally-derived wheel distribution factors for the interior and exterior beams at midspan and pier locations. It is apparent that the computed distribution factor is relatively close in value to the AASHTO distribution factors. In

fact, experimental factors were greater than the AASHTO factors for all of the multiple lane load conditions. This is an unusual result because the standard distribution factors are generally assumed to be conservative. The relatively poor distribution behavior of this bridge was primarily due to the high flexibility of the deck.

Table 18 Vehicle rating factors – R/C T-beam bridge.

Load Type: tons (kN)	Allowable Stress R.F.		Load Factor R.F.	
	Inventory	Operating	Inventory	Operating
H-20: 20 (178)	1.08	2.09	1.33	2.21
HS-20: 36 (320)	0.79	1.55	0.98	1.64
Type 3*: 22 (196)	1.03	2.00	1.27	2.11
Type 3S2*: 40 (356)	0.95	1.85	1.17	1.95
Type 3-3*: 40.5 (361)	0.93	1.81	1.15	1.92
Permit 1: 126** (1,121)	0.59	1.16	0.74	1.23
Permit 2: 79** (703)	0.97	1.90	1.21	2.02

* Modified to Wyoming load configurations.
** Single lane loading (permit truck only).

Table 19 Wheel line load distribution factors – R/C T-beam bridge.

Beam	Single Lane Loaded	2 Lanes Loaded	3 Lanes Loaded
Int. Beam midspan	0.98	1.29	1.36
Ext. Beam midspan	1.01	1.14	1.17
Int. Beam @ pier	1.10	1.32	1.41
Ext. Beam @ pier	0.72	1.16	1.20

When applying these factors to the results of a conventional beam analysis, it is important to note that the longitudinal stiffness characteristics of the beams must also be realistically represented if the ratings are to be accurate. This means that the appropriate boundary conditions (beam supports) must be applied as well as the appropriate dimensional properties such as pier and abutment widths.

CONCLUSIONS

Based on the model calibration results it was noted that this structure was more flexible than the majority of R/C bridges. Generally, gross concrete sections provided relatively accurate moment-of-inertia estimate for R/C beams. The fact that the resulting beam stiffnesses were less than those obtained for gross concrete sections suggests that the crack density in the concrete has become significant. The lower-than-predicted stiffness parameters were obtained for the interior T-beams and the concrete deck. The apparent flexibility of the structure had two notable effects. One was the relatively large dynamic (impact) responses observed from the high-speed load tests. The other was the relatively poor lateral distribution of loads that yielded wheel distribution factors equal to and greater than the AASHTO S/6.5 formula. This does not imply

that the bridge is deficient, but it does indicate that there is relatively little reserve "stiffness", commonly associated with beam/slab structures.

The unusual measurements obtained from the center beam near the pier are an indication that some type of deterioration has occurred or that some defect is present. The effects appeared to very localized and were not factored into the final model calibration or rating results. It is recommended, however, that this location be examined closely on future inspections.

There was a considerable difference between the critical rating values obtained by the ASD and LFD rating methods. This is typical of continuous structures because there is a relatively high ratio of dead-load to live-load at the pier locations. Since the inherent factor-of-safety applied to the dead-load effects is greater for ASD ratings, the available live-load capacity is smaller compared to LFD ratings. Due to the redundant nature of this structure and the probable redistribution of dead load over time, the LFD ratings are probably more representative of the structure's actual condition.

MEASURED AND COMPUTED STRAIN COMPARISONS

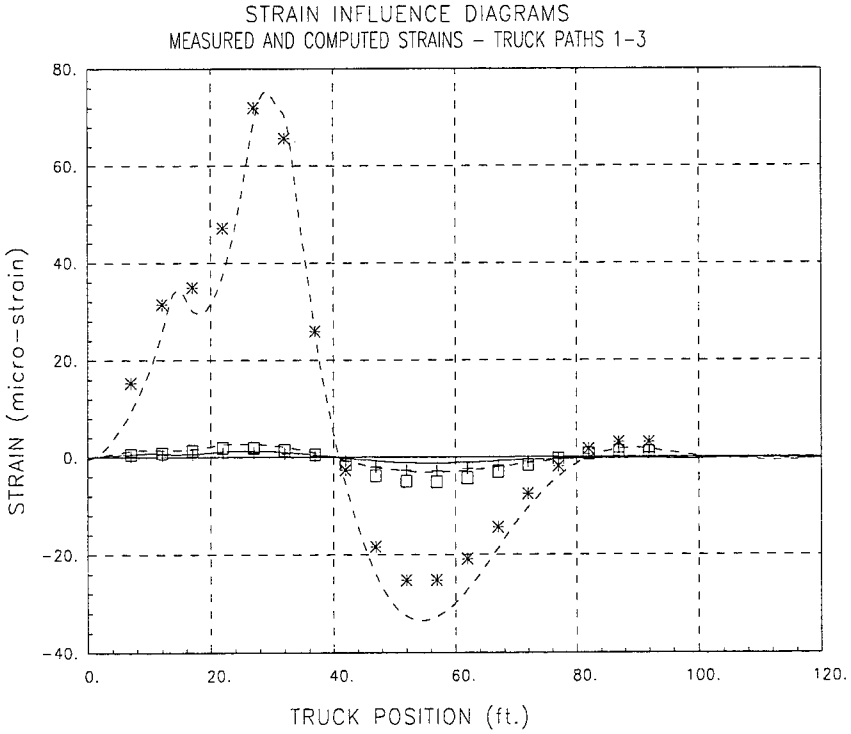

Figure 25 Strain comparison at midspan beam 5 - span 1 (3 axle truck).

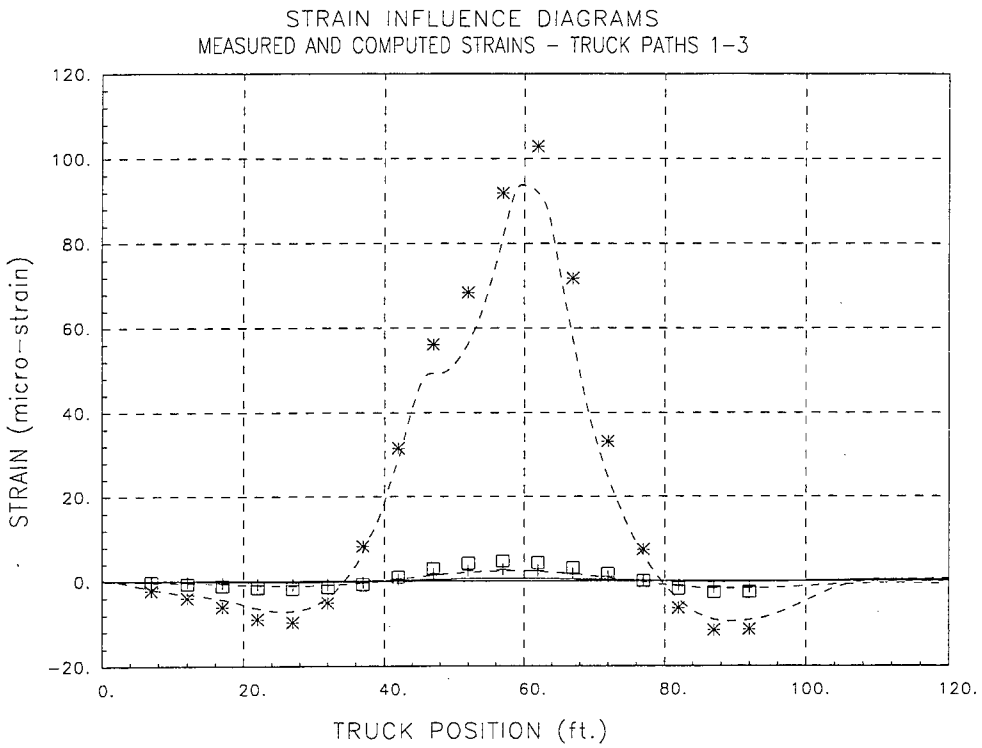

Figure 26 Strain comparison at midspan beam 5 - span 2 (3 axle truck).

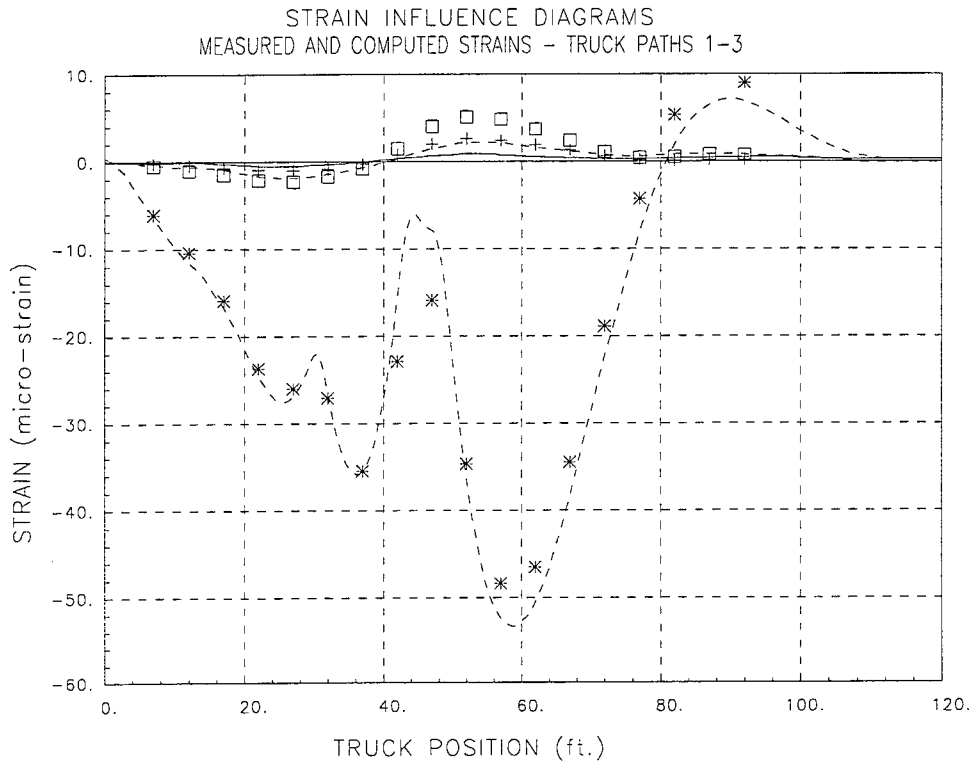

Figure 27 Strain comparison at beam 5 - pier 1 (3 axle truck).

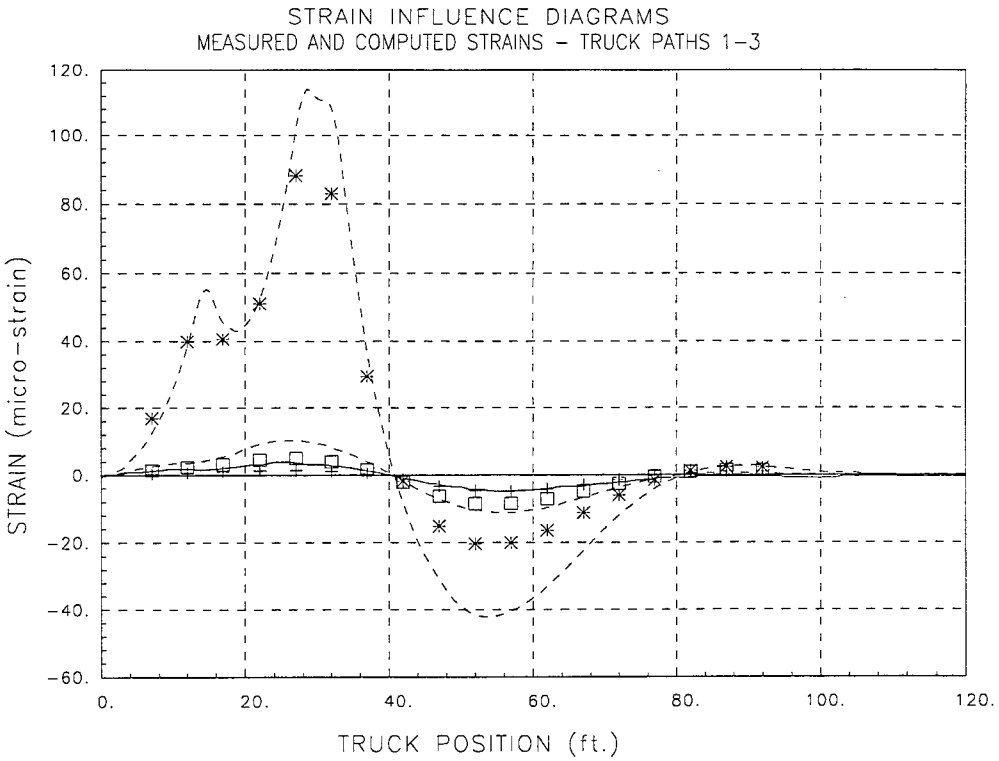

Figure 28 Strain comparison at midspan beam 4 - span 1 (3 axle truck).

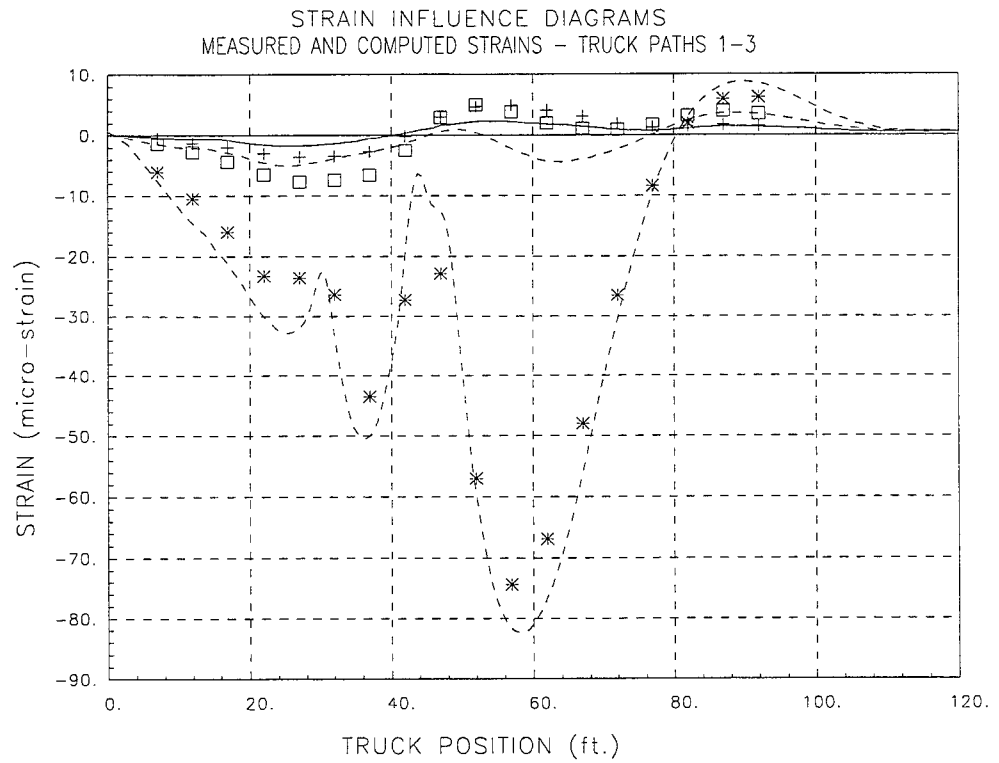

Figure 29 Strain comparison at beam 4 - pier 1 (3 axle truck).

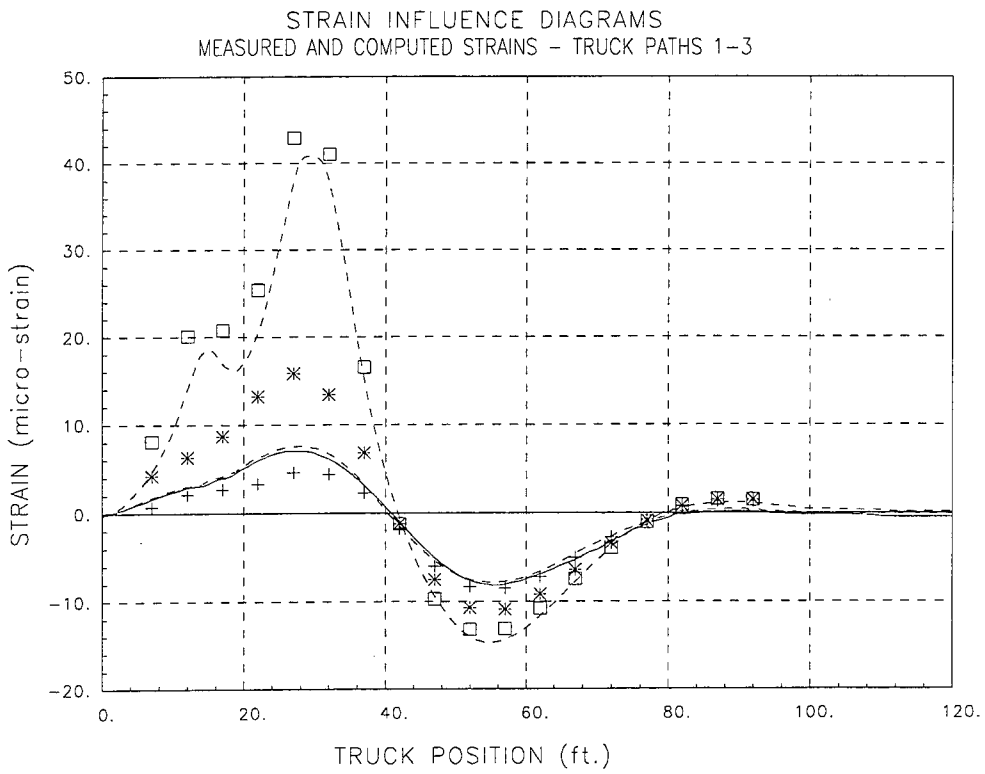

Figure 30 Strain comparison at midspan beam 3 - span 1 (3 axle truck).

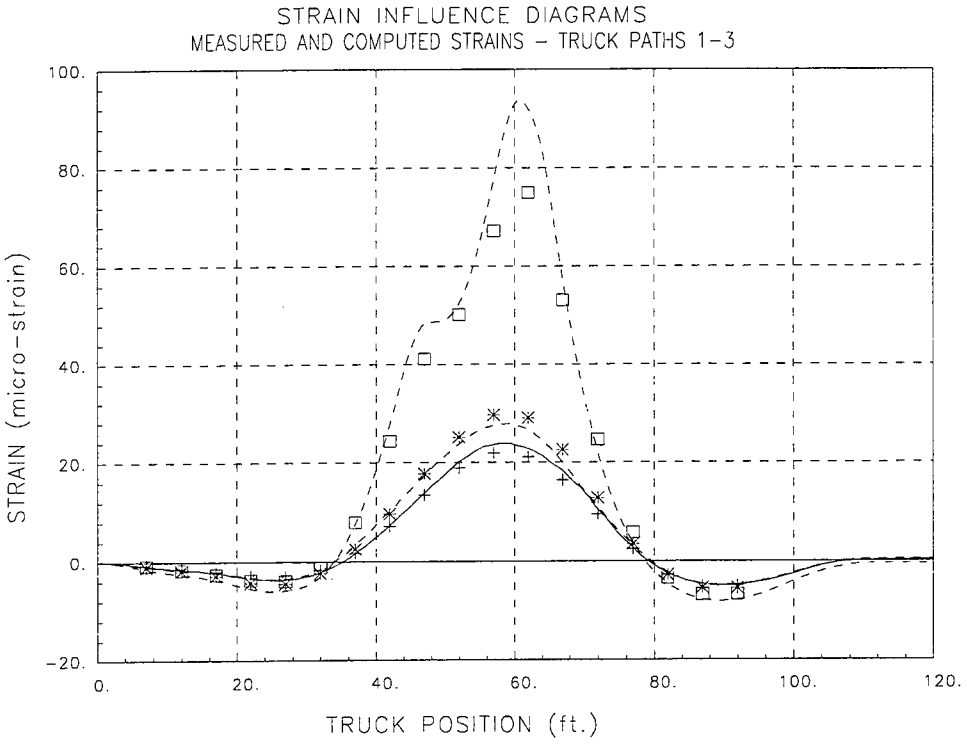

Figure 31 Strain comparison at midspan beam 3 - span 2 (3 axle truck).

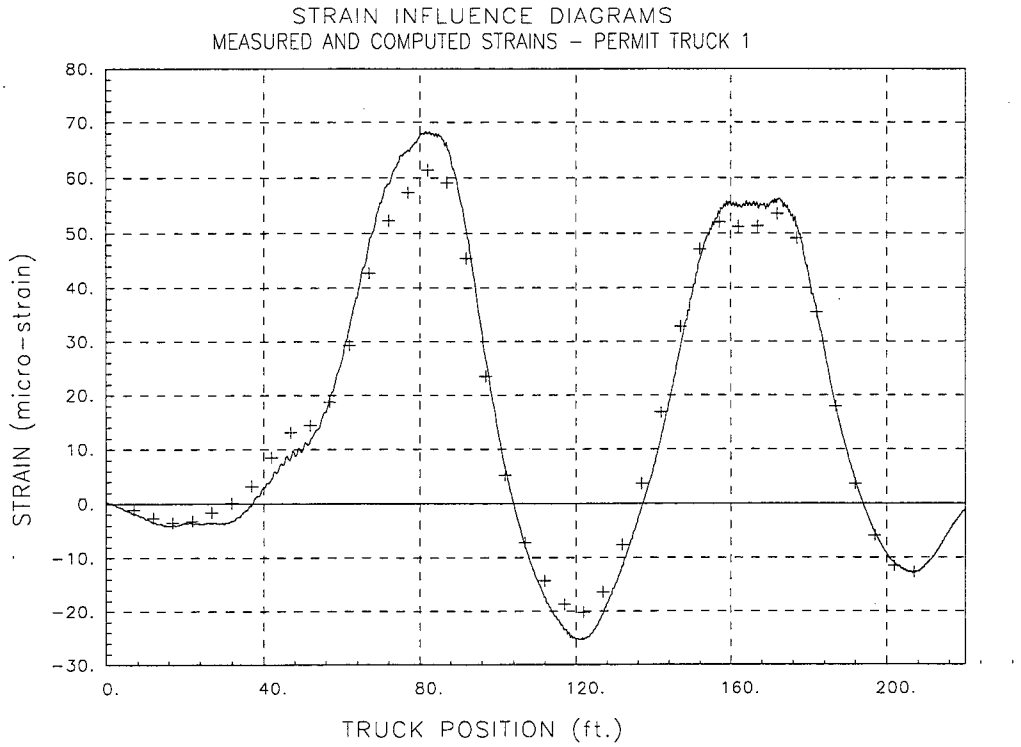

Figure 32 Strain comparison at midspan beam 1 - span 2 (permit truck 1).

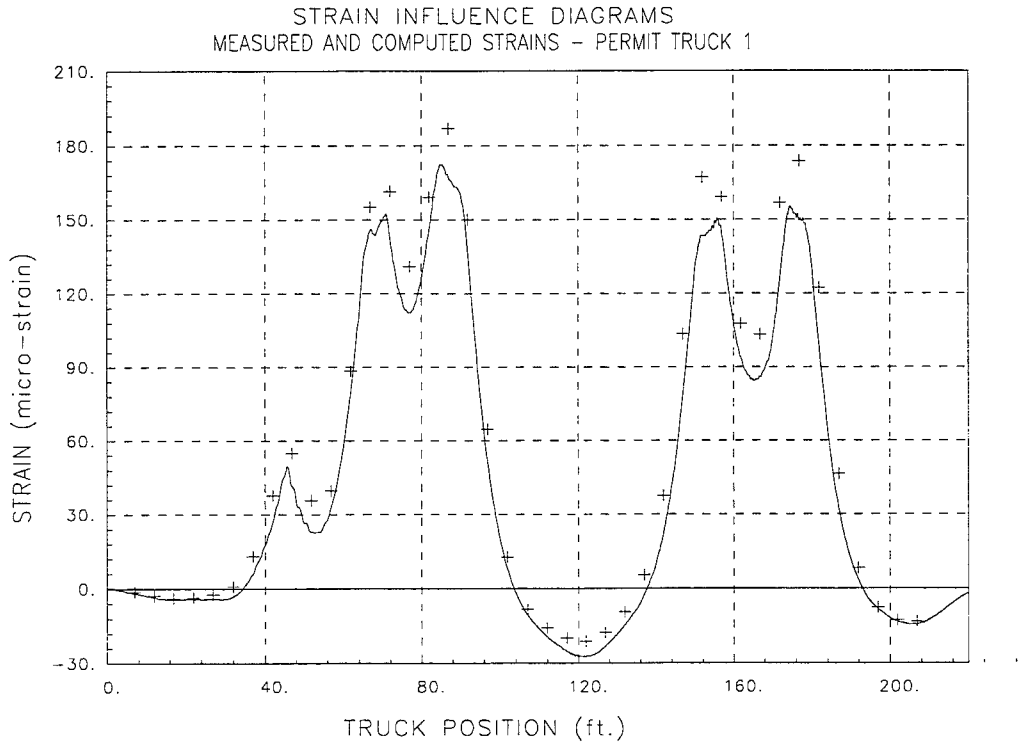

Figure 33 Strain comparison at midspan beam 2 - span 2 (permit truck 1).

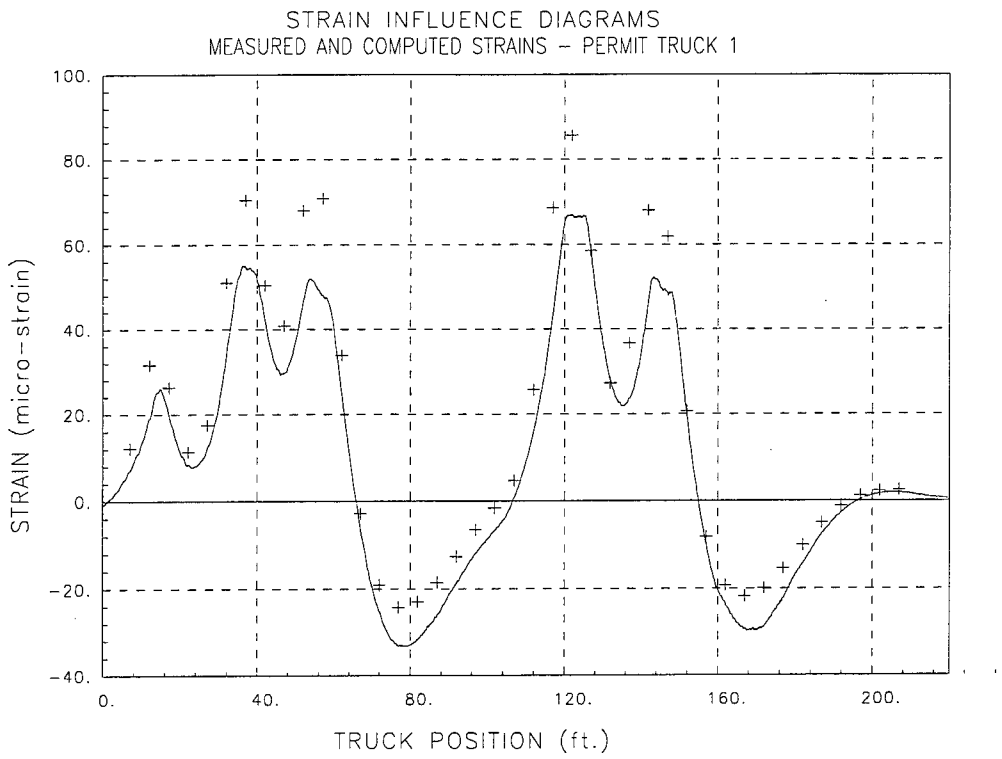

Figure 34 Strain comparison at midspan beam 3 - span 1 (permit truck 1).

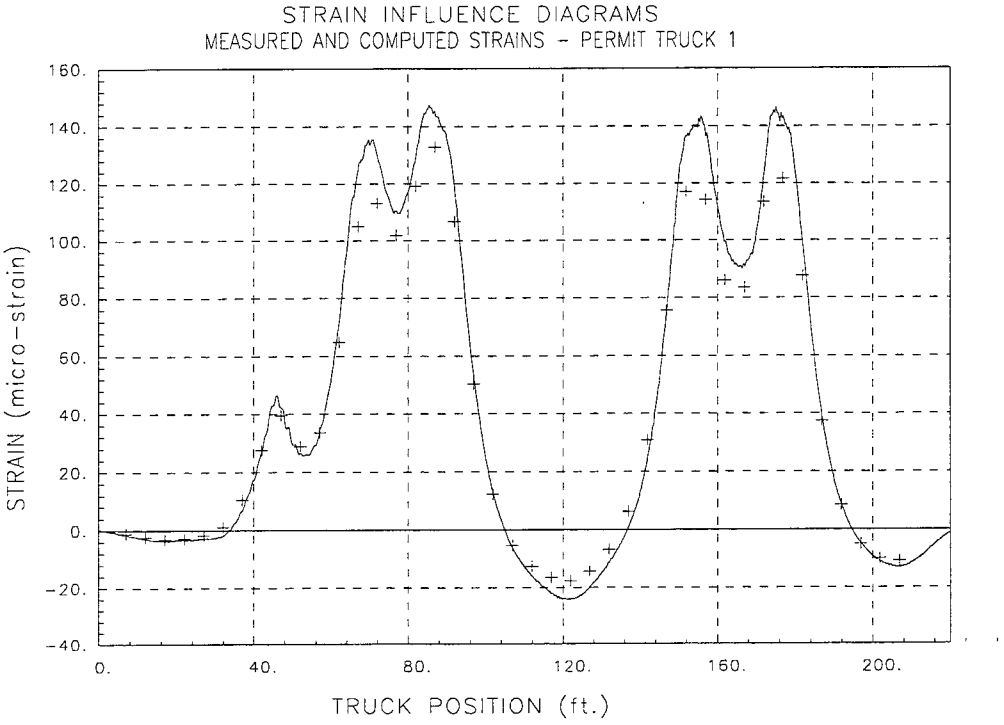

Figure 35 Strain comparison at midspan beam 3 - span 2 (permit truck 1).

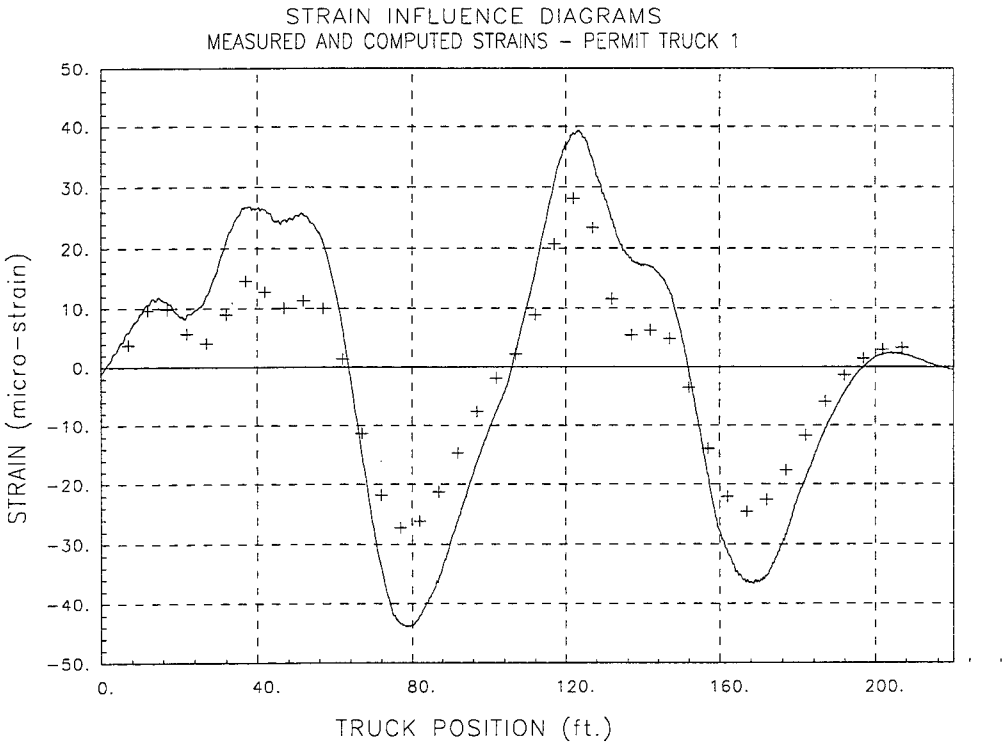

Figure 36 Strain comparison at midspan beam 1 - span 1 (permit truck 1).

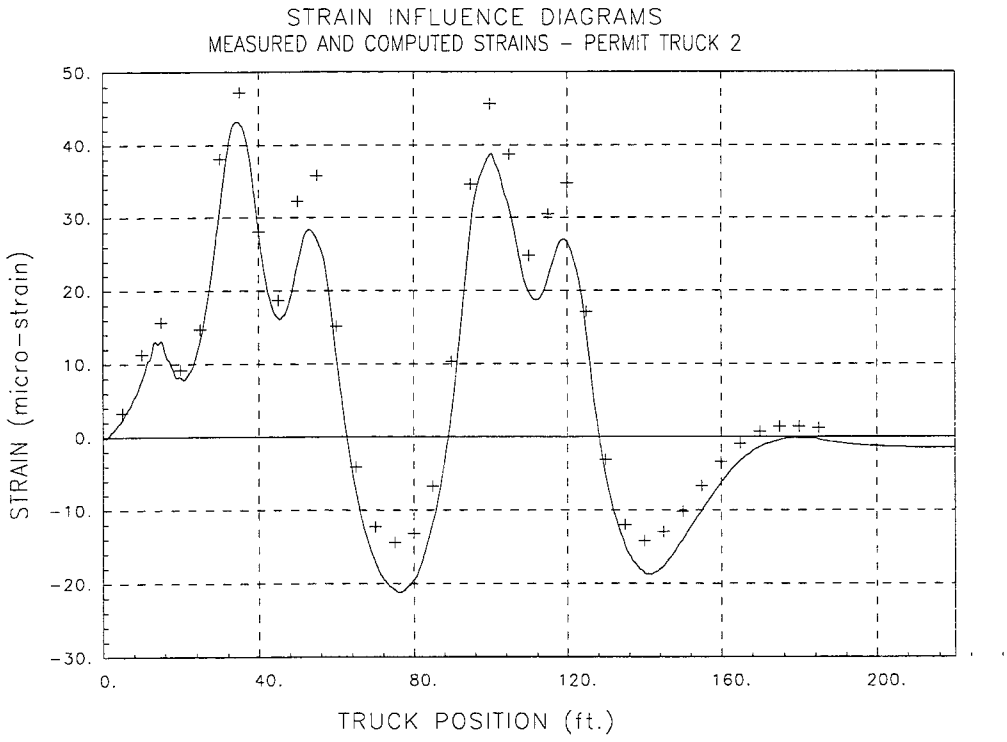

Figure 37 Strain comparison at midspan beam 3 - span 1 (permit truck 2).

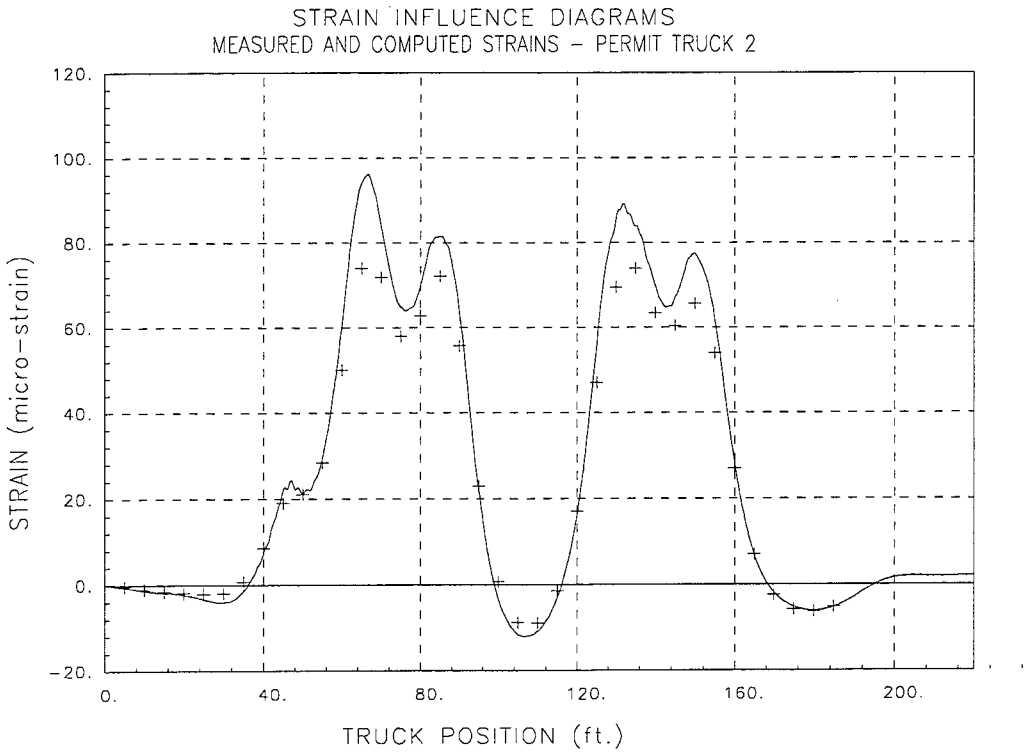

Figure 38 Strain comparison at midspan beam 3 - span 2 (permit truck 2).

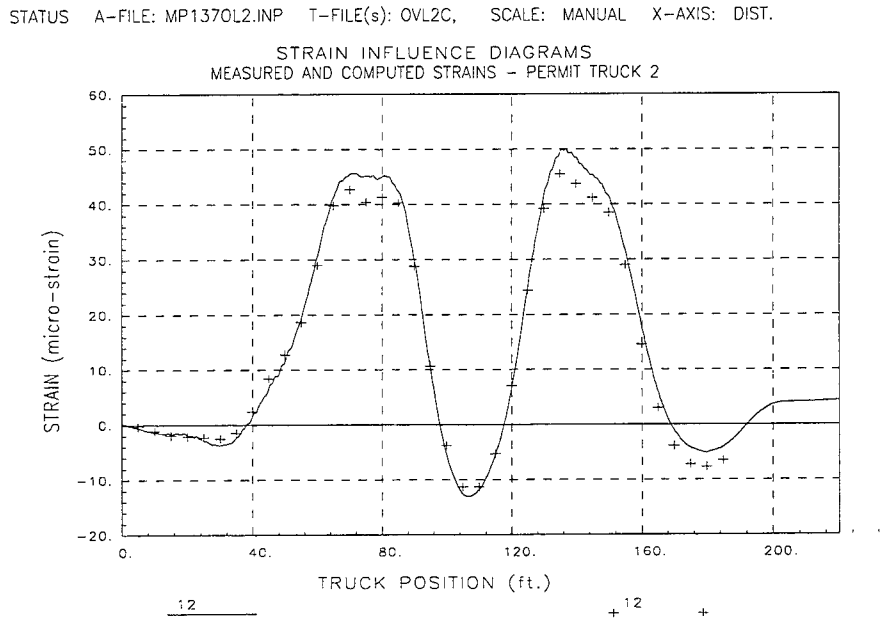

Figure 39 Strain comparison at midspan beam 1 - span 2 (permit truck 2).

APPENDIX C – SLAB/STEEL GIRDER BRIDGE

DESCRIPTION OF STRUCTURE

Table 20 Structure description – slab/girder bridge.

Structure Identification	Structure ID CHD
Location	Wyoming, Northbound I-25 mile 114.69
Structure Type	Steel I-beam, 3-span continuous, partially composite (nc, c, nc)
Span Length(s)	37ft-0in - 59ft-0in – 37ft-0in (11.3m – 18m – 11.3m)
Skew	18° from perpendicular
Roadway/Structure Widths	42ft-0in / 44ft-8in (12.8m/13.6m)
Beam Spacing	(5) W33x130 @ 9ft-3in (2.8m)
Slab Depth(s)	Varies 8in to 8½in (203mm to 216mm)
Beam dimensions	W33x130 typical Non-composite design @ end spans and over piers. Composite design in positive moment region of span 2.
Exterior Beams	3ft-10in (1.2m) deck overhang from beam centerline including 16in (406mm) wide by 6in (152mm) deep concrete curb.
Beam supports	North abutment pinned. Rockers at south abutment and piers.
Reinforced Concrete	f'c = 3,250 lbf/in^2 (22.4MPa), f'c=1,300 lbf/in^2 (9.0MPa)
Structural Steel	ASTM A36, fb = 20,000 lbf/in^2 (138MPa)
Comments	Structural appearance was good. No apparent deterioration in steel beams or deck.

INSTRUMENTATION PROCEDURES

The primary goal of the instrumentation was to measure the longitudinal flexural characteristics of the beams and capture the lateral load distribution of the super-structure. Due to the symmetrical span lengths and the structure's apparent good condition, instrumentation was limited to the southern approach span and middle span. The superstructure of the bridge was instrumented with 32 re-usable strain transducers as shown in Figure 40. Transducers were located in pairs at 16 different beam cross-sections; one centered on the bottom flange and the other on the web approximately 31in (787mm) from the bottom flange. All of the transducers were oriented longitudinally to measure axial strain responses. Beam flexural responses and neutral axis locations were measured directly since strains were obtained at two depths on each cross-section.

Instrumented beam cross-sections included midspan of the approach span and midspan of the center span for all beams, two beams near the south abutment, three beams near the first pier to monitor negative flexure, and one diaphragm. Based on the construction details of the

superstructure and experience with similar structures, it was desired to obtain the following stiffness parameters:

- Effective stiffness of the interior beams in positive and negative moment regions, including the degree of composite action and effective flange width and thickness.
- Effective stiffness of the exterior beams in positive and negative moment regions including the degree of composite action, effective flange width and thickness, and effects of the attached curb.
- Effective rotational end restraints of the beams provided by the abutments.
- End restraint provided by abutment pins and rockers and rotational restraint provided by interior rockers.
- Effective transverse stiffness of the R/C deck including the effective thickness with overlay, presence of cracks, and concrete stiffness.
- Effective transverse stiffness provided by diaphragms.

All of these parameters significantly affect the structure's load distribution characteristics. Therefore, evaluation of these parameters was necessary to accurately assess the load effect on each component due to an applied load condition. All of the instrumentation procedures were accomplished during the afternoon of August 18th, 1997. Access to the underside of the structure was obtained by a 20 ft (6.1m) extension ladder.

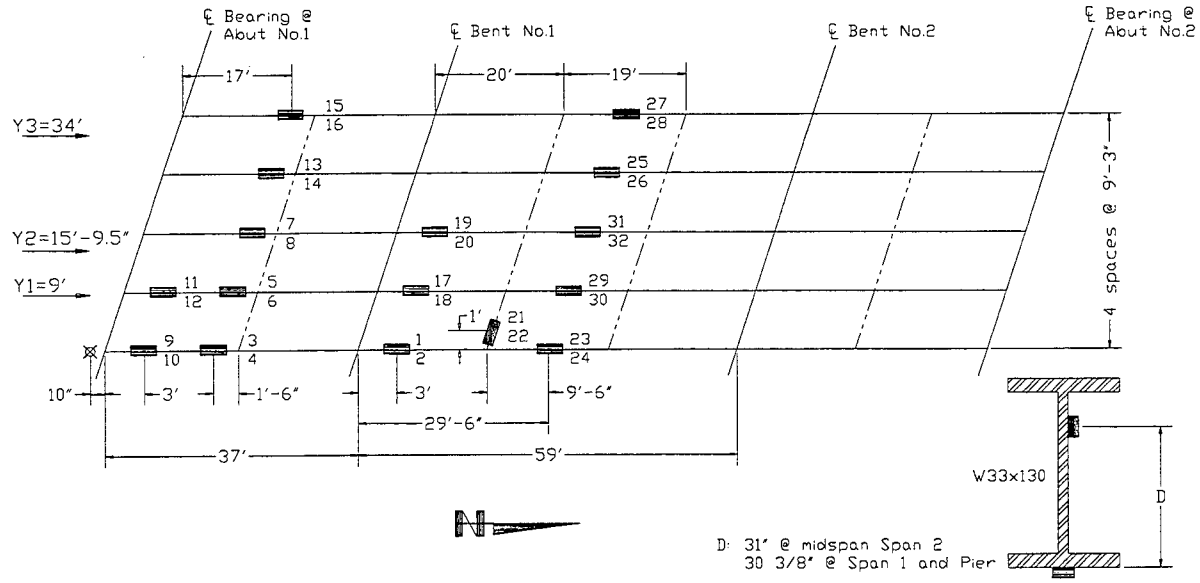

Figure 40 Instrumentation plan for slab/girder bridge.

LOAD TEST PROCEDURES

A loaded, three-axle tandem dump truck provided by WYDOT was used for the initial controlled loading applications. The test truck had a gross weight of 63.02 kips (280 kN) with wheel weights and axle configurations as shown in Figure 41. Three transverse truck paths (east shoulder, east lane, and west lane) were defined so that the lateral load transfer characteristics

could be established. The load tests were performed by driving the truck across the bridge at crawl speed along the prescribed paths. Data was recorded continuously at 32 Hz during each pass and the truck position was monitored in order to record strain as a function of vehicle position. Truck crossings from each path were performed twice to ensure data reproducibility. A total of six slow-speed truck crossings were performed along with two high-speed passes along paths 2 and 3. Traffic control, provided by WYDOT, consisted of a single lane closure and approximately one-minute road blocks as the test truck crossed the bridge. The entire testing process took approximately one hour.

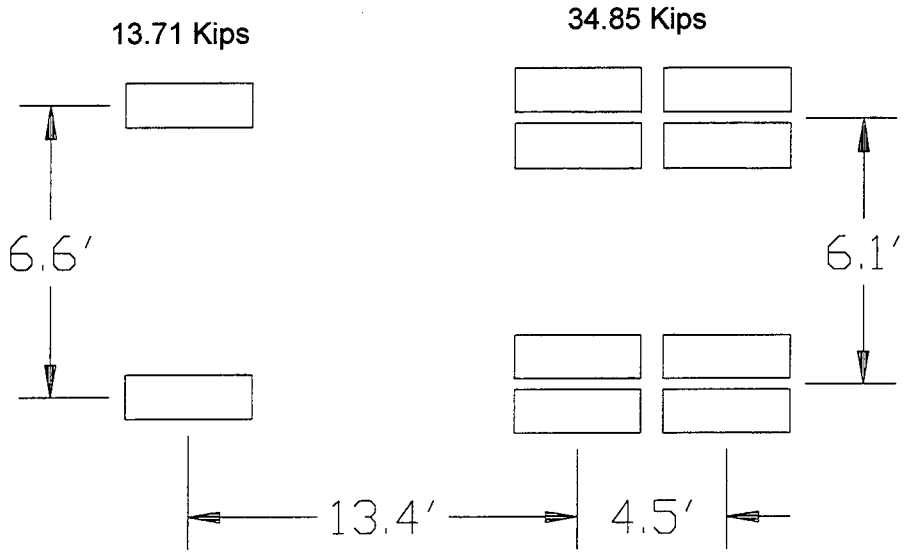

Figure 41 Load configuration of initial test truck – slab/girder bridge.

After the load testing procedures with the 3-axle test truck were completed, strains were measured during a single crossing of an overload permit vehicle. The permit vehicle had a gross weight of 285.38 kips (1,270 kN) carried by 15 axles as shown in Figure 42. As with the initial test, the longitudinal position of the truck was monitored as the permit load followed a pre-defined path at crawl speed. The path for the overload vehicle was the same as path 2 of the test truck (passenger side steering wheel over the right lane line).

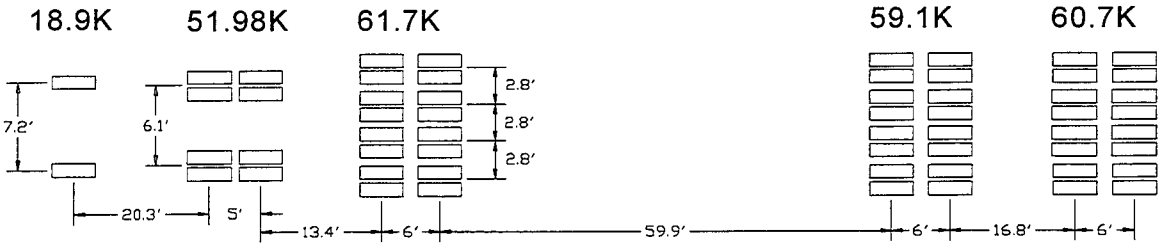

Figure 42 Permit vehicle for slab/girder bridge test.

PRELIMINARY INVESTIGATION OF TEST RESULTS

A visual examination of the field data was first performed to assess the quality of the data and to make a qualitative assessment of the bridge's live-load response. It was determined that the structural responses were elastic since all of the strains returned to zero after each truck crossing. It was also immediately apparent that regions designed as non-composite (end spans and regions over the pier) were in fact acting partially composite. The semi-composite behavior was observed by fluctuations in the upper web strain measurements and corresponding neutral axis locations (see Figure 43). In contrast, all measurements taken from the midspan of span 2 had a consistent relationship between upper and lower strain magnitudes indicating full composite action as shown in Figure 44.

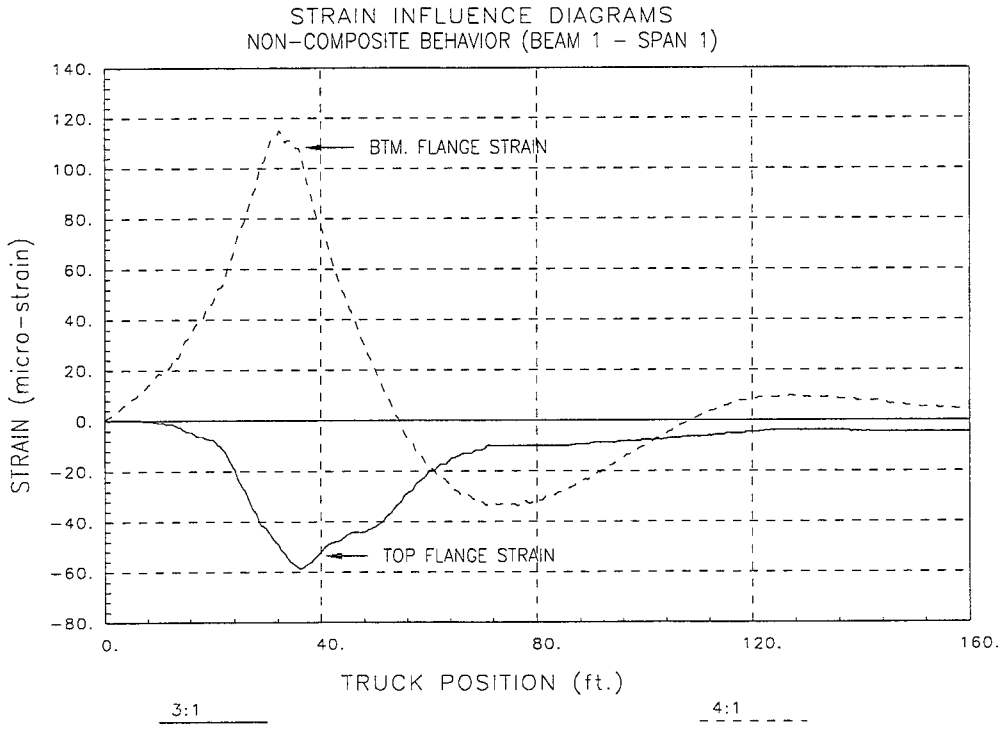

Figure 43 Strain responses indicating non-composite beam behavior.

Neutral axis calculations obtained at the non-composite regions varied significantly with respect to load magnitude (truck position), however, the neutral axes never dropped to the centroid of the steel I-beams. Therefore, even though there was not a rigid bond between the deck and top flange of the I-beam, shear friction was providing some additional stiffness to the beam cross-sections. It was interesting to note that the varying beam stiffness was only observed by the gages mounted near the tops of the beams. As shown in Figure 45, the bottom flange strains were more consistent and reproducible from duplicated load tests than were the upper web strains. Reproducibility of all the bottom flange strains and all of the strains in the composite region was excellent, indicating that the partial composite behavior of the superstructure did not have any adverse effects on the structure's load response.

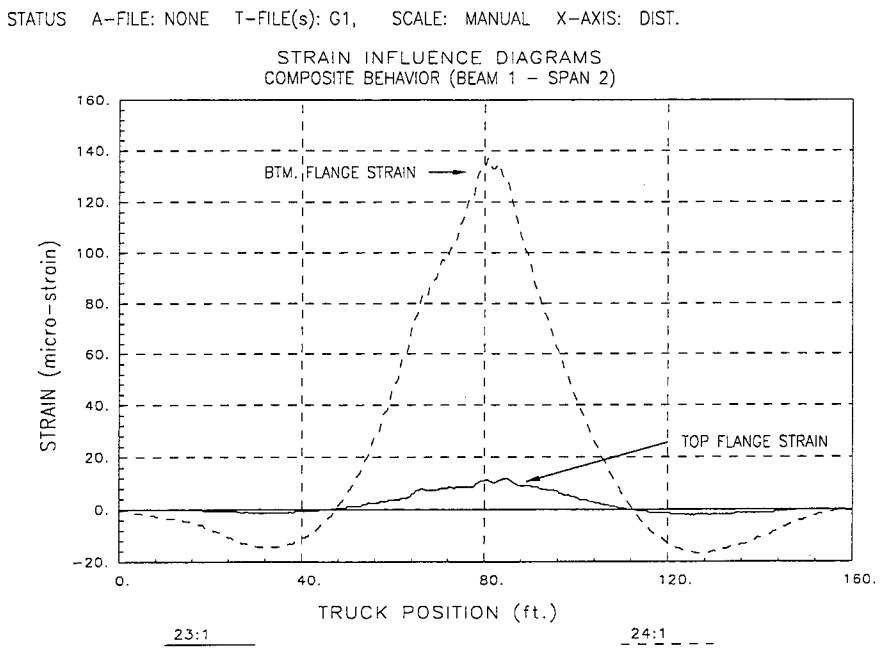

Figure 44 Strain responses indicating composite beam behavior.

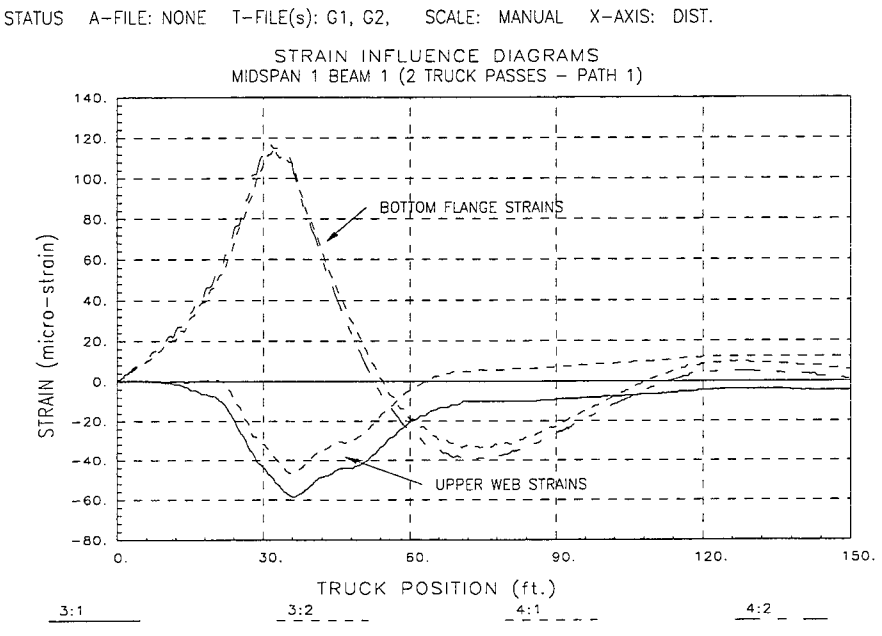

Figure 45 Consistency of bottom flange strain measurements – slab/girder bridge.

The measured strains were considered normal for the span length and truck weight. The largest measured positive moment strain was +138 in^{-6}/in (4.0 ksi (27.4 MPa) in steel) and the largest negative moment strain was –81 in^{-6}/in (-2.4 ksi (-16.6 MPa) in steel). Table 21 contains the maximum measured strains at various locations on the structure for each truck path and for the permit truck. A comparison of the maximum measured strains between the test truck path 2 and the permit truck indicated that the permit load generated responses approximately 27 percent higher in positive moment and 116 percent higher in negative moment.

As a means of determining cross-section properties and relative stiffnesses of the interior and exterior beams, neutral axis measurements were calculated from the strain histories. This was done using strain measurements at the different depths of the beam cross-sections and assuming linear strain distributions throughout the beam depth. Table 22 contains the measured neutral axis values for the various beam cross-sections and provides averaged values for the interior and exterior beams in the positive moment region of span 2. From these results, it is apparent that the curbs make up for the reduced flange width on the exterior beams such that the interior and exterior beams have approximately the same cross-sectional stiffness.

Table 21 Maximum strains – slab/girder bridge.

Gage ID	Location	3 Axle Path 1	3 Axle Path 2	3 Axle Path 3	Permit Truck Path 2
4	Beam 1 Midspan 1	115	31	1	50
6	Beam 2 Midspan 1	116	118	1	122
8	Beam 3 Midspan 1	32	92	36	97
14	Beam 4 Midspan 1	1	16	136	16.6
16	Beam 5 Midspan 1	2	-4	87	0
24	Beam 1 Midspan 2	137	46	1	84
30	Beam 2 Midspan 2	118	124	8	157
32	Beam 3 Midspan 2	41	107	48	151
26	Beam 4 Midspan 2	7	28	138	47
28	Beam 5 Midspan 2	1	1	115	1
2	Beam 1 Near Pier	-60	-21	-1	-47
18	Beam 2 Near Pier	-57	-50	-4	-108
20	Beam 3 Near Pier	-20	-49	-23	-95

Strains were recorded from high-speed crossings of the test truck along paths 2 and 3 to assess any impact or dynamic effects on the structure. Figure 46 contains strain histories from a midspan span gage for both the slow speed and high-speed crossings along path 2 (right lane). These strain histories show that there was a slight dynamic component (structure vibration) from this high-speed crossing. However, there was also significant load amplification due to impact of the truck. The maximum observed increase in strain occurred at span 2 with a magnitude of 22 percent. Based on these observations, the AASHTO impact factor of 29 percent appeared to be reasonable and was used in the subsequent rating calculations.

Table 22 Measured neutral axis values – slab/girder bridge.

Cross-section location	Gage #s	Neutral axis location measured From bottom of beam (in).
Beam 1 span 1	3, 4	20.5
Beam 2 span 1	5, 6	20.3
Beam 3 span 1	7, 8	21.7
Beam 4 span 1	13, 14	24.7
Beam 5 span 1	15, 16	24.9
Beam 1 span 2	23, 24	32.8
Beam 2 span 2	29, 30	31.5
Beam 3 span 2	31, 32	32.8
Beam 4 span 2	25, 26	32.1
Beam 5 span 2	27, 28	34.1
Beam 1 @ pier	1, 2	22.0
Beam 2 @ pier	17, 18	18.7
Beam 3 @ pier	19, 20	21.7
Average Int. Beam (span 2 +Moment)		32.1
Average Ext. Beam (span 2 +Moment)		33.5

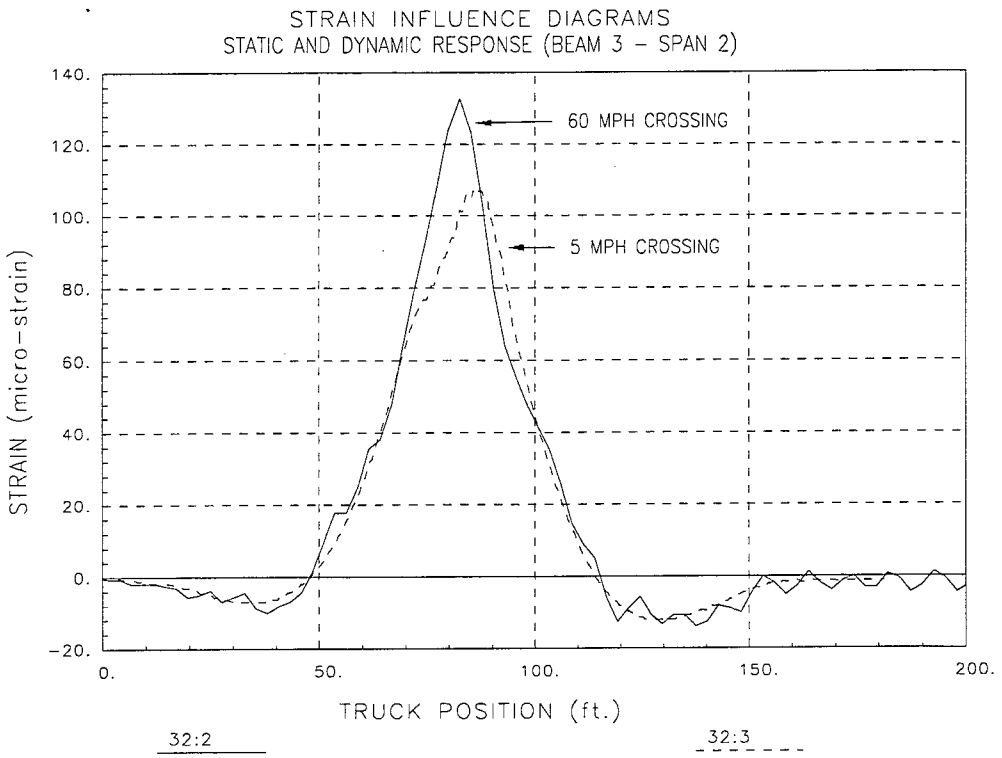

Figure 46 Static and dynamic strain history (beam 2 - span 2).

It should be noted that all of the above information was extracted directly from the field data only. The following section illustrates how the field data was used to generate and "calibrate" an analytical model of the structure.

MODELING, ANALYSIS, AND DATA CORRELATION

A simple finite element model (FEM) of the structure was defined and the entire field testing operation was reproduced in the analysis procedures. Two-dimensional frame elements were used to represent the beams and quadrilateral plate elements simulated the load transfer characteristics of the deck. Nodal points were defined longitudinally at the abutment and pier support locations, beam splices, and diaphragm locations. Intermediate nodal points were then defined to limit beam segment lengths to $1/12^{th}$ of the span length. Transverse node placement was based on the overall width of the bridge and at beam centerline locations. To maintain a desirable aspect ratio for the plate elements, intermediate node lines were located halfway between the beam lines. Based on the observed bending responses, rotational spring elements were placed at the abutment nodes and at all pier locations. To facilitate comparison of the computed and measured responses, gage locations were defined on the beams corresponding to the same locations defined in the field. The vertical location of the gages with respect the neutral axes were defined based on the measured neutral axis locations.

The entire model including geometry, boundary conditions, member cross-sections, and gage locations was generated graphically and is shown in Figure 47. This approach allowed a quick and accurate representation of the bridge and the testing procedures to be developed. Even though the geometry of the structure was well-defined, there were various structural parameters that were not well known. These parameters included the effective stiffness (EI) of the interior and exterior beams in the composite and non-composite regions, the effective stiffness of the deck (Et^3), and the moment resistance of the support conditions (K). For the initial model, all beams were assumed to be fully composite and the initial stiffness constants of the support springs were assumed to be zero. These properties were later modified based on the comparison of the computed and measured response behavior.

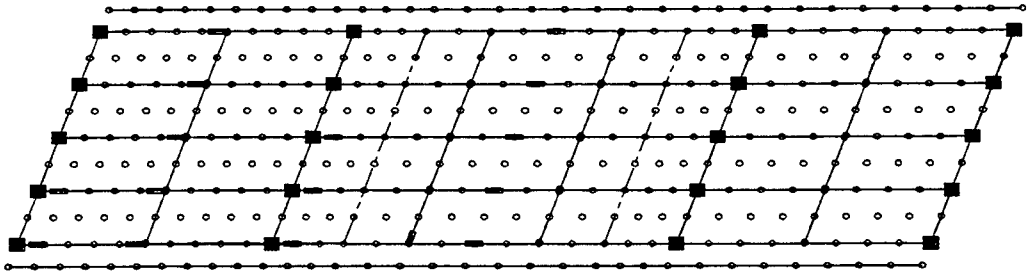

Figure 47 Computer model of slab/girder bridge.

Loading of the model was accomplished by defining a two-dimensional model (foot print) of the test vehicle consisting of a group of point loads and then placing the truck model on

structure model. Truck crossings were simulated by moving the truck model at discrete positions along the same paths used during the field test. During the comparison process, 22 longitudinal truck positions were defined for each test path. Therefore, for each analysis run, strains were computed at 32 gage locations for 12 truck positions on 3 truck paths. Accuracy of the analysis was determined by comparing 1152 (32x12x3) computed strain values with their corresponding measured strains.

Initial comparisons between the computed and measured strains indicated that significant differences existed between the model and the actual structure. In general, the magnitudes of the computed strains in the non-composite regions were too low due to the initial assignment of full composite behavior. However, initial strain comparisons in the composite region were good. The differences in ratios of the beam-end and midspan curvatures also indicated that some end restraint was being provided by the beam supports. It was also apparent that the lateral distribution was in error by observing the relative errors at the midspan gages for the various truck passes.

To improve the model's accuracy, the above-mentioned stiffness terms were modified through a parameter identification process until a best-fit correlation between the measured and computed strain was obtained. Reasonable upper and lower limits were defined for each parameter and the parameters were evaluated within those constraints. For example, the upper and lower bound moment-of-inertia (I) values for the beam members were defined by the composite and non-composite beam cross-sections. An additional allowance of 30 percent on upper and lower limits was provided to account for likely inaccuracies in the assumed steel and concrete modulus as well as the effective flange thickness provided by the deck.

The effective slab thickness was given a range of plus and minus 50 percent to account for the stiffening effect of the reinforcement, the presence of cracks, and any error in the estimated concrete modulus. Lower and upper bounds for the abutment spring stiffnesses were defined by the ratio of EI/KL, where E, I and L refer to the beam properties and span lengths, and K is the rotational spring stiffness in terms of moment per unit measure of rotation. Reasonable ranges for this ratio are between 0.1 and 4.0, which correspond to nearly fixed and nearly simple supports. Common end restraints for typical beam supports have a stiffness ratio (EI/KL) of around 1.0. It was assumed that the stiffnesses of the interior and exterior beams might be different due the slight differences in measured neutral axis values. Therefore, the interior and exterior beams were treated separately.

A total of seven different stiffness parameters were calibrated through an iterative process of analysis, data comparison, and structural identification. At the end of this cycle, an excellent correlation was obtained. Table 23 contains the initial and final values for each of the variable properties. To illustrate how the parameter modification improved the accuracy of the model, initial and final error values are shown in Table 24.

Table 23 Initial and final parameter values – slab/girder bridge.

Member Property	Units	Initial Value	Identified Value
Int. Beams span 1 and pier - I	in^4, (cm^4)	197,200 (8,207,464)	24,000 (998,880)
Int. Beams span 2 - I	in^4, (cm^4)	197,200 (8,207,464)	24,000 (998,880)
Ext. Beams span 1 and pier - I	in^4, (cm^4)	197,200 (8,207,464)	10,280 (427,854)
Ext. Beams span 2 - I	in^4, (cm^4)	197,200 (8,207,464)	10,770 (448,247)
Rotational restraint supports- Ka	k-in/rad (kN-m/rad)	0 (0)	300,000 (33,900)
Diaphragm connection stiffness (I)	In^4, (cm^4)	315 (13,110)	11 (458)
Deck Thickness	In (mm)	8 (203)	7.4 (188)

Table 24 Accuracy of initial and refined models – R/C T-beam bridge.

Error Value	Initial Model	Refined Model
Absolute Error	4,975	3,510
Percent Error	23.5	7.7
Scale Error	6.3	4.3
Correlation Coefficient	0.88	0.96

Following the parameter identification procedure, a 2-D model of the permit loads were generated and applied to the calibrated model. The purpose of this exercise was to verify that the model could reasonably predict the responses from much heavier loads with completely different geometries. The analysis was run for the single pass of the permit load with the truck positions were incremented at 10ft (3.1m) intervals. A total of 25 truck positions were defined and strains were computed at each gage location. As shown in Table 25, a reasonable level of accuracy was obtained from the permit load crossings when compared to the results obtained for the dump truck. The increase in error values is somewhat misleading because most of the error is due to the top gages in the non-composite regions. Bottom flange gages and gages in the composite section of span 2 yielded excellent correlations. Measured and computed strain comparisons are provided for the test truck and the permit vehicles in Figure 48 through Figure 73.

Table 25 Accuracy of calibrated model for permit load – slab/girder bridge.

Error Value	Permit Truck
Absolute Error	4726
Percent Error	9.7
Scale Error	27.0
Correlation Coefficient	0.95

Results from the structural identification process indicated that the beam stiffnesses in the non-composite regions were approximately 53 percent greater than calculated (I) for a purely non-composite cross-section. Since the beams' semi-composite stiffnesses apparently varied with load magnitude, it was likely that the additional stiffness could not be relied upon with extremely heavy load applications. Therefore, it was desirable to determine the accuracy of the model if pure non-composite cross-sections were used for the regions designed as non-composite. Corresponding (I) values and neutral axis locations were modified to represent non-composite behavior, and the analysis and comparison procedure was repeated with the permit truck using only the bottom flange gages in the non-composite regions. It was interesting to note that the accuracy of the composite/non-composite model was nearly as good as the calibrated model. Results from the comparison are shown in Table 26.

Table 26 Accuracy of composite/non-composite model (btm flanges only).

Error Value	Calibrated Model	Composite/non-composite model
Absolute Error	1759	2100
Percent Error	2.1	2.7
Scale Error	16.6	17.2
Correlation Coefficient	0.99	0.99

Based on the intended design and the observed response behavior of the superstructure, it is apparent that non-composite section properties should be assumed for the non-composite regions. Even though some beam stiffening was induced by friction between the top flange and deck, the bottom flange strains could be reasonably well predicted by the non-composite model.

At this point, the model has been "calibrated" to the field measurements and it has been verified that the model will provide the same degree of accuracy regardless of the load configuration. Since the load responses of the model are very similar to those of the actual structure, it can be assumed that the stiffness and load transfer characteristics are correct.

DISCUSSION OF RESULTS

The accuracy obtained by this evaluation process was typical of steel bridge structures. Some variations were observed in the upper regions of the beam cross-sections due to the friction between the top flange and deck in the non-composite regions. However, the bottom flange strains were predicted within the tolerance obtainable by the load test. The main observations made from the load test data evaluation and during the parameter identification process are as follows:

- The exterior beams had approximately the same stiffness as the interior beams. This indicated that the additional curb made up for the loss of effective flange width in the exterior beams.
- Fully-composite behavior was observed in the positive moment region of span 2. The resulting beam stiffnesses were 22 percent greater than the initial stiffness calculated for a composite

section. This could be a result of the concrete modulus being greater than assumed or the asphalt overlay contributing to the beam stiffness.

- Beam sections designed as non-composite were observed to behave partially composite due to friction between the top flange of the steel I-beam and concrete deck. The degree of composite action was observed to vary with load magnitude. Bottom flange strains were reasonably-well predicted by the model containing non-composite beam cross-sections, therefore non-composite behavior should be assumed during subsequent rating calculations.
- There was minimal rotational restraint provided by the rocker supports (midspan stresses reduced by less than five percent). Because the amount of restraint was small and was dependent on the rocker angle, it could effectively be ignored in subsequent rating evaluations.
- The measured dynamic or impact effects obtained during the high-speed truck crossings were in the range of 0 to 22 percent. Average values obtained from the most heavily loaded beams were approximately 15 percent, indicating that the AASHTO impact factor of 29 percent is reasonable.
- Strain comparisons from the permit load produced approximately the same degree of accuracy as did the test vehicle used to calibrate the model. This verifies that the majority of measured responses were linear with respect to load magnitude and that the accuracy is not dependent on the applied load. Strains measured near the top flange, varied significantly due to shifts in the neutral axis. However, bottom flange strains were very consistent.

LOAD RATING PROCEDURES AND RESULTS

In this section, a discussion of the load rating procedures is given and load limits are provided for standard Wyoming load configurations and for the permit load vehicle used in the field test.

Inventory and operating rating factors were computed using Allowable Stress Design (ASD) and Load Factor Design (LFD) methods. Member capacities were computed for the interior and exterior beams based on positive moment, negative moment, and shear using AASHTO design specifications. Allowable stress flexural capacities of the beams were based on steel stresses of 20 ksi (138 MPa) for inventory ratings and 27 ksi (186 MPa) for operating limits. Load factor capacities were based on yield strength of the various beam sections.

The rating equation specified by the AASHTO *Manual for Condition Evaluation of Bridges* given in appendix F was used to generate inventory and operating load limits. The appropriate load factors were applied to the dead- and live-load effects based on the level of rating ($A_1 = A_2 = 1.0$ for ASD ratings, A_1=1.3 & A_2=2.17 for LFD Inventory ratings, and A_1=1.3 & A_2=1.3 for LFD Operating ratings). An impact factor of 29.0 percent, specified by AASHTO, was applied to the live load effects.

Since the span 2 beams were design as composite, the calculation of dead-load effects had to be performed in two phases. The self-weight of the beams and deck were applied to the fully non-composite structure model. Maximum computed non-composite dead-load stresses were subtracted from the various capacity stress limits to obtain composite member capacities. Resulting composite member capacities, listed in Table 27, were used in the rating equation.

Table 27 Component capacities minus non-composite dead-load effects

	Moment Capacity: k-in (kN-m)			Shear Capacity: kips (kN)		
Member	Inv.	Oper.	L. F.	Inv.	Oper.	L. F.
Int. Beams Spans 1&3	7,300 (825)	10,150 (1,147)	13,800 (1,559)	230 (1,023)	311 (1,384)	401 (1,785)
Ext. Beams Spans 1&3	7,300 (825)	10,150 (1,147)	13,800 (1,559)	230 (1,023)	311 (1,384)	401 (1,785)
Int. Beams @ Pier	-5,160 (-583)	-8,000 (-904)	-11,650 (-1,317)	230 (1,023)	311 (1,384)	401 (1,785)
Ext. Beams @ Pier	-5,160 (-583)	-8,000 (-904)	-11,650 (-1,317)	230 (1,023)	311 (1,384)	401 (1,785)
Int. Beams Span 2	10,885 (1,230)	16,050 (1,814)	22,690 (2,564)	230 (1,023)	311 (1,384)	401 (1,785)
Ext. Beams Span 2	10,885 (1,230)	16,050 (1,814)	22,690 (2,564)	230 (1,023)	311 (1,384)	401 (1,785)

It is important to note that the primary benefit of the integrated approach is that the load effects are more realistically determined. With the exception of estimating accurate section properties, the approach has little impact on component capacity calculations. In the rating equation, dead- and live-load effects were computed from the calibrated model. Additional dead load of 60 lb/ft^2 (2,874 N/m^2) to account for 3in (76mm) of asphalt and railings, was applied uniformly to the deck of the composite/non-composite model. Critical live-load effects were determined by computing shear and moment envelopes for several different truck paths. Multiple lane load situations (2 and 3 lanes) were obtained by superimposing envelopes for truck paths separated by 12ft (3.7m) or more. Effects of three-lane loading were reduced by 10 percent as specified by AASHTO 3.12.1. All rating factors were limited by bending moment. Rating values for various components are listed in Table 28.

Table 29 contains the critical rating factors for the five standard Wyoming truck configurations including the HS-20 and H-20 and also for the permit vehicle used during the test. In general, rating factors for the shorter vehicles were obtained from midspan of span 2 of the interior beams (positive moment), while rating factors for longer vehicles were obtained from the interior beams over the interior piers (negative moment). The next-most critical location was the positive moment region in span 2 of the interior beams.

Table 28 Component rating factors – slab/girder bridge.

Truck	Member	A.S. Rating Factors		L.F. Rating Factors	
		Inventory	Operating	Inventory	Operating
H-20	Int. beam spans 1&3	2.90	4.12	2.59	4.32
	Ext. beam spans 1&3	4.23	5.99	3.76	6.28
	Int. beam @ Pier	2.73	4.70	3.22	5.37
	Ext. beam @ Pier	4.42	7.61	5.21	8.69
	Int. beam span 2	2.25	3.50	2.30	3.84
	Ext. beam span 2	3.20	4.96	3.26	5.44
HS-20	Int. beam spans 1&3	2.29	3.27	2.05	3.43
	Ext. beam spans 1&3	3.23	4.61	2.90	4.83
	Int. beam @ Pier	1.48	2.60	1.79	2.98
	Ext. beam @ Pier	2.49	4.37	3.00	5.00
	Int. beam span 2	1.55	2.44	1.60	2.68
	Ext. beam span 2	2.08	3.25	2.14	3.57
Type3*	Int. beam spans 1&3	2.81	3.99	2.51	4.18
	Ext. beam spans 1&3	4.04	5.72	3.59	5.99
	Int. beam @ Pier	2.49	4.29	2.93	4.90
	Ext. beam @ Pier	4.20	7.22	4.94	8.24
	Int. beam span 2	2.19	3.41	2.24	3.74
	Ext. beam span 2	3.02	4.68	3.08	5.14
Type 3S2*	Int. beam spans 1&3	3.11	4.43	2.78	4.64
	Ext. beam spans 1&3	4.27	6.07	3.81	6.37
	Int. beam @ Pier	1.57	2.71	1.85	3.10
	Ext. beam @ Pier	2.58	4.44	3.04	5.07
	Int. beam span 2	2.39	3.72	2.44	4.08
	Ext. beam span 2	3.34	5.18	3.40	5.68
Type 3-3*	Int. beam spans 1&3	3.00	4.25	2.67	4.45
	Ext. beam spans 1&3	4.11	5.84	3.67	6.12
	Int. beam @ Pier	1.50	2.58	1.77	2.95
	Ext. beam @ Pier	2.40	4.12	2.82	4.71
	Int. beam span 2	2.11	3.29	2.16	3.61
	Ext. beam span 2	2.92	4.53	2.97	4.96
Permit Truck **	Int. beam spans 1&3	2.86	4.07	2.56	4.27
	Ext. beam spans 1&3	3.02	4.26	2.67	4.46
	Int. beam @ Pier	1.19	2.05	1.41	2.35
	Ext. beam @ Pier	1.41	2.43	1.66	2.77
	Int. beam span 2	1.86	2.89	1.90	3.17
	Ext. beam span 2	1.71	2.65	1.74	2.91

* Modified to Wyoming rating specifications.

** Single lane loading (permit truck only).

Table 29 Critical vehicle rating factors – slab/girder bridge.

Load Type: tons (kN)	Allowable Stress R.F.		Load Factor R.F.	
	Inventory	Operating	Inventory	Operating
H-20 20 (178)	2.25	3.50	2.30	3.84
HS-20 36 (320)	1.55	2.48	1.63	2.72
Type 3* 22 (196)	2.19	3.41	2.24	3.74
Type 3S2* 40 (356)	1.57	2.71	1.85	3.10
Type 3-3* 40.5 (361)	1.50	2.58	1.77	2.95
Permit Vehicle 143** (1,273)	1.19	2.05	1.41	2.35

* Modified to Wyoming rating specifications.

** Single lane loading (permit truck only).

To facilitate a conventional beam load rating, lateral wheel load distribution factors where computed from the calibrated model. The distribution factors were computed for each beam by dividing the maximum computed beam moment obtained from multiple lane loads by the moment generated from a truck wheel line using a conventional beam analysis. Essentially, the distribution factor is computed by rearranging the standard AASHTO moment equation, as shown in Equation (1).

$$DF = \frac{M_{max}}{M_{AASHTO}} \quad (1)$$

Where:

M_{max}= Maximum beam moment generated by rating model with rating vehicle in multiple lanes.

M_{AASHTO} = Moment generated by conventional beam analysis with single wheel line of rating vehicle without distribution factor.

This approach is preferred to the alternate procedure, in which the maximum beam moment is divided by the sum of beam moments along a bridge cross-section because they become ambiguous when a significant skew is present. Table 30 contains the maximum lateral distribution factors for the interior and exterior beams for both positive and negative moment regions.

Table 30 Wheel distribution factors for multiple-lane loading.

Beam	Interior Beams	Exterior Beams	AASHTO S/5.5
Span 1 & 3 (+ moment)	1.26	0.90	1.68
Pier (- moment)	1.50	0.92	1.68
Span 2 (+ moment)	1.30	1.00	1.68

When applying these factors to the results of a conventional beam analysis, it is important to note that the longitudinal stiffness characteristics of the beams must be realistically represented if

the ratings are to be accurate. This means that the appropriate boundary conditions (beam supports) must be applied as well as the appropriate dimensional properties, such as pier and abutment widths.

CONCLUSIONS

Portions of superstructure designed as non-composite were observed to behave partially composite due to friction between the top flange and the deck. The degree of unintended composite action varied with load position (moment magnitude) which indicated that the response was somewhat nonlinear. Therefore, any additional stiffness provided by the beam/deck friction cannot be considered reliable and should not be used in subsequent ratings. Analysis results from a model based on non-composite section properties in span 1 and over the piers produced reasonably accurate strain histories for the bottom flange. All rating values presented in this report were computed from the model containing the calibrated section properties in the composite regions and non-composite section properties in the regions designed as non-composite.

Even though some secondary stiffening factors were ignored during rating calculations (i.e. partial composite behavior and rotational resistance of the supports), the rating factor summary indicates that this structure had a relatively high load capacity. Two factors contributed to the favorable rating values. First, the identified section properties of the composite beam sections in span 2 were approximately 22 percent greater than the initial hand calculation indicated. Secondly, the observed lateral distribution was significantly greater than the S/5.5 value specified by the 1994 AASHTO design code. Because the analysis was performed on a two-dimensional model of the superstructure, the lateral distribution characteristics were provided by the deck stiffness, transverse members, and effects of skew.

MEASURED AND COMPUTED STRAIN COMPARISONS

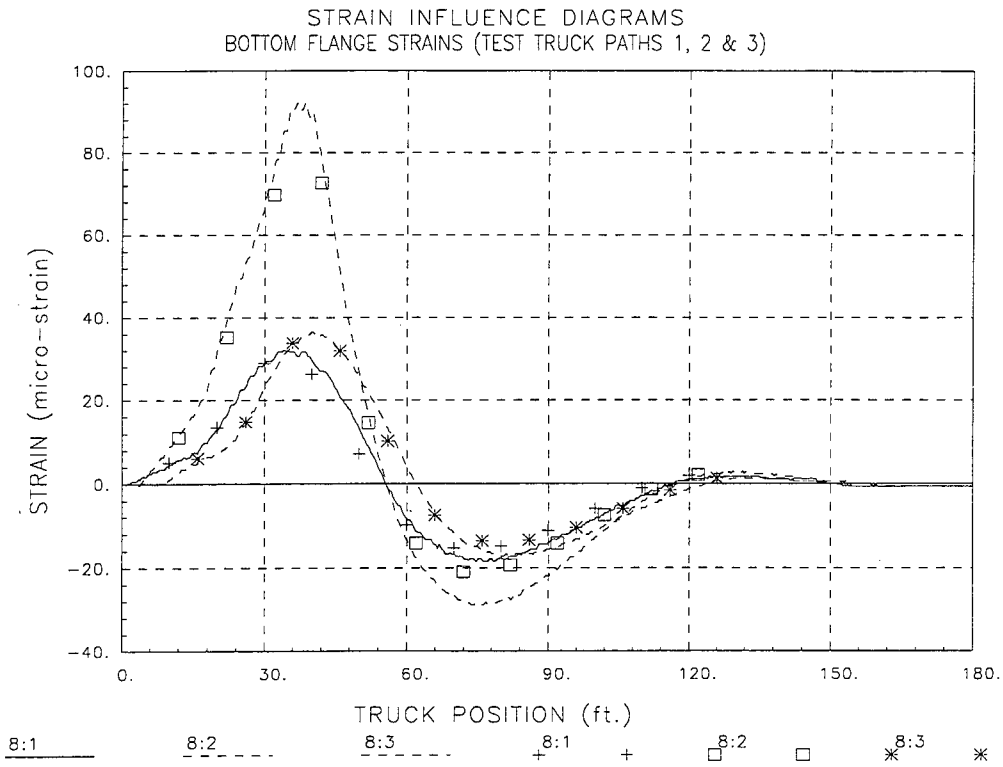

Figure 48 Strain history - beam 1 midspan 1 - truck paths 1, 2 & 3.

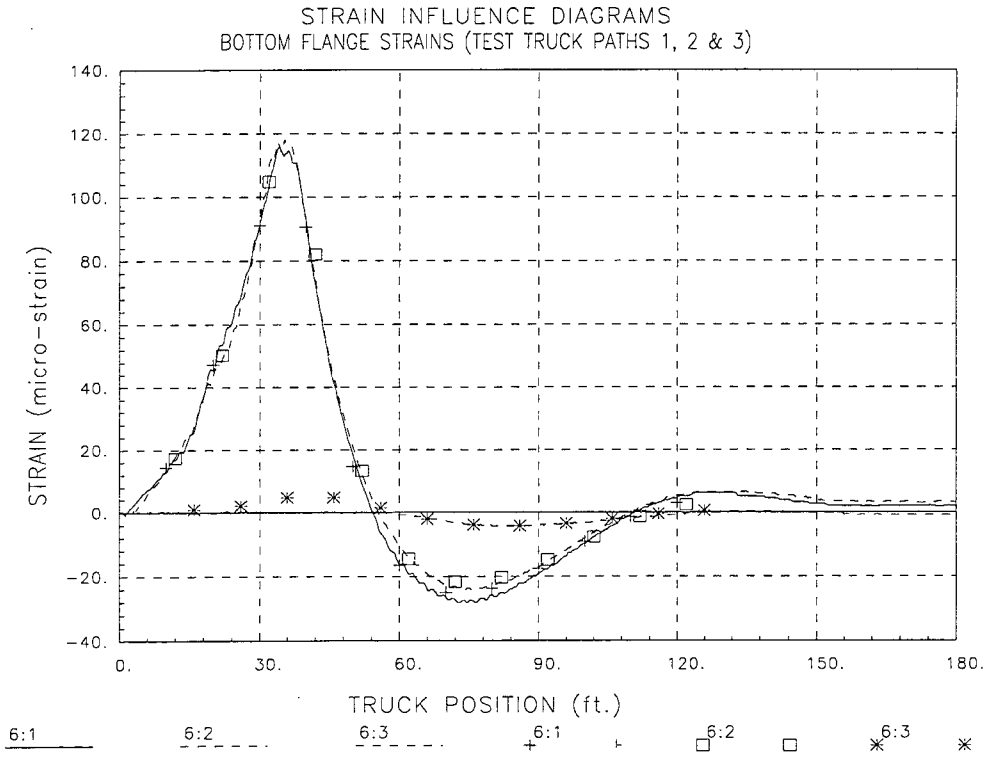

Figure 49 Strain history - beam 2 midspan 1 - truck paths 1, 2 & 3.

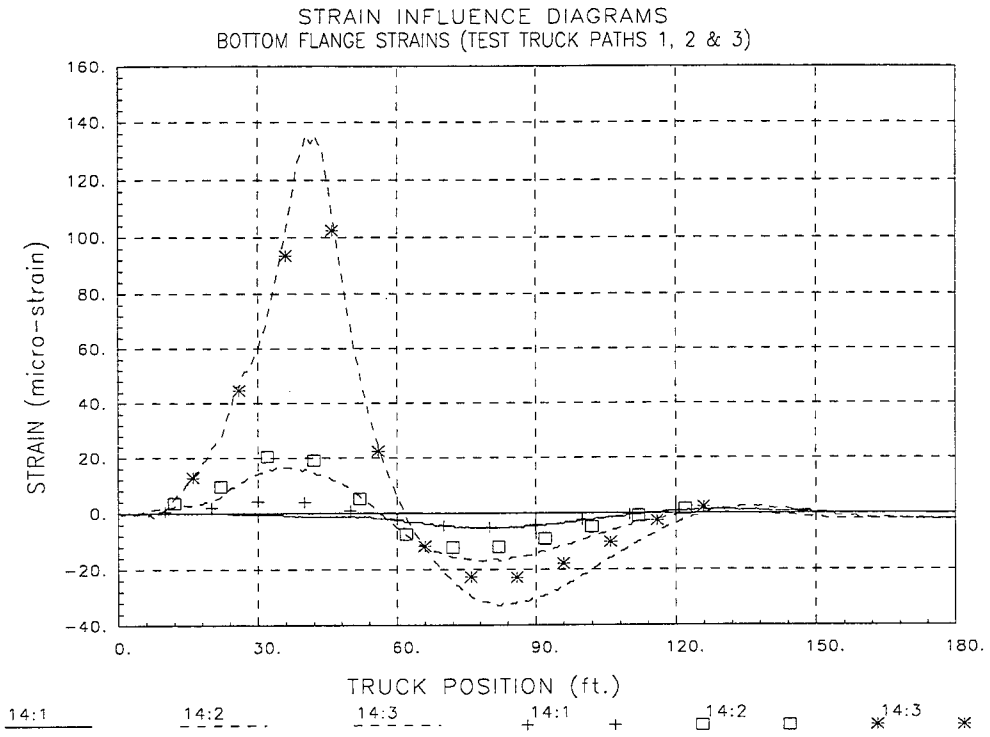

Figure 50 Strain history - beam 4 midspan 1 - truck paths 1, 2 & 3.

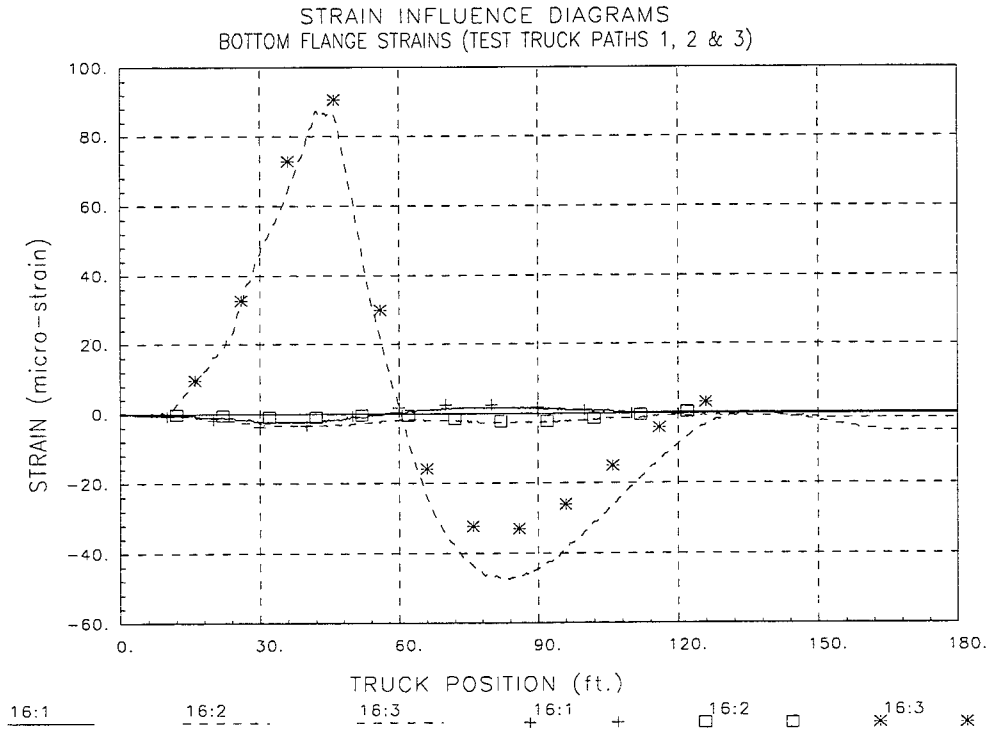

Figure 51 Strain history - beam 5 midspan 1 - truck paths 1, 2 & 3.

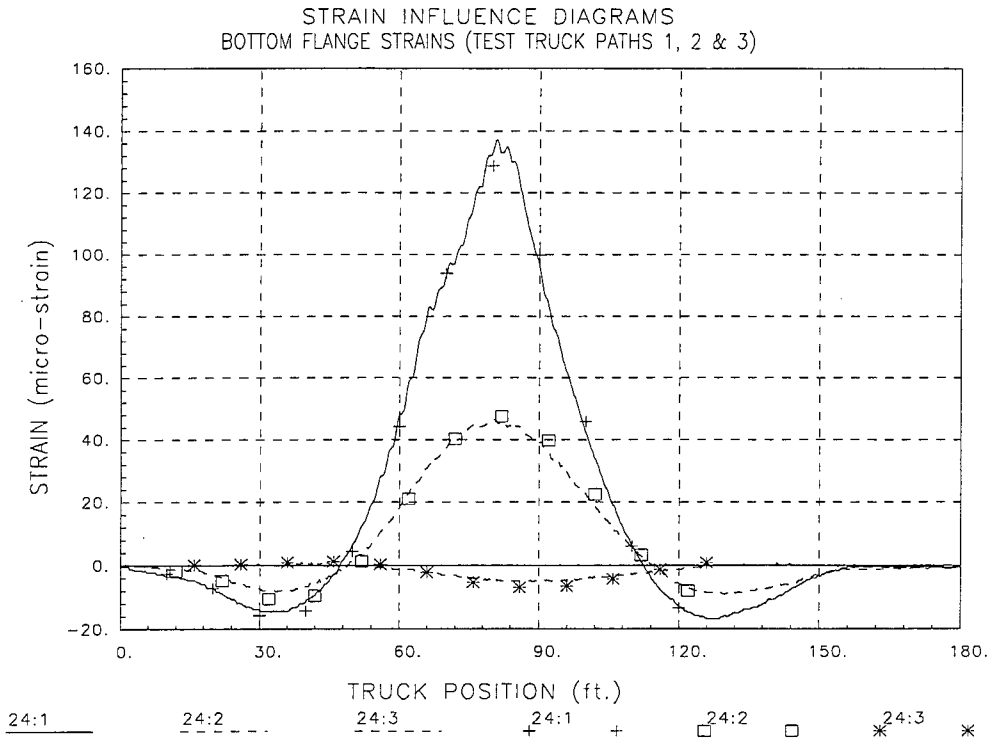

Figure 52 Strain history - beam 1 midspan 2 - truck paths 1, 2 & 3.

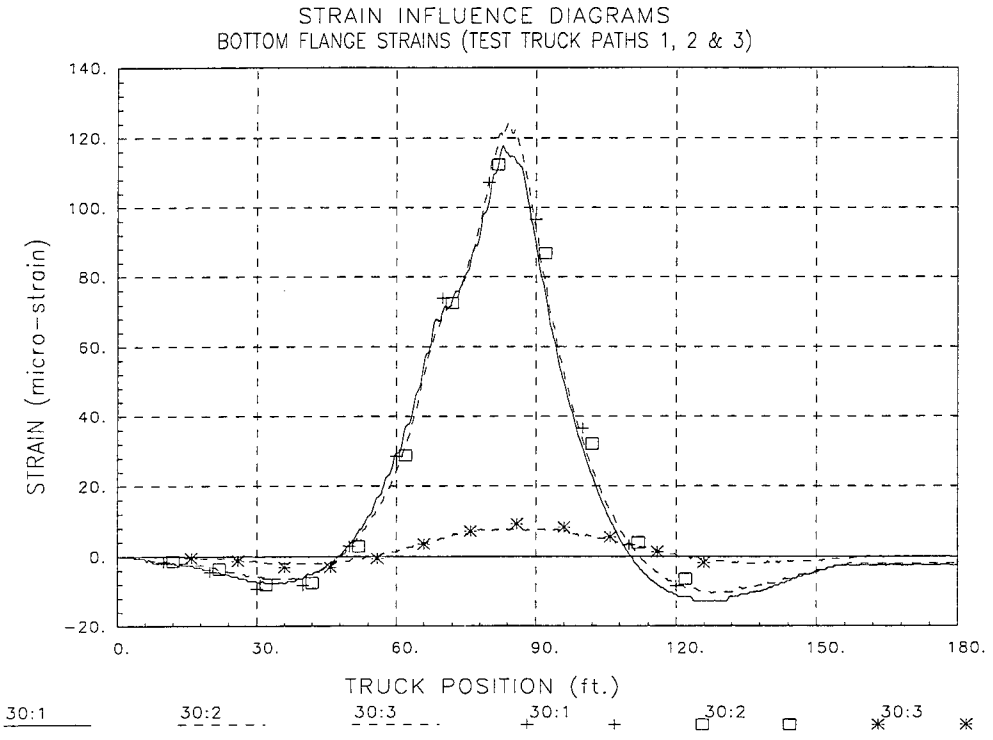

Figure 53 Strain history - beam 2 midspan 2 - truck paths 1, 2 & 3.

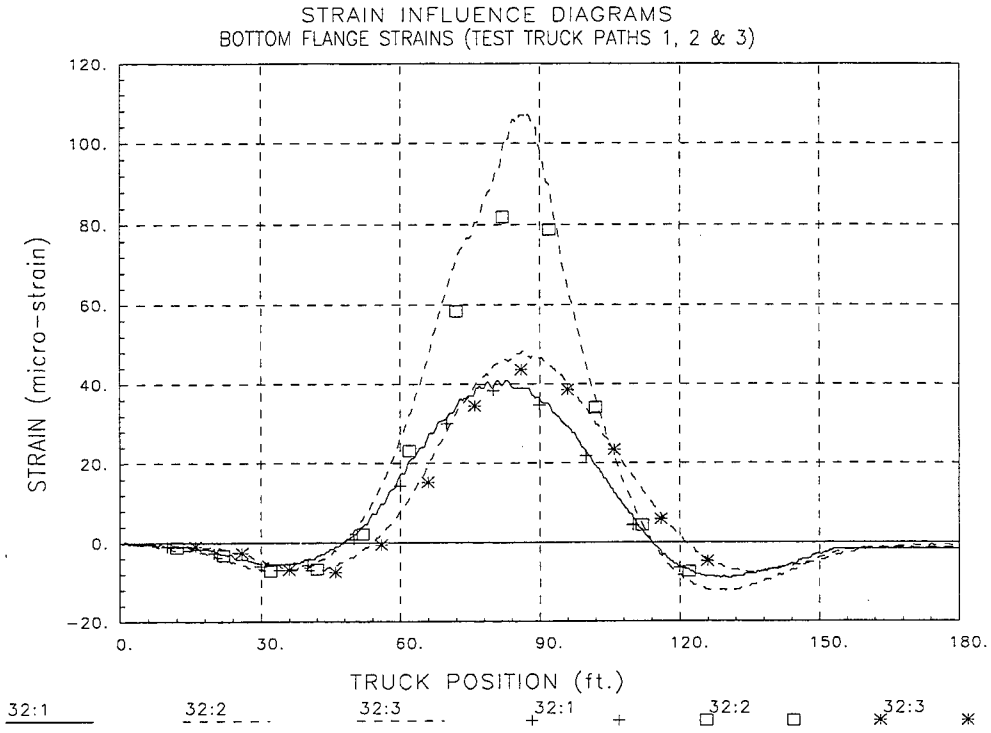

Figure 54 Strain history - beam 3 midspan 2 - truck paths 1, 2 & 3.

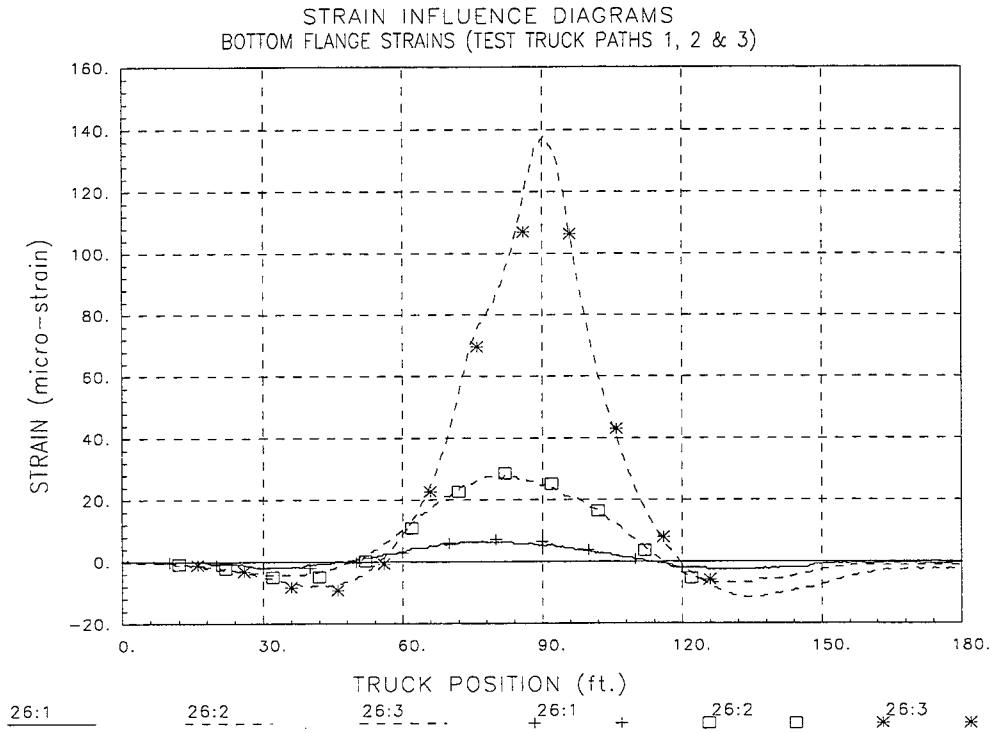

Figure 55 Strain history - beam 4 midspan 2 - truck paths 1, 2 & 3.

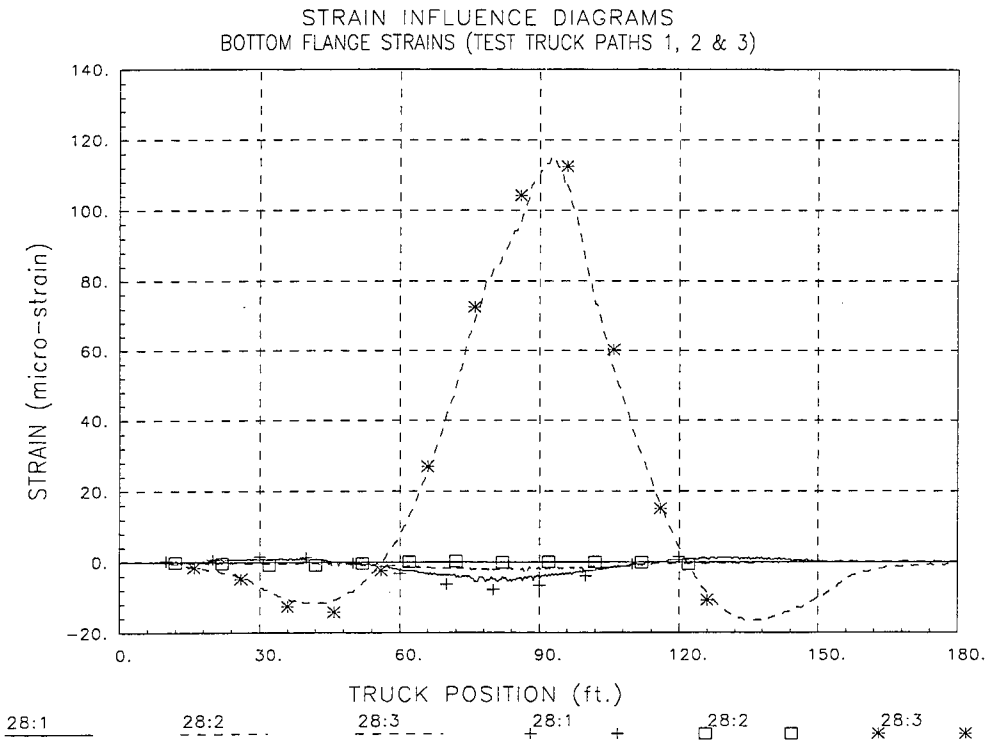

Figure 56 Strain history - beam 5 midspan 2 - truck paths 1, 2 & 3.

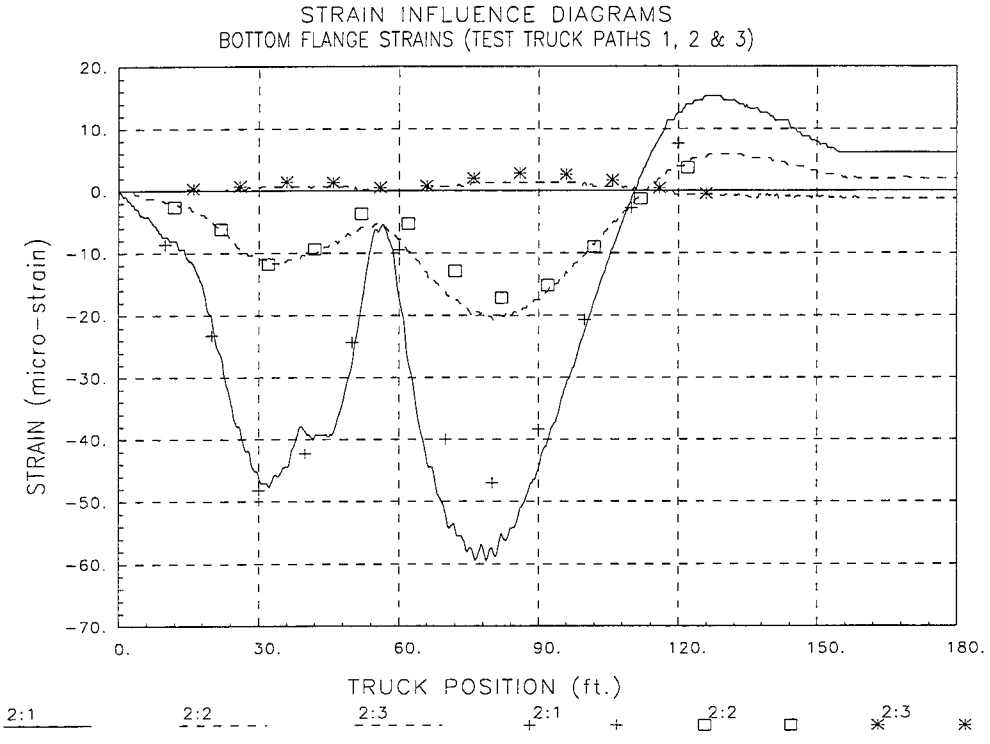

Figure 57 Strain history - beam 1 near pier 1 - truck paths 1, 2 & 3.

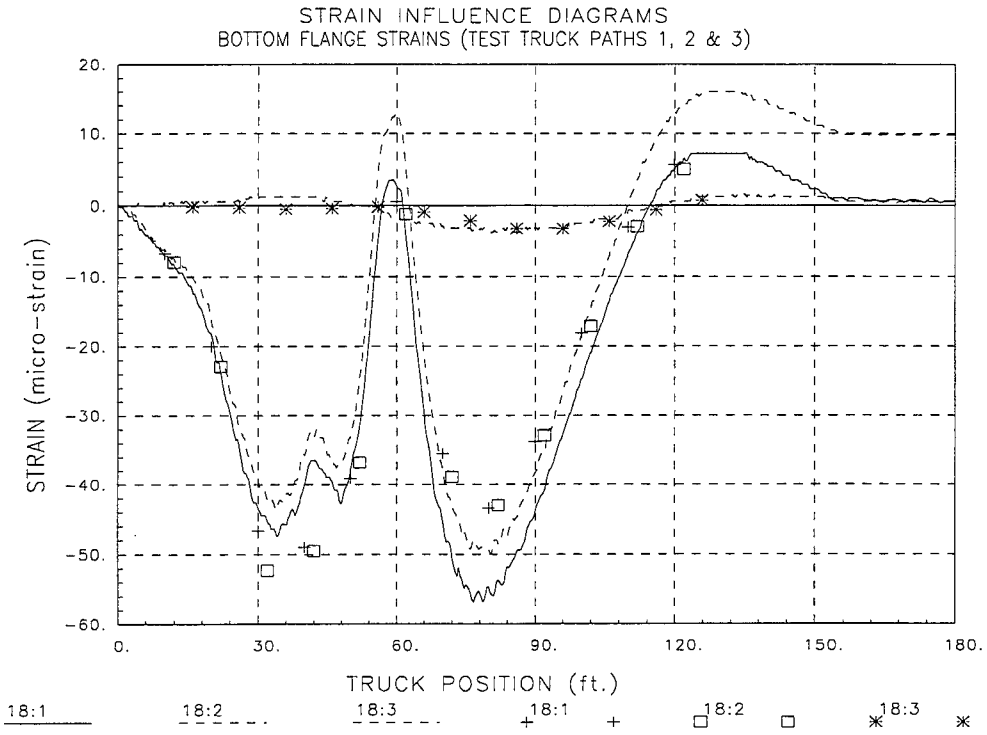

Figure 58 Strain history - beam 2 near pier 1 - truck paths 1, 2 & 3.

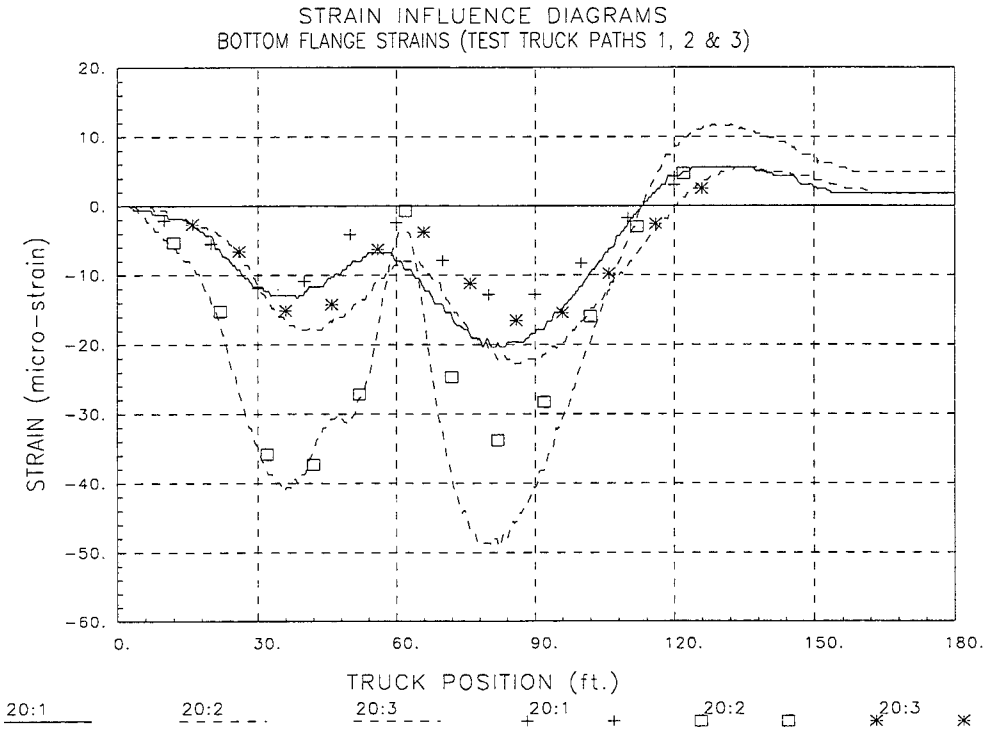

Figure 59 Strain history - beam 3 near pier 1 - truck paths 1, 2 & 3.

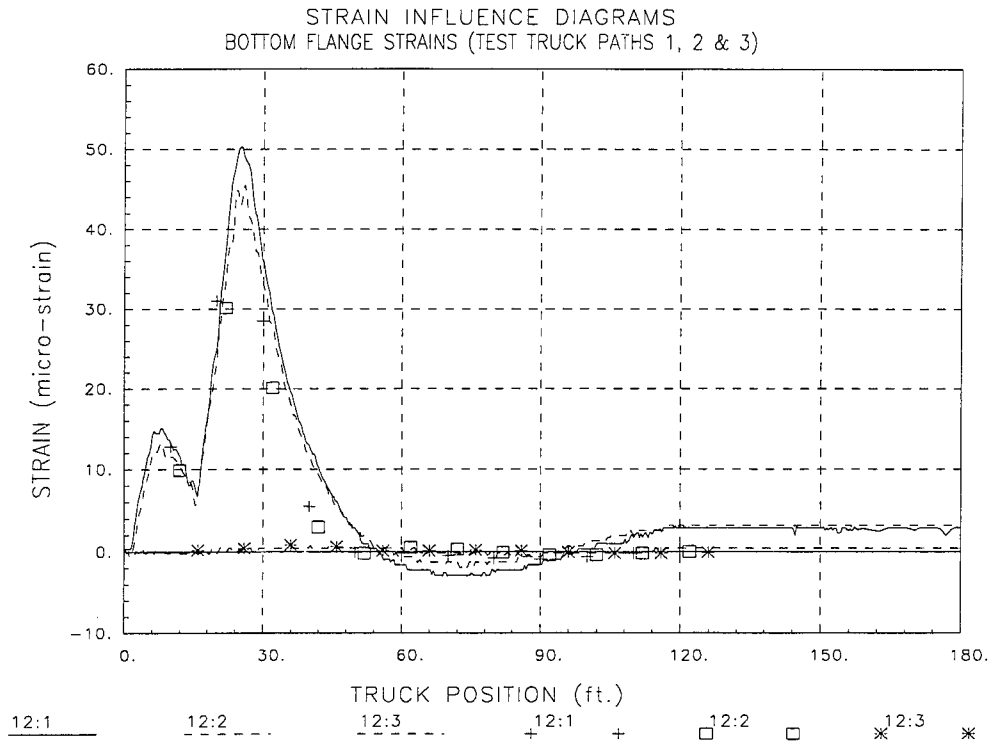

Figure 60 Strain history - beam 2 near south abutment - truck paths 1, 2 & 3.

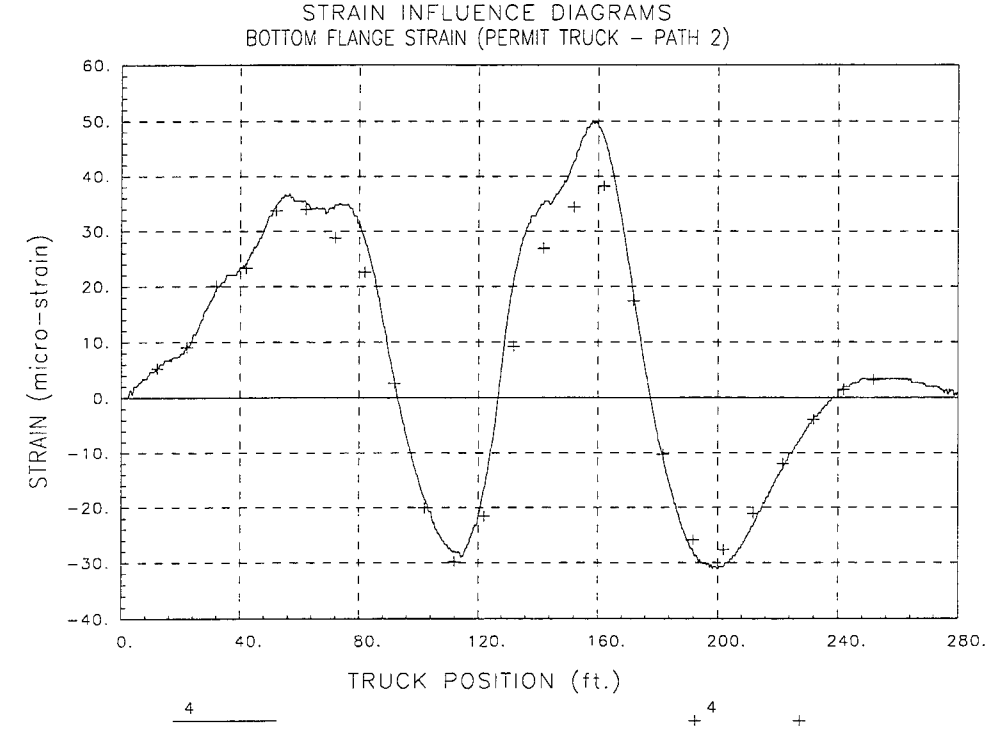

Figure 61 Strain history - beam 1 midspan 1 – permit truck path 2.

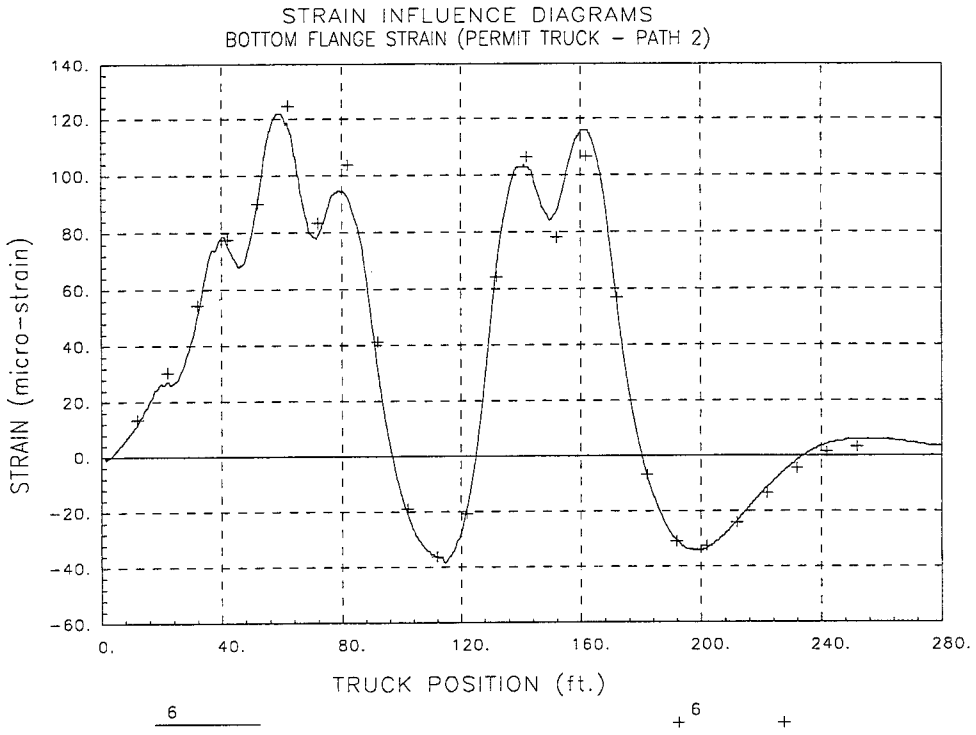

Figure 62 Strain history - beam 2 midspan 1 – permit truck path 2.

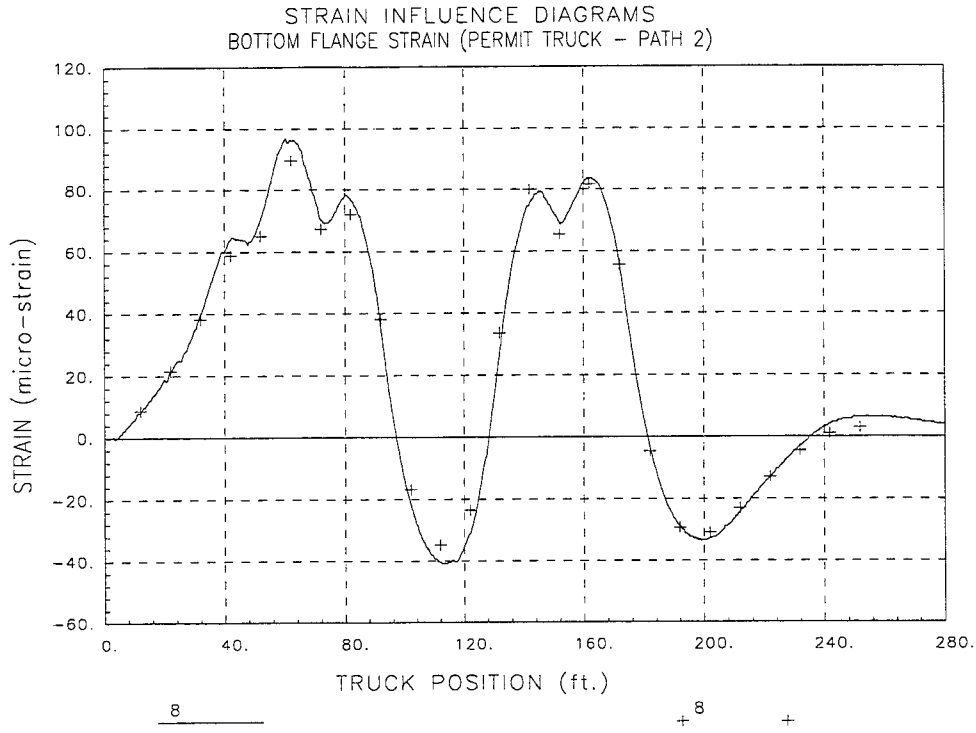

Figure 63 Strain history - beam 3 midspan 1 – permit truck path 2.

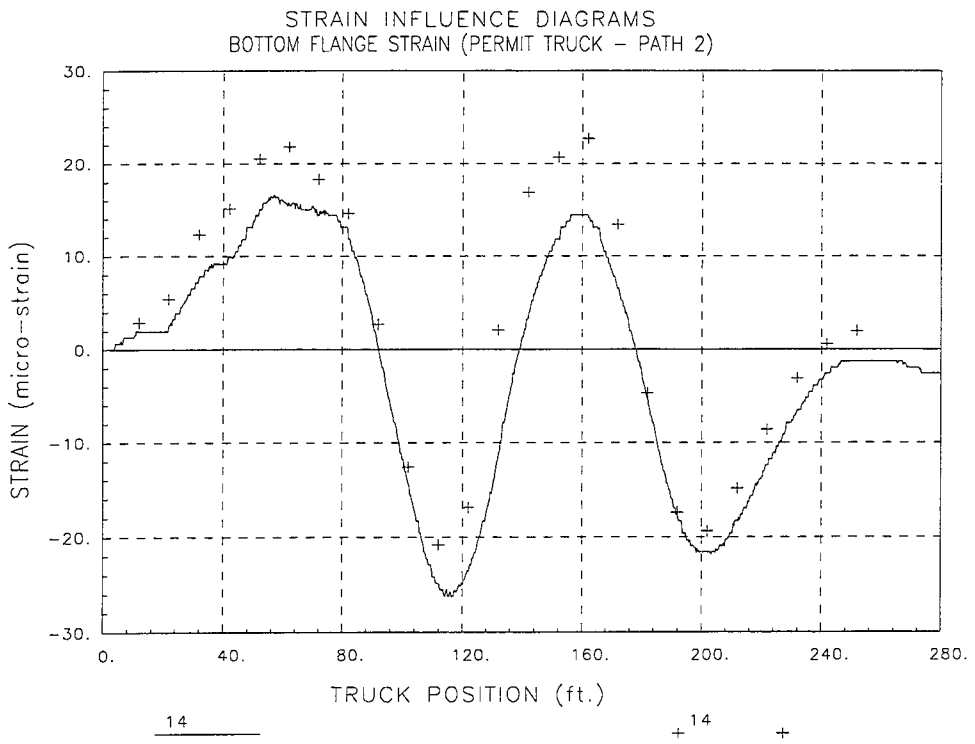

Figure 64 Strain history - beam 4 midspan 1 – permit truck path 2.

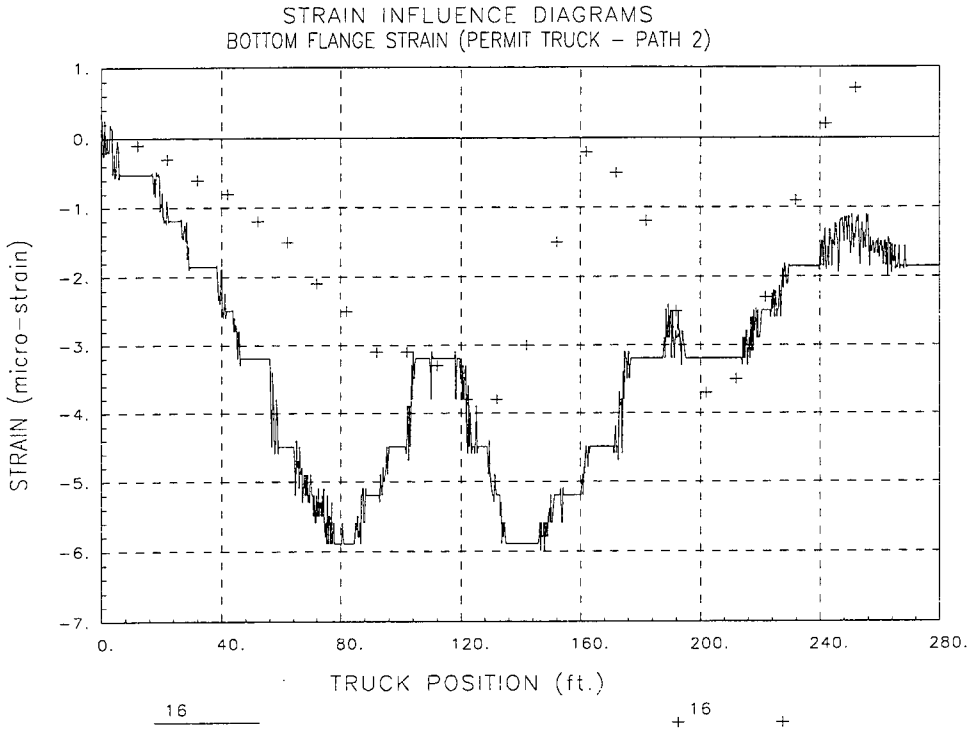

Figure 65 Strain history - beam 5 midspan 1 – permit truck path 2.

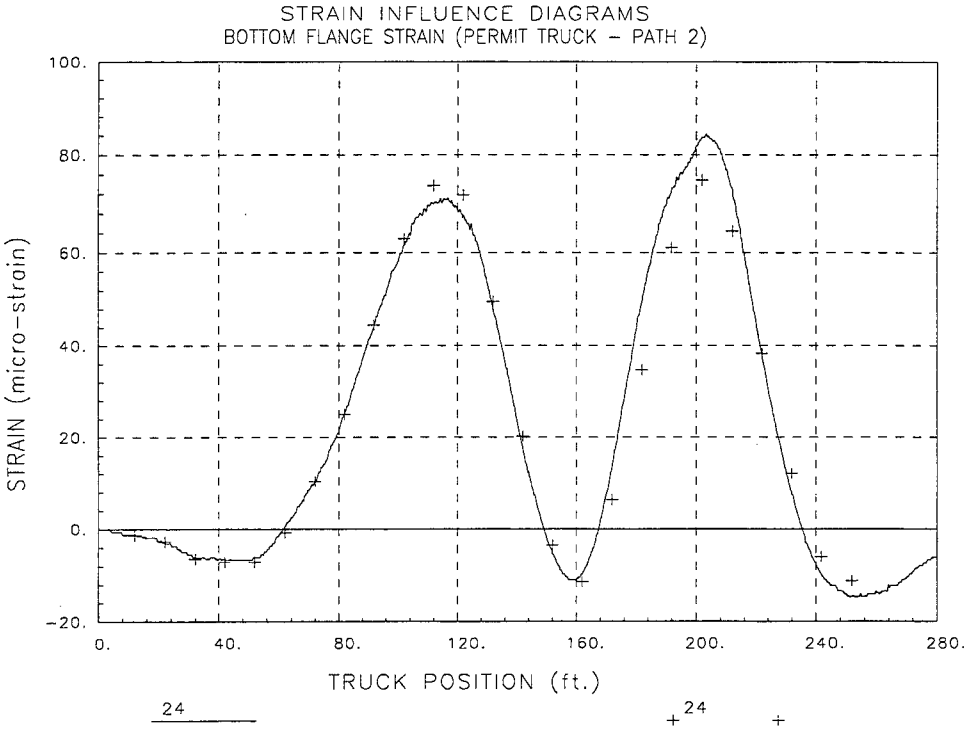

Figure 66 Strain history - beam 1 midspan 2 – permit truck path 2.

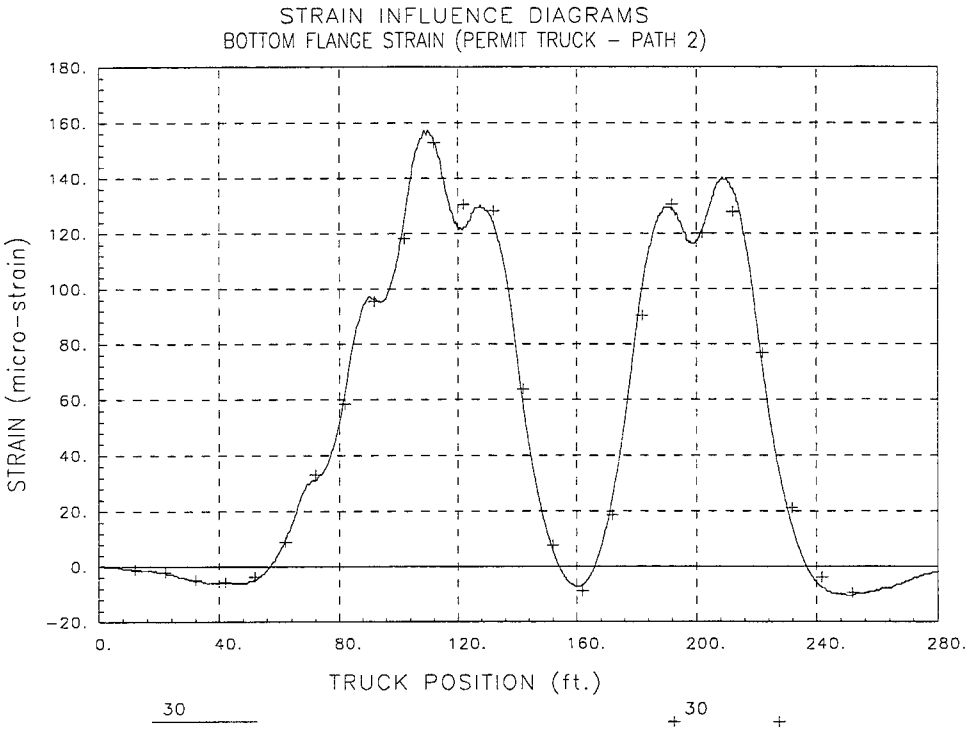

Figure 67 Strain history - beam 2 midspan 2 – permit truck path 2.

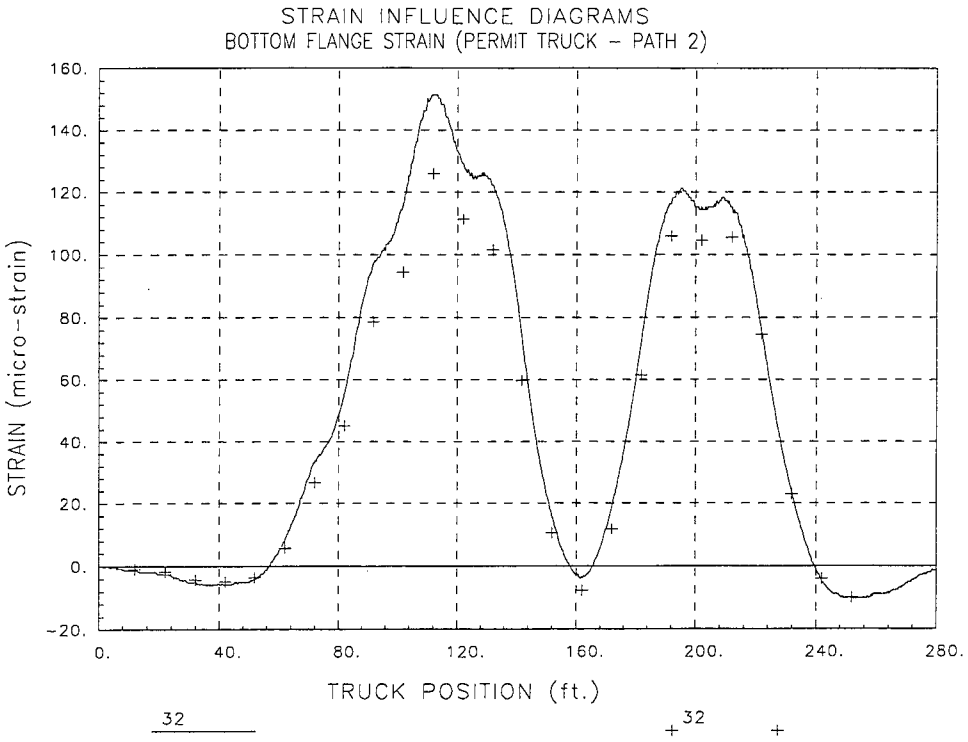

Figure 68 Strain history - beam 3 midspan 2 – permit truck path 2.

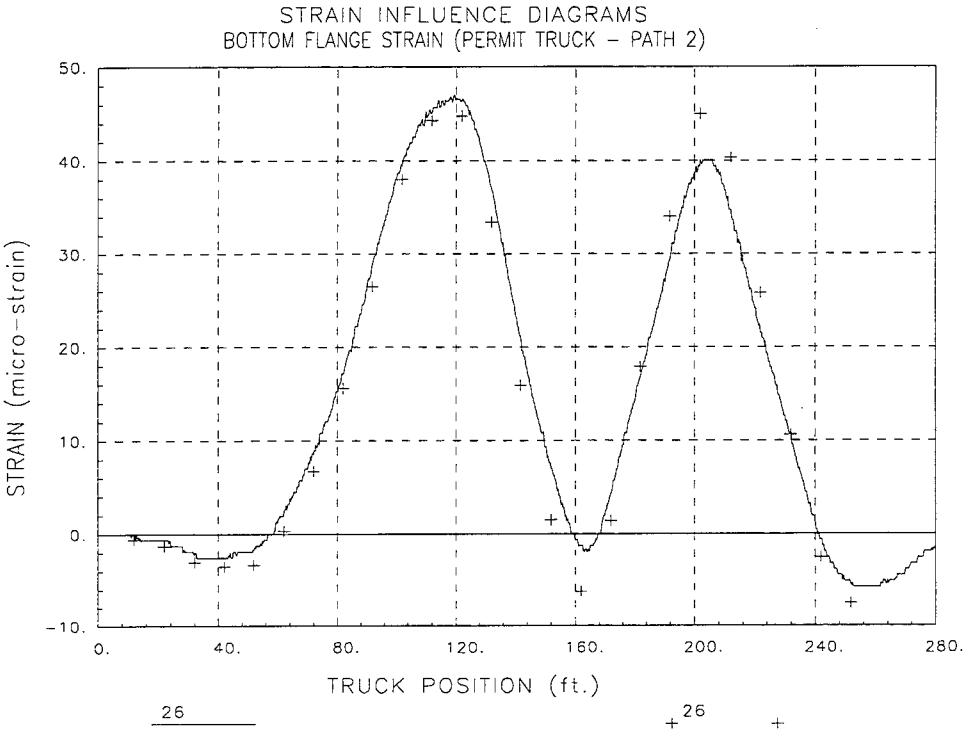

Figure 69 Strain history - beam 4 midspan 2 – permit truck path 2.

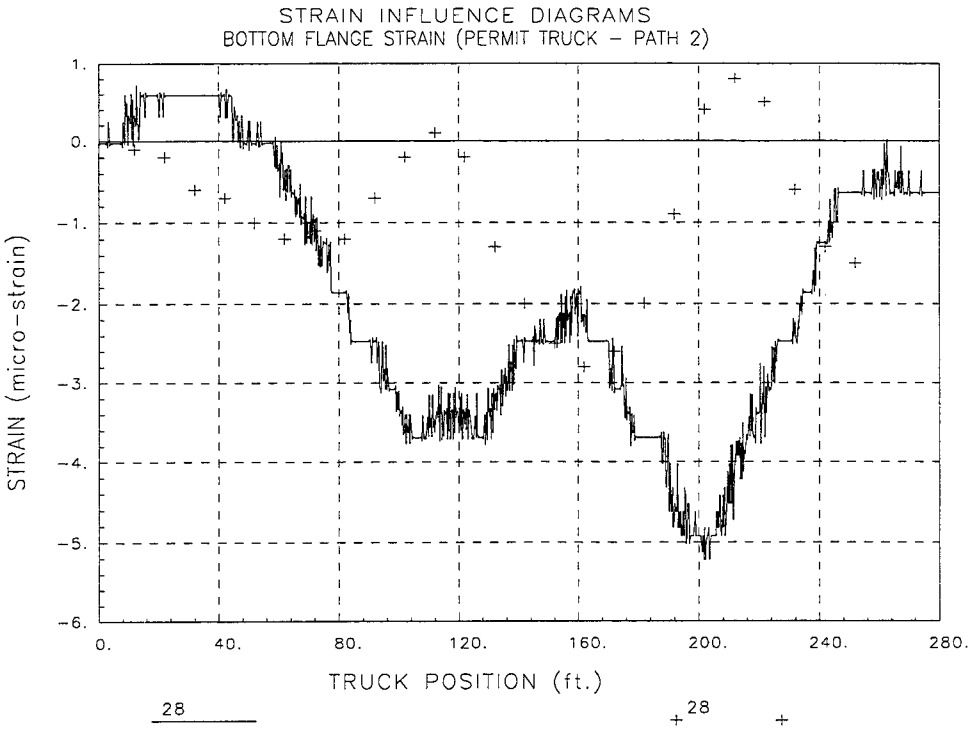

Figure 70 Strain history - beam 5 midspan 2 – permit truck path 2.

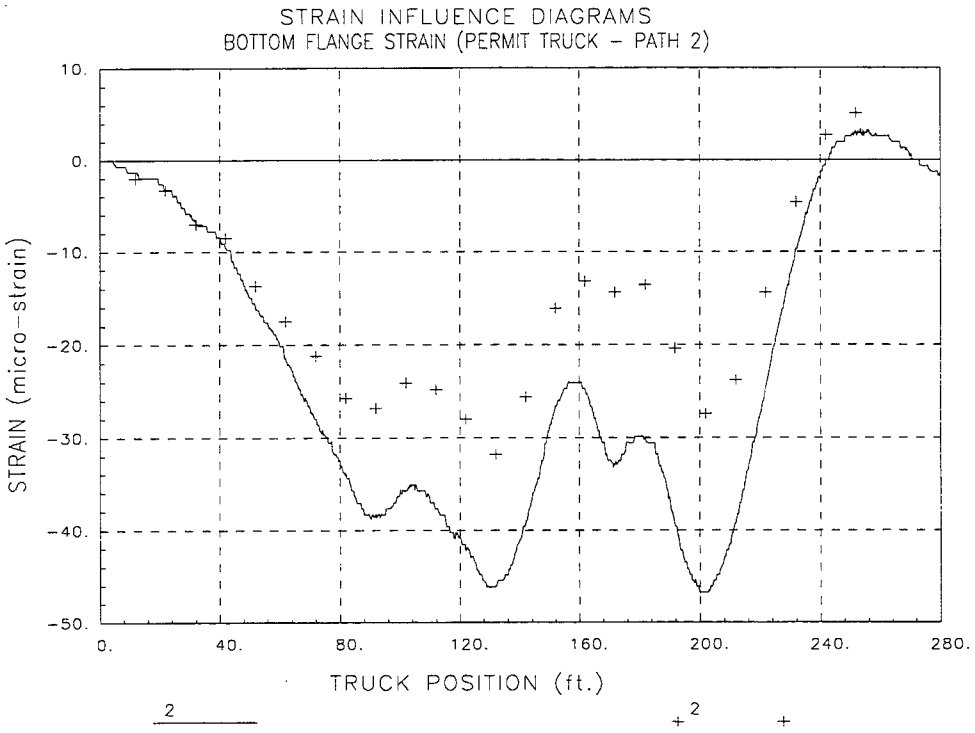

Figure 71 Strain history - beam 1 near pier 1 – permit truck path 2.

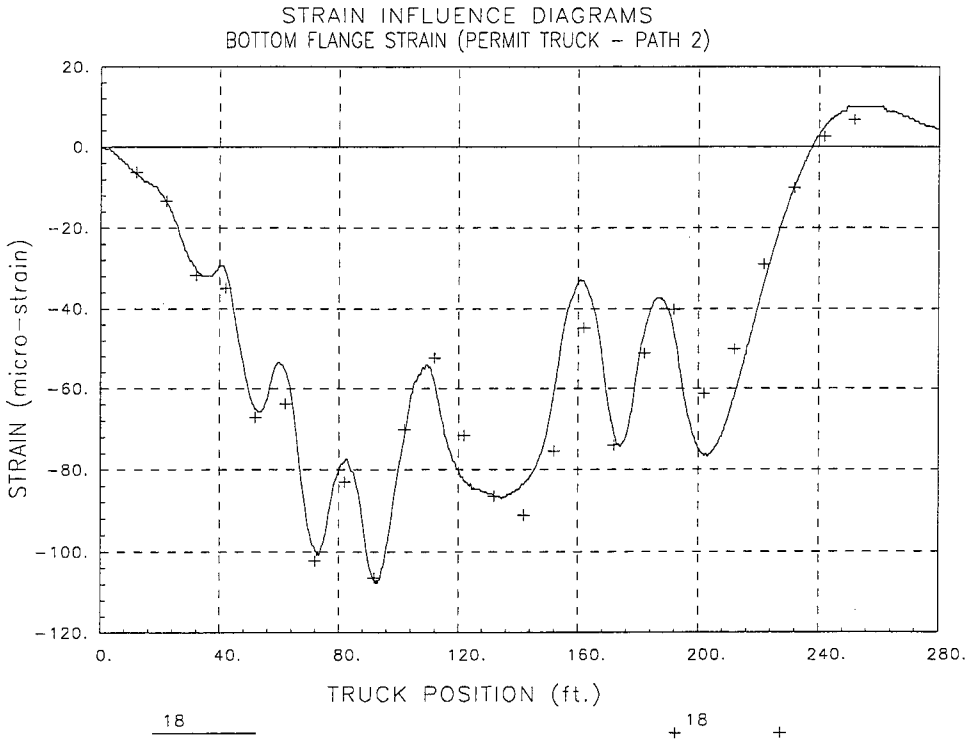

Figure 72 Strain history - beam 2 near pier 1 – permit truck path 2.

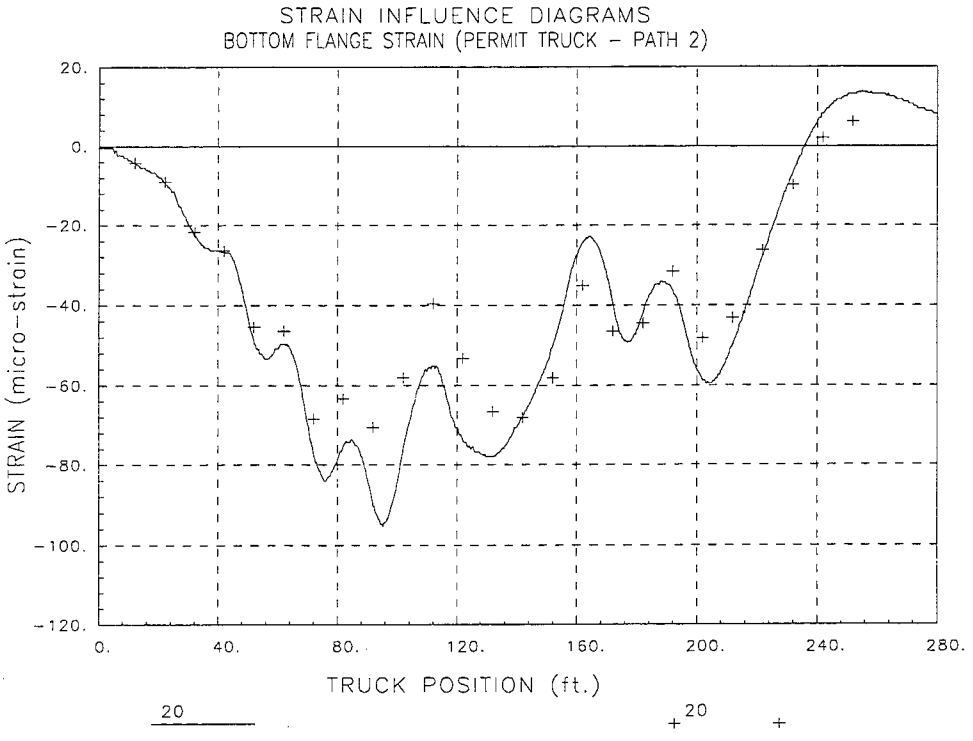

Figure 73 Strain history - beam 3 near pier 1 – permit truck path 2.

APPENDIX D – FIELD TESTING PROCEDURES

The motivation for developing a relatively easy-to-implement field testing system was to allow short and medium span bridges to be tested on a routine basis. Original development of the hardware was started in 1988 at the University of Colorado under a contract with the Pennsylvania Department of Transportation (PennDOT). Subsequent to that project, the Integrated technique was refined on another study funded by the Federal Highway Administration (FHWA) in which 35 bridges located on the Interstate system throughout the country were tested and evaluated. Further refinement has been implemented over the last several years through testing and evaluating several more bridges, lock gates, and other structures.

The real key to being able to complete the field testing quickly is the use of strain transducers (rather than standard foil strain gages) that can be attached to the structural members in just a few minutes. These sensors were originally developed for monitoring dynamic strains on foundation piles during the driving process. They have been adapted for use in structural testing through special modifications and have an accuracy of 3% to 4% and are periodically re-calibrated to NIST standards.

In addition to the strain sensors, the data acquisition hardware has been designed specifically for field use through the use of rugged cables and military-style connectors. This allows quick assembly of the system and keeps bookkeeping to a minimum. The analog-to-digital converter (A/D) is an off-the-shelf-unit, but all signal conditioning, amplification, and balancing hardware has been specially designed for structural testing. The test software has been written to allow easy configuration (test length, etc.) and operation. The end result is a system that can be used by people other than computer experts or electrical engineers. Other enhancements include the use of a remote-control position indicator. As the test vehicle crosses the structure, one of the testing personnel walks along-side and depresses a button on the communication radio each time the front axle of the vehicle crosses one of the chalk lines laid out on the deck. This action sends a signal to the strain measurement system which receives it and puts a mark in the data. This allows the field strains to be compared to analytical strains as a function of vehicle position, not only as a function of time.

The use of a moving load as opposed to placing the truck at discrete locations has two major benefits. First, the testing can be completed much quicker, meaning there is less impact on traffic. Second, and more importantly, much more information can be obtained (both quantitative and qualitative). Discontinuities or unusual responses in the strain histories, which are often signs of distress, can be easily detected. Since the load position is monitored as well, it is easy to determine what loading conditions cause the observed effects. If readings are recorded only at discreet truck locations, the risk of losing information between the points is great. The advantages of continuous readings have been proven over and over again.

This outline is intended to describe the general procedures used for completing a successful field test on a highway bridge using a Structural Testing System (STS). Other types of structures can be tested as well with only slight deviations from the directions given here.

Once a tentative instrumentation plan has been developed for the structure in question, the strain transducers must be attached and the STS prepared for running the test.

ATTACHING STRAIN TRANSDUCERS

There are two methods for attaching the strain transducers to the structural members: C-clamping or with tabs and adhesive. For steel structures, quite often the transducers can be clamped directly to the steel flanges of rolled sections or plate girders. If significant lateral bending is assumed to be present, then one transducer may be clamped to each edge of the flange. If the transducer is to be clamped, insure that the clamp is centered over the mounting holes. In general, the transducers can be clamped directly to painted surfaces. However, if the surface being clamped to is rough or has very thick paint, it should be cleaned first with a grinder. The alternative to clamping is the tab attachment method outlined below.

1) Place two tabs in mounting jig. Place transducer over mounts and tighten the 1/4-20 nuts until they are snug (approximately 50 in-lb.). This procedure allows the tabs to mounted without putting stress on the transducer itself. When attaching transducers to R/C members, transducer extensions are used to obtain a longer gage length. In this case the extension is bolted to one end of the transducer and the tabs are bolted to the free ends of the transducer and the extension.

2) Mark the centerline of the transducer location on the structure. Place marks 1-1/2 inches on either side of the centerline and using a hand grinder, remove paint or scale from these areas. If attaching to concrete, lightly grind the surface to remove any scale. If the paint is quite thick, use a chisel to remove most of it before grinding.

3) Very lightly grind the bottom of the transducer tabs to remove any oxidation or other contaminants.

4) Apply a thin line of adhesive to the bottom of each transducer tab.

5) Spray each tab and the contact area on the structural member with the adhesive accelerator.

6) Mount transducer in its proper location and apply a light force to the tabs (not the center of the transducer) for approximately 10 seconds.

If the above steps are followed, it should be possible to mount each transducer in approximately five minutes. When the test is complete, *carefully* loosen the 1/4-20 nuts from the tabs and remove transducer. If one is not careful, the tab will pop loose from the structure and the transducer may be damaged. Use vice grips to remove the tabs from the structure.

PERFORMING LOAD TEST

The general testing sequence is as follows:

1) Transducers are mounted and the system is connected together and turned on.

2) The deck is marked out for each truck pass. Locate the point on the deck directly above the first bearing for one of the fascia beams. If the bridge is skewed, the first point encountered from the direction of travel is used and an imaginary line extended across and normal to the roadway as shown in Figure 74. All tests are started from this line. In order to track the position of the loading vehicle on the bridge during the test, an X-Y coordinate system, with the origin at the selected reference point is laid out. Longitudinal marks are placed with chalk powder the length of the bridge in even increments. For spans less than 100-ft (30.5-m), 10-ft (3.05-m) increments are used, although for very short spans, use 5-ft (1.5-m) For longer spans, marks are placed at 20-foot (6.1-m) intervals. This is done for each lane that the truck travels over. A typical deck layout is shown in Figure 74.

In addition to monitoring the longitudinal position, the vehicle's transverse position must be known. The transverse truck position is kept uniform by first aligning the truck in the center of the lane where it would normally travel at highway speed. Next, a chalk mark is made on the deck locating the transverse location of the driver's side front wheel. By making a measurement from this mark to the reference point, the transverse ("Y") position of the truck is always known. The truck is aligned on this mark for all subsequent tests in this lane. For two lane bridges with shoulders, tests are run on the shoulder (driver's side front wheel along the white line) and in the center of each lane. If the bridge has only two lanes and very little shoulder, tests are run in the center of each lane only. If the purpose of the test is to calibrate a computer model, it is sometimes more convenient to simply use the lane lines as guides since it is easier for the driver to maintain a constant lateral position. Responses due to critical truck positions are then obtained by the analysis.

The driver is instructed that the test vehicle must be kept in the proper location on the bridge. For example, the left front wheel needs to be kept on the white line for the shoulder tests. Another important item was that the vehicle maintain a constant rate of speed during the entire test.

Two more pieces of information are then needed: the axle weights and dimensions of the test vehicle. The axle weights are generally provided by the driver, who stops at a local scale. However, a weight enforcement team can use portable scales and weigh the truck at the bridge site. Wheel base and axle width dimensions are made with a tape measure and recorded.

3) The program is started and the number of channels indicated is verified. If the number of channels indicated do not match the number of channels actually there, a malfunction has occurred and must be corrected before testing commences.

4) The transducers are initialized (zeroed out) with the Balance option. If a transducer cannot be initialized, it should be inspected to ensure that it has not been damaged.

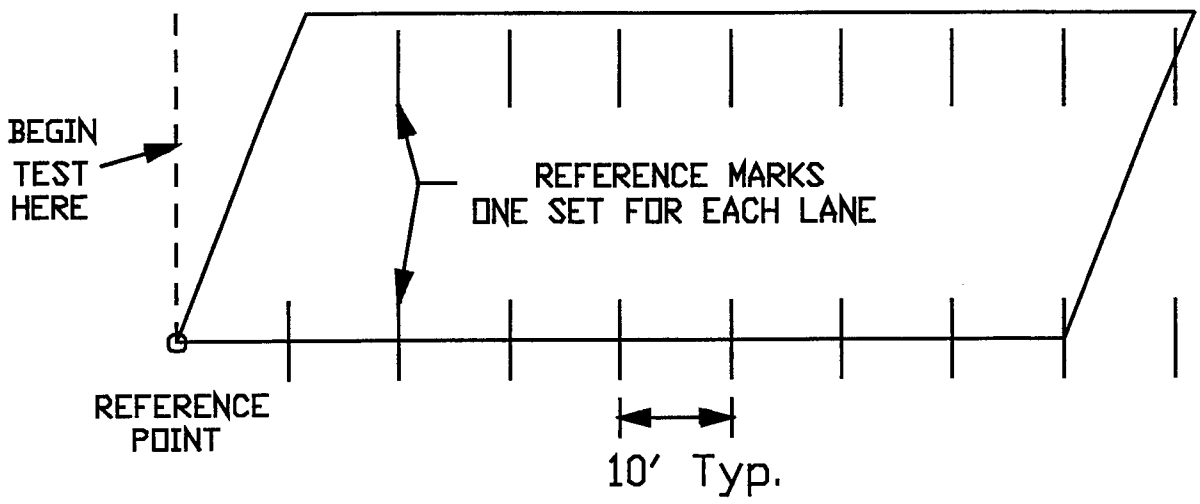

Figure 74 Typical deck layout for monitoring load position.

5) The desired test length, sample rate, and output file name are selected. In general, a longer test time than the actual event is selected. For most bridge tests, a one or two minute test length will suffice since the test can be stopped as soon as the truck crosses completely over the structure.

6) To facilitate presenting data as a function of load position, rather than time, two items describing the PI information must be defined. The starting position and PI interval distance allow the data to be plotted using position coordinates that are consistent with a numeric analysis. The starting position refers to the longitudinal position of the load vehicle in the model coordinate system when the data recording is started. The interval distance(s) is the distance between position marks using the units and sign convention of the coordinate system. Typically, all of the intervals are defined with the same length, however, in some cases this may not be possible and some other reference points must be used. The distance between each position mark can be defined. It is important that this information be clearly defined in the field notes.

7) If desired, the Monitor option can be used to verify transducer output during a trial test. Also, it is useful to run a Position Indicator (PI) test while in Monitor to ensure that the clicks are being received properly.

8) When all parties are ready to commence the test, the Run Test option is selected which places the system in an activated state. When the PI is first depressed, the test will start. Also, the PI is depressed each time the front axle crossed a chalk mark. The PI operator should either ride on the truck sidestep or walk beside the truck as it crosses the bridge. An effort should be made to get the truck across with no other traffic on the bridge. There should be no talking over the radios during the test as a "position" will be recorded each time the microphones are activated.

9) When the test has been completed and the system is still recording data, hit "S" to stop collecting data and finish writing the recorded data to disk. If the data files are large, they can be compressed and copied to floppy disk.

10) It is important to record the field notes very carefully. Having data without knowing where it was recorded can be worse than having no data at all. Transducer location and serial numbers must be recorded accurately.

APPENDIX E – ANALYSIS AND DATA CORRELATION PROCEDURES.

INTRODUCTION

In order for load testing to be a practical means of evaluating short- to medium-span bridges, it is apparent that testing procedures must be economic to implement in the field and the test results translatable into a load rating. A well-defined set of procedures must exist for the field applications as well as for the interpretation of results. An evaluation approach based on these requirements was first developed at the University of Colorado during a research project sponsored by the Pennsylvania Department of Transportation (PennDOT). Over several years, the techniques originating from this project have been refined and expanded into a complete bridge rating system.

The ultimate goal of the Integrated approach is to obtain realistic rating values for highway bridges in a cost effective manner. This is accomplished by measuring the response behavior of the bridge due to a known load and determining the structural parameters that produce the measured responses. With the availability of field measurements, many structural parameters in the analytical model can be evaluated that are otherwise conservatively estimated or ignored entirely. Items that can be quantified through this procedure include the effects of structural geometry, effective beam stiffnesses, realistic support conditions, effects of parapets and other non-structural components, lateral load transfer capabilities of the deck and transverse members, and the effects of damage or deterioration. Often, bridges are rated poorly because of inaccurate representations of the structural geometry or because the material and/or cross-sectional properties of main structural elements are not well defined. A realistic rating can be obtained, however, when all of the relevant structural parameters are defined and implemented in the analysis process.

One of the most important phases of this approach is a qualitative evaluation of the raw field data. Much is learned during this step to aid in the rapid development of a representative model.

INITIAL DATA EVALUATION

The first step in structural evaluation consists of a visual inspection of the data in the form of graphic response histories. Graphic software was developed to display the raw strain data in various forms. Strain histories can be viewed in terms of time or truck position. Since strain transducers are typically placed in pairs, neutral axis measurements, curvature responses, and strain averages can also be viewed. Linearity between the responses and load magnitude can be observed by the continuity in the strain histories. Consistency in the neutral axis measurements from beam to beam and as a function of load position provides great insight into the nature of the bridge condition. The direction and relative magnitudes of flexural responses along a beam line are useful in determining if end restraints play a significant role in the response behavior. In general, the initial data inspection provides the engineer with information concerning modeling requirements and can help locate damaged areas.

Having strain measurements at two depths on each beam cross-section, flexural curvature and the location of the neutral axis can be computed directly from the field data. Figure 75 illustrates how curvature and neutral axis values are computed from the strain measurements.

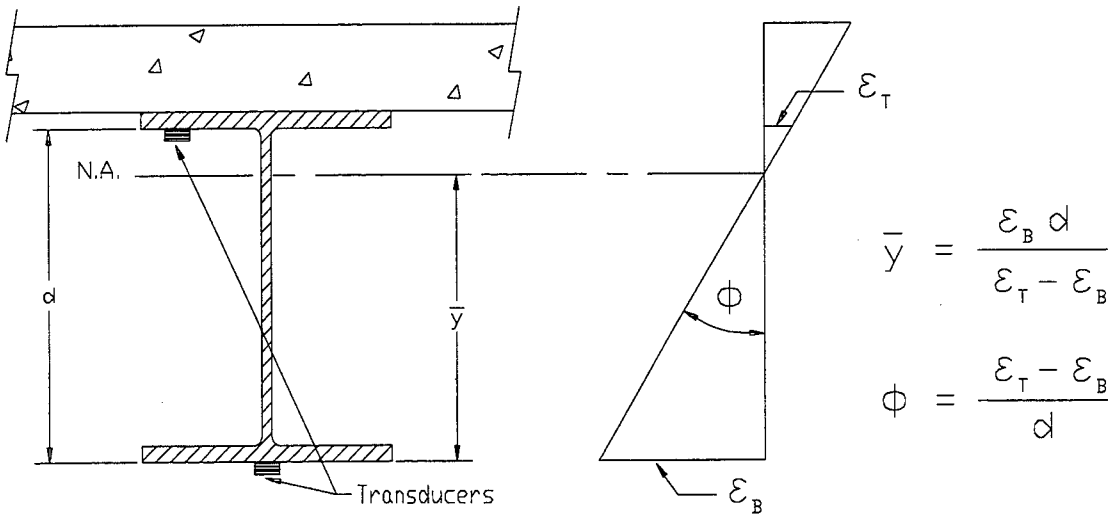

Figure 75 Illustration of neutral axis and curvature calculations.

The consistency in the N.A. values between beams indicate the degree of consistency in beam stiffnesses. Also, the consistency of the N.A. measurement on a single beam as a function of truck position provides a good quality check for that beam. If for some reason a beam's stiffness changes with respect to the applied moment (i.e. loss of composite action or loss of effective flange width due to a deteriorated deck), it will be observed by a shift in the N.A. history.

Since strain values are translated from a function of time into a function of vehicle position on the structure and the data acquisition channel and the truck position tracked, a considerable amount of book keeping is required to perform the strain comparisons. In the past, this required manipulation of result files and spreadsheets which was tedious and a major source of error. This process in now performed automatically by the software and all of the information can be verified visually.

FINITE ELEMENT MODELING AND ANALYSIS

The primary function of the load test data is to aid in the development of an accurate finite element model of the bridge. Finite element analysis is used because it provides the most general tool for evaluating various types of structures. Since a comparison of measured and computed responses is performed, it is necessary that the analysis be able to represent the actual response behavior. This requires that actual geometry and boundary conditions be realistically represented. In maintaining reasonable modeling efforts and computer run times, a certain amount of simplicity

is also required, so a planar grid model is generated for most structures and linear-elastic responses are assumed. A grid of frame elements are assembled in the same geometry as the actual structure. Frame elements represent the longitudinal and transverse members of the bridge. The load transfer characteristics of the deck are provided by attaching plate elements to the grid. When end restraints are determined to be present, elastic spring elements having both translational and rotational stiffness terms are inserted at the support locations.

Loads are applied in a manner similar to the actual load test. A model of the test truck, defined by a two-dimensional group of point loads, is placed on the structure model at discrete locations along the same path that the test truck followed during the load test. Gage locations identical to those in the field are also defined on the structure model so that strains can be computed at the same locations under the same loading conditions.

CORRELATIONS AND PARAMETER MODIFICATIONS

The accuracy of the model is determined numerically by the analysis using several statistical relationships and through visual comparison of the strain histories. The numeric accuracy values are useful in evaluating the effect of any changes to the model, where as the graphical representations provide the engineer with the best perception for why the model is responding differently than the measurements indicate. Member properties that cannot be accurately defined by conventional methods or directly from the field data are evaluated by comparing the computed strains with the measured strains. These properties are defined as variable and are evaluated such that the best correlation between the two sets of data is obtained. It is the engineer's responsibility to determine which parameters need to be refined and to assign realistic upper and lower limits to each parameter. The evaluation of the member property is accomplished with the aid of a parameter identification process (optimizer) built into the analysis. In short, the process consists of an iterative procedure of analysis, data comparison, and parameter modification. It is important to note that the optimization process is merely a tool to help evaluate various modeling parameters. The process works best when the number of parameters is minimized and reasonable initial values are used.

During the optimization process, various error values are computed by the analysis program that provide quantitative measure of the model accuracy and improvement. The error is quantified in four different ways, each providing a different perspective of the model's ability to represent the actual structure; an absolute error, a percent error, a scale error and a correlation coefficient.

The **absolute error** is computed from the absolute sum of the strain differences. Algebraic differences between the measured and theoretical strains are computed at each gage location for each truck position used in the analysis, therefore, several hundred strain comparisons are generally used in this calculation. This quantity is typically used to determine the relative accuracy from one model to the next and to evaluate the effect of various structural parameters. It is used by the optimization algorithm as the objective function to minimize the error. Because the absolute error is in terms of micro-strain (m) the value can vary significantly depending on the magnitude of the strains, the number of gages and number of different loading scenarios. For this reason, it has little conceptual value except for determining the relative improvement of a particular model.

A **percent error** is calculated to provide a better qualitative measure of accuracy. It is computed as the sum of the strain differences squared divided by the sum of the measured strains squared. The terms are squared so that error values of different sign will not cancel each other out, and to put more emphasis on the areas with higher strain magnitudes. A model with acceptable accuracy will usually have a percent error of less than 10%.

The **scale error** is similar to the percent error except that it is based on the maximum error from each gage divided by the maximum strain value from each gage. This number is useful because it is based only on strain measurements recorded when the loading vehicle is in the vicinity of each gage. Depending on the geometry of the structure, the number of truck positions, and various other factors, many of the strain readings are essentially negligible. This error function uses only the most relevant measurement from each gage.

Another useful quantity is the **correlation coefficient** which is a measure of the linearity between the measured and computed data. This value determines how well the shape of the computed response histories match the measured responses. The correlation coefficient can have a value between 1.0 (indicating a perfect linear relationship) and -1.0 (exact opposite linear relationship). A good model will generally have a correlation coefficient greater than 0.90. A poor correlation coefficient is usually an indication that a major error in the modeling process has occurred. This is generally caused by poor representations of the boundary conditions or the loads were applied incorrectly (i.e. truck traveling in wrong direction).

The following table contains the equations used to compute each of the statistical error values:

Table 31. Error functions used for data correlation.

ERROR FUNCTION	EQUATION
Absolute Error	$\Sigma\lvert\varepsilon_m - \varepsilon_c\rvert$
Percent Error	$\Sigma(\varepsilon_m - \varepsilon_c)^2 \,/\, \Sigma(\varepsilon_m)^2$
Scale Error	$\dfrac{\Sigma \max\lvert\varepsilon_m - \varepsilon_c\rvert_{gage}}{\Sigma \max\lvert\varepsilon_m\rvert_{gage}}$
Correlation Coefficient	$\dfrac{\Sigma(\varepsilon_m - \overline{\varepsilon_m})(\varepsilon_c - \overline{\varepsilon_c})}{\Sigma\sqrt{(\varepsilon_m - \overline{\varepsilon_m})^2(\varepsilon_c - \overline{\varepsilon_c})^2}}$

In addition to the numerical comparisons made by the program, periodic visual comparisons of the response histories are made to obtain a conceptual measure of accuracy. Again, engineering judgment is essential in determining which parameters should be adjusted so as to obtain the most

accurate model. The selection of adjustable parameters is performed by determining what properties have a significant effect on the strain comparison and determining which values cannot be accurately estimated through conventional engineering procedures. Experience in examining the data comparisons is helpful, however, two general rules apply concerning model refinement. When the shapes of the computed response histories are similar to the measured strain records but the magnitudes are incorrect this implies that member stiffnesses must be adjusted. When the shapes of the computed and measured response histories are not very similar then the boundary conditions or the structural geometry are not well represented and must be refined.

In some cases, an accurate model cannot be obtained, particularly when the responses are observed to be non-linear with load position. Even then, a great deal can be learned about the structure and intelligent evaluation decisions can be made.

APPENDIX F - LOAD RATING PROCEDURES

For borderline bridges (those that calculations indicate a posting is required), the primary drawback to conventional bridge rating is an oversimplified procedure for estimating the load applied to a given beam (i.e. wheel load distribution factors) and a poor representation of the beam itself. Due to lack of information and the need for conservatism, material and cross-section properties are generally over-estimated and beam end supports are assumed to be simple when in fact even relatively simple beam bearings have a substantial effect on the midspan moments. Inaccuracies associated with conservative assumptions are compounded with complex framing geometries. From an analysis standpoint, the goal here is to generate a model of the structure that is capable of reproducing the measured strains. Decisions concerning load rating are then based on the performance of the model once it is proven to be accurate.

The main purpose for obtaining an accurate model is to evaluate how the bridge will respond when standard design loads, rating vehicles or permit loads are applied to the structure. Since load testing is generally not performed with all of the vehicles of interest, an analysis must be performed to determine load rating factors for each truck type. Load rating is accomplished by applying the desired rating loads to the model and computing the stresses on the primary members. Rating factors are computed using the equation specified in the AASHTO Manual for Condition Evaluation of Bridges - see equation (2).

It is important to understand that diagnostic load testing and the integrated approach are most applicable to obtaining Inventory (service load) rating values. This is because it is assumed that all of the measured and computed responses are linear with respect to load. The integrated approach is an excellent method for estimating service load stress values but it generally provides little additional information regarding the ultimate strength of particular structural members. Therefore, operating rating values must be computed using conventional assumptions regarding member capacity. This limitation of the integrated approach is not viewed as a serious concern, however, because load responses should never be permitted to reach the inelastic range.

Operating and/or Load Factor rating values must also be computed to ensure a factor of safety between the ultimate strength and the maximum allowed service loads. The safety to the public is of vital importance but as long as load limits are imposed such that the structure is not damaged then safety is no longer an issue. Following is an outline describing how field data is used to help in developing a load rating for the superstructure. These procedures will only complement the rating process, and must be used with due consideration to the substructure and inspection reports.

1) *Preliminary Investigation:* Verification of linear and elastic behavior through continuity of strain histories, locate neutral axis of flexural members, detect moment resistance at beam supports, qualitatively evaluate behavior.

2) *Develop representative model:* Use graphic pre-processors to represent the actual geometry of the structure, including span lengths, girder spacing, skew, transverse members, and deck. Identify gage locations on model identical to those applied in the field.

3) *Simulate load test on computer model:* Generate 2-dimensional model of test vehicle and apply to structure model at discrete positions along same paths defined during field tests. Perform analysis and compute strains at gage location for each truck position.

4) *Compare measured and initial computed strain values:* Various global and local error values at each gage location are computed and visual comparisons made with post-processor.

5) *Evaluate modeling parameters:* Improve model based on data comparisons. Engineering judgment and experience is required to determine which variables are to be modified. A combination of direct evaluation techniques and parameter optimization are used to obtain a realistic model. General rules have been defined to simplify this operation.

6) *Model evaluation:* In some cases it is not desirable to rely on secondary stiffening effects if it is likely they will not be effective at higher load levels. It is beneficial, though, to quantify their effects on the structural response so that a representative computer model can be obtained. The stiffening effects that are deemed unreliable can be eliminated from the model prior to the computation of rating factors. For instance, if a non-composite bridge is exhibiting composite behavior, then it can conservatively be ignored for rating purposes. However, if it has been in service for 50 years and it is still behaving compositely, chances are that very heavy loads have crossed over it and any bond-breaking would have already occurred. Therefore, probably some level of composite behavior can be relied upon. When unintended composite action is allowed in the rating, additional load limits should be computed based on an allowable shear stress between the steel and concrete and an ultimate load of the non-composite structure.

7) *Perform load rating:* Apply HS-20 and/or other standard design, rating and permit loads to the calibrated model. Rating and posting load configuration recommended by AASHTO are shown in Figure 76.The same rating equation specified by the **AASHTO - Manual for the Condition Evaluation of Bridges** is applied:

$$RF = \frac{C - A_1 D}{A_2 L(1 + I)} \tag{2}$$

where:

RF = Rating Factor for individual member.
C = Member Capacity.
D = Dead-Load effect.
L = Live-Load effect.
A_1 = Factor applied to dead-load.
A_2 = Factor applied to live-load.
I = Impact effect, either AASHTO or measured.

The only difference between this rating technique and standard beam rating programs is that a more realistic model is used to determine the dead-load and live-load effects. Two-dimensional loading techniques are applied because wheel load distribution factors are not applicable to a planar model. Stress envelopes are generated for several truck paths, envelopes for paths separated by normal lane widths are combined to determine multiple lane loading effects.

8) *Consider other factors:* Other factors such as the condition of the deck and/or substructure, traffic volume, and other information in the inspection report should be taken into consideration and the rating factors adjusted accordingly.

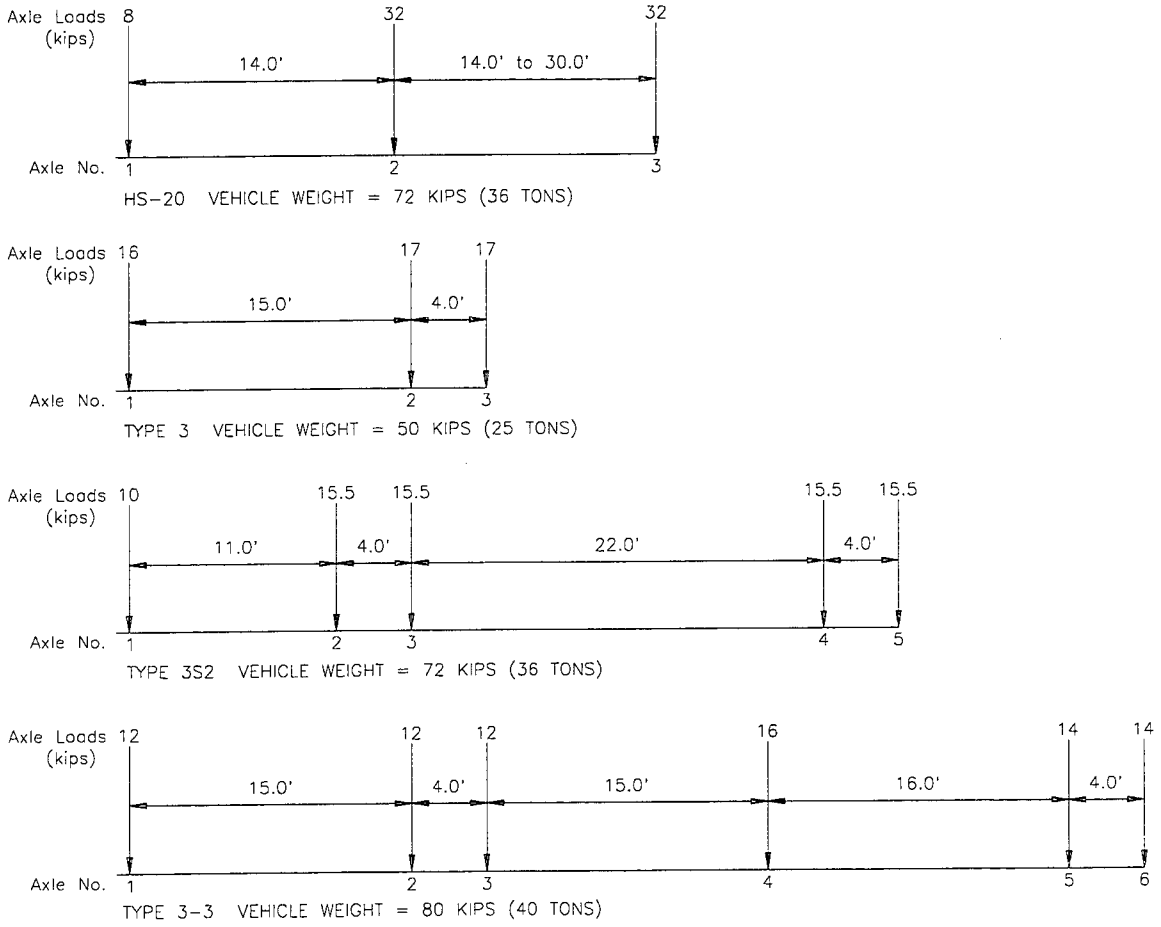

Figure 76 AASHTO rating and posting load configurations.

APPENDIX G - REFERENCES

AASHTO (1989). "Standard Specification for Highway Bridges." Washington,D.C.

AASHTO, (1994). "Manual for the Condition Evaluation of Bridges", Washington,D.C.